

NAVAL POSTGRADUATE SCHOOL

Monterey, California



THESIS

**THE ROLE OF THE PLANETARY BETA EFFECT ON
CURRENTS AND MEDDIES IN THE NORTHERN
CANARY CURRENT SYSTEM**

by

Patrick J. Murray

June 2000

Thesis Advisor:
Second Reader:

Mary L. Batteen
Curtis A. Collins

Approved for public release; distribution is unlimited.

DTIC QUALITY INSPECTED 4

20000807 062

REPORT DOCUMENTATION PAGE			Form Approved OMB No. 0704-0188	
Public reporting burden for this collection of information is estimated to average 1 hour per response, including the time for reviewing instruction, searching existing data sources, gathering and maintaining the data needed, and completing and reviewing the collection of information. Send comments regarding this burden estimate or any other aspect of this collection of information, including suggestions for reducing this burden, to Washington headquarters Services, Directorate for Information Operations and Reports, 1215 Jefferson Davis Highway, Suite 1204, Arlington, VA 22202-4302, and to the Office of Management and Budget, Paperwork Reduction Project (0704-0188) Washington DC 20503.				
1. AGENCY USE ONLY (Leave blank)		2. REPORT DATE June 2000		3. REPORT TYPE AND DATES COVERED Master's Thesis
4. TITLE AND SUBTITLE The Role of the Planetary Beta Effect on Currents and Meddies in the Northern Canary Current System				5. FUNDING NUMBERS
6. AUTHOR(S) Murray, Patrick J.				
7. PERFORMING ORGANIZATION NAME(S) AND ADDRESS(ES) Naval Postgraduate School Monterey, CA 93943-5000				8. PERFORMING ORGANIZATION REPORT NUMBER
9. SPONSORING / MONITORING AGENCY NAME(S) AND ADDRESS(ES)				10. SPONSORING / MONITORING AGENCY REPORT NUMBER
11. SUPPLEMENTARY NOTES The views expressed in this thesis are those of the author and do not reflect the official policy or position of the Department of Defense or the U.S. Government.				
12a. DISTRIBUTION / AVAILABILITY STATEMENT Approved for public release; distribution is unlimited.				12b. DISTRIBUTION CODE
13. ABSTRACT (maximum 200 words) To investigate the role of planetary beta on classical as well as unique features in the northern Canary Current System (NCCS), four numerical experiments are conducted with varying Coriolis parameterizations (f -plane or β -plane). The first two experiments use a closed boundary and annual salinity forcing for the Mediterranean Outflow (MO). The latter two experiments use an open Mediterranean Sea at the Strait of Gibraltar and seasonal forcing for MO to permit a more accurate investigation of the role of the beta effect on subsurface spreading of MO and Meddies. All four experiments use seasonal climatological winds and seasonal thermohaline gradients along the western boundary to force the model. Experiments run on a β -plane (Experiments 2 and 4) accurately portray classical eastern boundary current (EBC) mesoscale features. In addition, these experiments depict unique NCCS features associated with a large embayment (the Gulf of Cadiz), poleward spreading of MO, and the generation of Meddies. Experiments run on an f -plane (Experiments 1 and 3) show the unrealistic dominance of a continuously strengthening equatorward jet that inhibits development of classical EBC and unique NCCS features. The complex upper layer and subsurface flow regimes of Experiment 4 most realistically portray currents, mesoscale features and Meddies similar to NCCS observations.				
14. SUBJECT TERMS Primitive equation model, California Current System, currents, meanders, eddies, filaments, Columbia River plume				15. NUMBER OF PAGES 115
				16. PRICE CODE
17. SECURITY CLASSIFICATION OF REPORT Unclassified	18. SECURITY CLASSIFICATION OF THIS PAGE Unclassified	19. SECURITY CLASSIFICATION OF ABSTRACT Unclassified		20. LIMITATION OF ABSTRACT UL

Approved for public release; distribution is unlimited

**THE ROLE OF THE PLANETARY BETA EFFECT ON CURRENTS AND
MEDDIES IN THE NORTHERN CANARY CURRENT SYSTEM**

Patrick J. Murray
Lieutenant Commander, United States Navy
B.S., United States Naval Academy, 1988

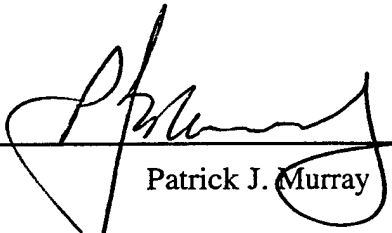
Submitted in partial fulfillment of the
requirements for the degree of

**MASTER OF SCIENCE IN METEOROLOGY AND PHYSICAL
OCEANOGRAPHY**

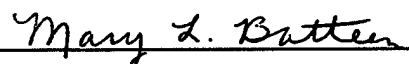
from the


**NAVAL POSTGRADUATE SCHOOL
June 2000**

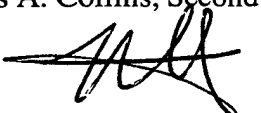
Author:


Patrick J. Murray

Approved by:


Mary L. Batteen, Thesis Advisor


Curtis A. Collins, Second Reader


Roland W. Garwood, Chairman
Department of Oceanography

ABSTRACT

To investigate the role of planetary beta on classical as well as unique features in the northern Canary Current System (NCCS), four numerical experiments are conducted with varying Coriolis parameterizations (f -plane or β -plane). The first two experiments use a closed boundary and annual salinity forcing for the Mediterranean Outflow (MO). The latter two experiments use an open Mediterranean Sea at the Strait of Gibraltar and seasonal forcing for MO to permit a more accurate investigation of the role of the beta effect on subsurface spreading of MO and Meddies. All four experiments use seasonal climatological winds and seasonal thermohaline gradients along the western boundary to force the model. Experiments run on a β -plane (Experiments 2 and 4) accurately portray classical eastern boundary current (EBC) mesoscale features. In addition, these experiments depict unique NCCS features associated with a large embayment (the Gulf of Cadiz), poleward spreading of MO, and the generation of Meddies. Experiments run on an f -plane (Experiments 1 and 3) show the unrealistic dominance of a continuously strengthening equatorward jet that inhibits development of classical EBC and unique NCCS features. The complex upper layer and subsurface flow regimes of Experiment 4 most realistically portray currents, mesoscale features and Meddies similar to NCCS observations.

TABLE OF CONTENTS

I. INTRODUCTION.....	1
II. MODEL DESCRIPTION	9
A. MODEL EQUATIONS	9
B. FORCING CONDITIONS AND EXPERIMENTAL DESIGN.....	12
III. RESULTS FROM MODEL SIMULATIONS.....	15
A. EXPERIMENT 1.....	15
1. Spin-up Phase.....	15
2. Quasi-equilibrium Phase	17
3. Discussion	19
B. EXPERIMENT 2.....	21
1. Spin-up Phase.....	21
2. Quasi-equilibrium Phase	24
3. Discussion	26
C. COMPARISON WITH OBSERVATIONS	30
IV. SUMMARY	33
LIST OF REFERENCES	93
INITIAL DISTRIBUTION LIST.....	97

LIST OF FIGURES

1. The model domain for the northern Canary Current System (NCCS) is bounded by 30°N to 42.5°N, 5°W to 17.5°W. The cross-shore (alongshore) resolution is 9 km (11 km). Geographical locations and prominent features are labeled. Model domain in (a) has a closed boundary along the entire coast, and in (b) has been modified at 5 grid points at the eastern boundary to open the Mediterranean Sea at the Strait of Gibraltar..... 37
2. Climatological (1980-1989) ECMWF winds in m/s for: (a) December, (b) February, (c) April, (d) August, and (e) October. Maximum wind vector is 8 m/s..... 39
3. Plot of Levitus climatological fields used as seasonal forcing along the western boundary (17.5°W) at 42.5°N (top) and 30°N (bottom) for (a) temperature and (b) salinity.....44
4. Salinities for Mediterranean Outflow (MO) used as seasonal forcing at the Strait of Gibraltar (from Levitus et al., 1994).....46
5. Experiment 1 plots of (a) temperature contours and velocity vectors at 10 m depth on day 27, (b) velocity vectors at 10 m depth on day 267, (c) cross-shore section of meridional velocity (v) at 35.3°N on day 330, and (d) temperature contours and velocity vectors at 10 m depth on day 216. Contour interval is 1°C in (a) and (d), and 10 cm/s in (c). Equatorward (poleward) flow is denoted by dashed (solid) lines in (c). Maximum velocity vector is 100 cm/s in (a), (b) and (d). To avoid clutter, velocity vectors are plotted every third gridpoint in the cross-shore direction in (a), (b), and (d), every third gridpoint in the alongshore direction in (a) and (b), and every fourth gridpoint in the alongshore direction in (d).....47
6. Cross-shore sections of meridional velocity (v) for Experiment 1 at (a) 37.3°N on day 231, and (b) 41.5°N on day 357. Contour interval is 10 cm/s for equatorward flow (dashed lines) in (a) and (b), with an additional 5 cm/s contour added in (b), 2 cm/s for poleward flow (solid lines) in (a), and 5 cm/s for poleward flow in (b).....51
7. Cross-shore section of salinity for Experiment 1 at 37.1°N on day 273. The contour interval for salinity is 0.01 (0.02) above (below) 35.69 values.....53
8. Horizontal maps of velocity vectors at 10 m depth for Experiment 1 on day (a) 519, (b) 561, and (c) 942. To avoid clutter, velocity vectors are plotted every third gridpoint in the cross-shore and alongshore directions. Maximum velocity vector is 100 cm/s.....54

9. Temperature contours and velocity vectors at 10 m depth for Experiment 1 on day 999. To avoid clutter, velocity vectors are plotted every fifth gridpoint in the cross-shore and alongshore directions. Contour interval is 1° C. Maximum velocity vector is 100 cm/s.....57
10. Cross-shore sections of meridional velocity (v) for Experiment 1 on day (a) 762 and (b) 1086. Contour interval is (a) 10 cm/s for equatorward flow (dashed lines) and 5 cm/s for poleward flow (solid lines), and (b) 10 cm/s for equatorward flow and 10 cm/s for poleward flow in (b).....58
11. Experiment 1 plots of (a) Cross-shore section of temperature at 39.3°N on day 828, and (b) Time-averaged plot of temperature contours and velocity vectors at 10m depth in the third year for October. The contour interval for temperature is 0.5°C in (a). In (b), to avoid clutter, velocity vectors are plotted every fifth gridpoint in the cross-shore and alongshore directions. Contour interval is 2° C. Maximum velocity vector is 100 cm/s.....60
12. Time-averaged plot of salinity contours and velocity vectors at 600 m depth for Experiment 1 in the third year for October. To avoid clutter, velocity vectors are plotted every sixth gridpoint in the cross-shore and alongshore directions. Contour interval is 0.04. Maximum velocity vector is 100cm/s.....62
13. Cross-shore section of salinity for Experiment 1 at 37.1°N on day 1002. The contour interval for salinity is 0.01 (0.02) above (below) 35.69 values.....63
14. Cross-shore section of meridional velocity (v) at 40.3°N for Experiment 2 on day 363. Contour interval is 10 cm/s for equatorward flow (dashed lines) and 2 cm/s for poleward flow (solid lines).....64
15. Temperature contours and velocity vectors at 10m depth for Experiment 2 on day 216. To avoid clutter, velocity vectors are plotted every third (fourth) gridpoint in the cross-shore (alongshore) direction. Contour interval is 1° C. Maximum velocity vector is 100 cm/s.....65
16. Cross-shore section of meridional velocity (v) at 37.3°N for Experiment 2 on day 210. Contour interval is 5 cm/s for equatorward flow (dashed lines) and 2 cm/s for poleward flow (solid lines).....66
17. Velocity vectors at 10 m depth for Experiment 2 on day 300. Velocity vectors are plotted every second gridpoint in the cross-shore and alongshore directions. Maximum velocity vector is 80 cm/s.....67

18. Experiment 2 plots of (a) velocity vectors at 1226 m depth on day 345, and (b) cross-shore section of salinity at 37.5°N on day 273. In (a), velocity vectors are plotted every second gridpoint in the cross-shore direction and at every gridpoint in the alongshore direction. Maximum velocity vector is 10 cm/s. In (b), the contour interval for salinity is 0.02 (0.03) above (below) 35.63 values.....68

19. Experiment 2 plots of (a) cross-shore section of meridional velocity (v) at 41.5°N on day 1089, (b) temperature contours and velocity vectors at 10 m depth on day 978, (c) Cross-shore section of meridional velocity (v) at 39.3°N on day 909, and (d) Cross-shore section of meridional velocity (v) at 32.3°N on day 816. In (a), contour interval is 5 cm/s for equatorward flow (dashed lines) and 5 cm/s for poleward flow (solid lines). In (b), velocity vectors are plotted every third gridpoint in the cross-shore and alongshore directions, contour interval is 1° C, and maximum velocity vector is 100 cm/s. In (c), contour interval is 10 cm/s for equatorward flow and 2.5 cm/s for poleward flow. In (d), contour interval is 10 cm/s for equatorward flow (with an additional 5 cm/s contour added) and 5 cm/s for poleward flow.....70

20. Horizontal maps at 10 m depth of average (a) mean kinetic energy (MKE) for Experiment 2 in the third year of the model simulation, (b) eddy kinetic energy (EKE) for Experiment 2, (c) mean kinetic energy (MKE) for Experiment 1, and (d) eddy kinetic energy (EKE) for Experiment 1. All plots are in the third year of the model simulation and time-averaged for July through September. Contour interval is 200 (cm/s)², in (a), (b), and (d), and 1000 (cm/s)² in (d).....74

21. Experiment 2 plots of (a) velocity vectors at 1226 m depth on day 1059, (b) cross-shore section of meridional velocity (v) at 35.5°N on day 1059, (c) cross-shore section of temperature at 35.5°N on day 1059, and (d) cross-shore section of salinity for at 35.5°N on day 1059. In (a), velocity vectors are plotted every second gridpoint in the cross-shore and alongshore directions. Maximum velocity vector is 20 cm/s. Meddies are labeled "A", "B", and "C". In (b), contour interval is 5 cm/s for equatorward flow (dashed lines) and 5 cm/s for poleward flow (solid lines). In (c), the contour interval for temperature is 0.2 °C. In (d), the contour interval is 0.01 (0.05) above (below) 35.66 (35.60) values.....78

22. Cross-shore section of salinity for Experiment 4 at 37.1°N on day 273. The contour interval for salinity is 0.01 (0.02) above (below) 35.63 (35.60) values.....82

23. Experiment 4 plots on day 1068 of (a) velocity vectors at 1226m depth, (b), cross-shore section of meridional velocity (v) at 37.7°N, (c) cross-shore section of temperature at 37.7°N, (d) cross-shore section of salinity at 37.7°N, and (e) temperature contours and velocity vectors 1226 m. In (a), velocity vectors are plotted every second gridpoint in the cross-shore and alongshore directions. Maximum velocity vector is 20 cm/s. Meddy "A" is labeled. In (b), the contour interval is 5

cm/s for equatorward flow (dashed lines) and 5 cm/s for poleward flow (solid lines). In (c), the contour interval for temperature is 0.2 °C. In (d), the contour interval for salinity is 0.01 (0.05) above (below) 35.63 (35.60) values. In (e), the contour interval for temperature is 0.2°C and the maximum current velocity is 20 cm/s.....83

LIST OF TABLES

Summary of Batteen (1989) specific experimental design.....	89
Summary of Batteen (1997) specific experimental design.....	89
Summary of Batteen(2000) specific experimental design.....	89
Summary of specific experimental design in this study.....	89
Values of constants used in the model.....	90
Annual salinity profiles for MO.....	91

ACKNOWLEDGEMENT

Dr. Mary Batteen, my advisor, generously provided outstanding professional guidance and instruction throughout the entire research process. I thank her for exceptional professional advice, patience, and support - all of which were essential in the completion of this study. Additionally, the constructive advice provided by Dr. Curtis Collins, as second reader, was greatly appreciated.

This study would have not been accomplished without the technical expertise of several individuals including, Frank Schenk, Donna Burych, Arlene Guest, and Eldor Magat. I am thankful for their support and assistance with the numerous technical issues surrounding the accomplishment of this study.

Above all, I would like to thank my family. The patience, flexibility, and encouragement of my wife Stacey and young son Jack were a wonderful comfort. Without their love and support, I could not have finished. Also, I would like to thank my parents for teaching me the importance of a well-rounded education. Thanks to all!

I. INTRODUCTION

The Canary Current System (CCS) on the eastern boundary of the central North Atlantic is a classical eastern boundary current (EBC) system. Stretching from $\sim 10^{\circ}\text{N}$ to $\sim 45^{\circ}\text{N}$ along the coasts of northwest Africa and the Iberian Peninsula (IP), it marks the closing eastern boundary of the North Atlantic Gyre. Typical of other EBCs, the mean equatorward Canary Current (CC), is a broad (~ 1000 km), relatively slow (~ 10 - 30 cm/s), yearlong surface flow extending to depths of ~ 500 m (Wooster *et al.*, 1976). The portion of the CC that stretches along the coast of the IP is often referred to as the Portugal Current (e.g., Tomczak and Godfrey, 1994).

As in other EBCs, a poleward undercurrent exists near the coast beneath the CC (e.g., Meincke *et al.*, 1975; Fiuza, 1980) as a relatively narrow (~ 10 - 40 km) and weak (~ 2 - 10 cm/s) flow, which is strongest between ~ 100 and ~ 600 m depth. The depth and strength of the undercurrent varies seasonally and latitudinally. In winter it shoals to the north near Cabo da Roca (see Figures 1a and 1b for geographic locations, and Figure 22.1 of Barton, 1998 for bathymetric contours and coastline geometry for the region), and forms a third flow component commonly referred to as the Iberian Current (IC) (Haynes and Barton, 1990). A narrow (25 - 40 km), relatively weak (~ 20 - 30 cm/s), seasonal surface current, the IC is found trapped near the coast against the shelf break (Fiuza, 1980; Frouin *et al.*, 1990; Haynes and Barton, 1990) and can occasionally be seen as far south as Cabo de Sao Vicente (Batteen *et al.*, 2000).

A unique feature that distinguishes the CCS from other EBCs is the existence of Mediterranean Outflow (MO) through the Strait of Gibraltar into the adjacent Gulf of Cadiz. A large embayment, the Gulf of Cadiz's pronounced east-west coastline orientation results in weaker upwelling in the Gulf of Cadiz than to the north or south of the Gulf of Cadiz, due to the dominant equatorward trade wind direction. The Gulf of Cadiz also creates a large separation between the two west coast upwelling regimes so that no continuous flow between the two appears to exist (Barton, 1998).

The salty MO plume that exits the Mediterranean Sea through the Strait of Gibraltar is diluted, thickens, and becomes vertically differentiated into two distinct cores as it flows westward into the Gulf of Cadiz (Iorga and Lozier, 1999). At $\sim 7^{\circ}\text{W}$ in the Gulf of Cadiz, both a shallow core at depths of $\sim 600\text{-}900\text{ m}$ and a deeper core at $\sim 1100\text{-}1200\text{ m}$ exist. Both cores continue to flow westward along the southern coast of Spain and turn poleward around Cabo de Sao Vicente (Amber and Howe, 1979; Iorga and Lozier, 1999). A third, shallower, poleward core of Mediterranean water has also been traced from the Strait of Gibraltar northward to $\sim 38.5^{\circ}\text{N}$ off western Portugal (Amber, 1982). In addition, a climatological cyclonic circulation in the southwestern Gulf of Cadiz acts to spread salty MO south of $\sim 34^{\circ}\text{N}$ (Iorga and Lozier, 1999).

The northern CCS (NCCS) is influenced predominantly by equatorward, upwelling favorable winds produced by the eastern half of the Azores High. Located in the northeastern part of the Atlantic Ocean, the Azores High is a semi-permanent subtropical high pressure system similar in nature and behavior to the North Pacific Subtropical High (Nelson, 1977). As such, the center of the Azores High migrates

meridionally with the seasons, reaching its southernmost extent near 27°N in March and ridging north to ~33°N by August. The building and migration of the Azores High cause wind stress values over the NCCS region to vary temporally, resulting in both alongshore and cross-shore variability of the predominantly equatorward winds along the west coast of the IP and the northwest coast of Africa. The east-west pressure contrast between Portugal and the center of the Azores High during summer is ~8 mb. In winter, this pressure gradient weakens to ~1 mb. As a result of this seasonally changing pressure gradient, considerably stronger northerly and northwesterly winds occur in the NCCS region in summer, while northerly and northwesterly winds become weaker to even slight southerly off the Iberian Peninsula in winter (Batteen *et al.*, 2000). The shift in maximum wind stress also causes upwelling favorable winds to shift from ~27°N near the Canary Islands in January, to ~43°N off Portugal by July (Fiuza, 1982).

Like other classical EBCs, observations of the sea surface in the NCCS region have shown highly energetic mesoscale features such as jet-like surface currents, meanders, eddies and filaments over the broad climatological mean flow of the CC. Satellite sea surface images have shown nearshore upwelling during periods of upwelling favorable winds with several narrow filaments of cooler water extending off the coast of the Iberian Peninsula (Fiuza and Sousa, 1989) and Cape Ghir in northwest Africa (Van Camp *et al.*, 1991; Hagen *et al.*, 1996). In these images, upwelling filaments often extend ~80-150 km offshore, with alongshore spacing of ~80-100 km between filaments (Haynes *et al.*, 1993), and often terminate with dipole eddy pairs (Fiuza *et al.*, 1982; Barton, 1998). Observations have also shown anticyclonic and cyclonic pairs of

mesoscale eddies on the order of 100 km off the IP coast (Fiuza, 1984; Stammer *et al.*, 1991). These mesoscale features have been observed during periods of predominantly upwelling favorable winds and appear to be located near prominent coastline irregularities such as capes. These observations provide evidence that wind forcing along coastline irregularities appear to be important mechanisms in the formation and sustainment of many of the mesoscale features found in the NCCS domain and other EBC regions (Batteen *et al.*, 2000).

Unique to the NCCS is the generation of anticyclonic submesoscale coherent vortices (SCVs) or Meddies. Numerical studies suggest that baroclinic instability of the northward dense plume of salty MO along the IP continental slope leads to the generation of Meddies (Kase *et al.*, 1989). As a result of numerous observations over the past decade, the primary generation region of Meddies is widely accepted to be near Cabo de Sao Vincente, off southwest Portugal. Several different trajectories of Meddies have been observed, including a southwestward movement into the Canary Basin, and westward translations south of the Azores (Richardson and Tychensky, 1998).

Over the last two decades numerous modeling studies have focused on the driving mechanisms of complex mesoscale activities in EBC regions, including upwelling filaments, highly energetic eddies, and meandering jets. For the California Current System, the classical EBC system, Ikeda *et al.* (1984a, b) and Haidvogel *et al.* (1991) studied baroclinic instability, coastline irregularities, and bottom topography as possible mechanisms, while Batteen *et al.* (1989), McCreary *et al.* (1991), Pares-Sierra *et al.*

(1993), Batteen (1997) and Batteen *et al.* (2000) studied wind forcing as a possible generation mechanism.

For over a decade, a high resolution, multi-level, primitive equation model has been used to examine the response to wind forcing of an idealized flat-bottomed oceanic regime along different eastern ocean boundaries (e.g., Batteen, 1989; Batteen, 1997, Batteen *et al.*, 2000). Results from sensitivity studies have produced various results depending on the type of wind forcing, coastline geometry and Coriolis parameterization used. A summary of experimental design for each of these studies is contained in Tables 1, 2 and 3.

For the California Current System, Batteen (1989) used a band of steady alongshore, upwelling favorable winds, either with or without alongshore variability, as forcing on both an f -plane and β -plane (see Table 1). This study was conducted using a straight California coast only. Eddies and jets with strong onshore and offshore directed flows were generated, along with a coastal jet and undercurrent on a scale and magnitude consistent with available observed data. The results supported the hypothesis that alongshore varying wind forcing on a β -plane is an important generation mechanism for eddies in the California Current System.

For the California Current System, Batteen (1997) forced the model from rest using seasonal climatological winds along a straight California coast on both an f -plane and β -plane (see Table 2). This study also included seasonal climatological wind forcing on an irregular coastline using β -plane only and focused on the role of the beta effect in generating, evolving and maintaining classical mesoscale features in the California

Current System. The results of this study showed that a surface equatorward current, upwelling of cooler water along the coast, and a poleward undercurrent develop in response to the prevailing wind direction. In addition, baroclinic and barotropic instabilities develop in the equatorward surface current and poleward flow, resulting in the generation of meanders near the coast, upwelling filaments extending offshore, and the subsequent development of seasonal or semi-permanent cyclonic and anticyclonic eddies farther offshore. While the meridional variability of f (β -plane) and variability in the equatorward component of wind stress were shown to be necessary ingredients for generating realistic vertical and horizontal structures for the cores of the surface equatorward and subsurface poleward currents, irregularities in the coastline geometry were shown to be important for “anchoring” upwelling and filaments, and for enhancing the growth of meanders and eddies. The results from several numerical experiments in this process-oriented study supported the hypothesis that wind forcing and coastline irregularities on a β -plane are important mechanisms for generation of observed mesoscale features of the California Current System (Batteen, 1997).

In a more recent study Batteen *et al.*, (2000) used the results of four numerical experiments of increasing complexity to investigate the unique and classical features of the NCCS (see Table 3). All four experiments were run on a β -plane. Experiment 1 included seasonal wind forcing on a straight coast, while Experiments 2 and 3 added the effects of irregular coastline geometry to the seasonal wind forcing. The most complex experiment, Experiment 4, added the effects of both thermohaline gradients and annual MO to the seasonal wind forcing and irregular coastline geometry. Consistent with

previous studies, wind forcing was shown to be a key generative mechanism for EBC mesoscale features, while capes were shown to be key areas for enhanced upwelling, extensive filaments, maximum current velocities and enhanced growth of cyclonic meanders and eddies. Unique features of the NCCS, including the development of anticyclonic meanders and eddies in an embayment like the Gulf of Cadiz and the generation of Meddies from MO, were also highlighted (Batteen *et al.*, 2000).

The objective of this study is to build on previous studies and to isolate the dependence of Coriolis parameterization (β -plane vs. f -plane) on classical as well as unique mesoscale features in the NCCS. Specifically, the generation, evolution, and maintenance of currents, meanders, eddies, filaments, MO, and Meddies is studied. The results of several numerical experiments (see Table 4) using a high-resolution, multi-level PE model are explored. In all experiments, irregular coastline geometry is used and the model is forced using seasonal climatological winds with both alongshore and cross-shore variability. In addition, each experiment includes the effects of thermohaline forcing on the western boundary and either annual or seasonal salinity forcing of MO. Experiments 1 and 2 are forced using annual values of salinity near the Strait of Gibraltar to include the effects of MO on the NCCS. In both experiments, the eastern Gulf of Cadiz exists as a closed boundary. Experiment 1 introduces the effect of running the model on an f -plane for the NCCS. Experiment 2 is the same as Experiment 1 except the model is run on a β -plane. The results of Experiment 2 are compared to the results of Experiment 1 to explore the role of the planetary beta effect on the NCCS. In order to more realistically examine the effects of MO on the NCCS, Experiments 3 and 4 are

forced using seasonal values of salinity for the MO. In addition, the Strait of Gibraltar is opened up to allow for the free exchange of water in and out of the Mediterranean Sea. Experiment 3 investigates the effect of MO when the model is run on an f -plane, while Experiment 4 is the same as Experiment 3 except the model is run on a β -plane. The results of Experiment 4 are compared to the results of Experiment 3 to explore the role of planetary beta effect on MO and Meddies in the NCCS. The results of Experiment 4, the most realistic experiment, are also compared to observations of surface and sub-surface mesoscale activities in the NCCS.

This study is organized as follows. In Chapter II we describe the numerical model and the specific experimental conditions. The results of the numerical experiments are presented in Chapter III along with a comparison with observations. A summary is presented in Chapter IV.

II. MODEL DESCRIPTION

A. MODEL EQUATIONS

This study uses the eddy-resolving, limited-area EBC model of Batteen (1997) with open northern, western, and southern boundaries. Additionally, for this study, the model has been adapted to have an open eastern boundary for the Strait of Gibraltar.

The model is multi-level, uses non-adiabatic primitive equations on a β -plane or f -plane, and has both baroclinic and barotropic velocity components. It is based on the hydrostatic, Boussinesq, and rigid lid approximations. Equations governing the model are as follows:

$$\frac{du}{dt} = \frac{-1}{\rho_0} \frac{\partial p}{\partial x} + fv - A_M \nabla^4 u + K_M \frac{\partial^2 u}{\partial z^2} \quad (1)$$

$$\frac{dv}{dt} = \frac{-1}{\rho_0} \frac{\partial p}{\partial y} - fu - A_M \nabla^4 v + K_M \frac{\partial^2 v}{\partial z^2} \quad (2)$$

$$\frac{\partial u}{\partial x} + \frac{\partial v}{\partial y} + \frac{\partial w}{\partial z} = 0 \quad (3)$$

$$\frac{\partial p}{\partial z} = -\rho g \quad (4)$$

$$\rho = \rho_0 [1 - \alpha(T - T_0) + \beta(S - S_0)] \quad (5)$$

$$\frac{dT}{dt} = -A_H \nabla^4 T + K_H \frac{\partial^2 T}{\partial z^2} \quad (6)$$

$$\frac{dS}{dt} = -A_H \nabla^4 S + K_H \frac{\partial^2 S}{\partial z^2} \quad (7)$$

In the above equations, t is time, T is temperature, S is salinity, ρ is density, and p is pressure. A right-handed Cartesian coordinate system (x,y,z) is used where x points toward shore, y alongshore, and z upward. The corresponding velocity components are (u,v,w) . Table 5 provides a list of symbols found in the model equations, as well as values of constants used throughout the study.

A space-staggered B-scheme (Arakawa and Lamb, 1977) is used for the horizontal finite differencing. Batteen and Han (1981) have shown this scheme to be appropriate when the grid spacing is approximately on the same order as, or less than, the Rossby radius of deformation. The horizontal grid spacing is 9 km in the east-west direction and 11 km in the north-south direction, while the internal Rossby radius of deformation is ~30 km, as determined by Feliks (1985). The model uses ten vertical layers, with constant z -levels, at depths of 10, 30, 75, 150, 250, 400, 600, 1226, 2283, and 3656 m. This vertical spacing scheme of the model concentrates more layers above the thermocline, which is in the dynamically active portion of the ocean.

The model domain (Figure 1a) encompasses the west coasts of Iberia and Morocco, from 30° N to 42.5° N (1408 km alongshore), and from 5° W to 17.5° W (1152 km cross-shore). The coastal boundaries of the model domain are closed for the first two experiments (e.g., see Figure 1a) and then opened at the Mediterranean for the second two experiments (e.g., see Figure 1b). Where closed, the coastal boundaries have both the tangential and normal components of velocity set to zero. Bottom topography has been omitted to focus on the roles of climatological wind forcing, thermohaline gradients, Coriolis parameterization, and the MO. The eastern boundary is modeled a vertical wall

(Figure 1a) or as an open boundary at the Strait of Gibraltar (Figure 1b) to account for more realistic exchange with the Mediterranean (Figure 1b). The constant depth used in the model is 4500 m.

The northern, southern, and western borders, as well as a portion of the eastern border in two experiments, are open boundaries, which use a modified version of the radiation boundary conditions of Camerlengo and O'Brien (1980). Biharmonic lateral heat and momentum diffusion is used in the model with the same choice of coefficients (i.e., $2.0 \times 10^{17} \text{ cm}^4/\text{s}$) as in Batteen (1997). Holland (1978) showed that highly scale-selective biharmonic diffusion acts predominantly on submesoscales, while Holland and Batteen (1986) found that baroclinic mesoscale processes could be damped by Laplacian lateral heat diffusion. As a result, the use of biharmonic lateral diffusion should allow mesoscale eddy generation via barotropic (horizontal shear) and/or baroclinic (vertical shear) instability mechanisms. Weak ($0.5 \text{ cm}^2/\text{s}$) vertical eddy viscosities and conductivities are also used. Bottom stress is parameterized by a simplified quadratic drag law (Weatherly, 1972), as in Batteen (1997).

The method of solution is straightforward with the rigid lid and flat bottom assumptions because the vertically integrated horizontal velocity is subsequently nondivergent. The vertical mean flow can be described by a streamfunction which can be predicted from the vorticity equation, while the vertical shear currents can be predicted after the vertical mean flow is subtracted from the original equations. The other variables, i.e. temperature, density, salinity, vertical velocity, and pressure, can be explicitly obtained from the thermodynamic energy equation (6), equation of state (5),

salinity equation (7), continuity equation (3), and hydrostatic equation (4), respectively (For more complete details on the method of solution, see Batteen, 1997).

B. FORCING CONDITIONS AND EXPERIMENTAL DESIGN

The model is forced from rest with climatological wind fields from a 2.5° by 2.5° grid of the European Centre for Medium Range Weather Forecasts (ECMWF) near-surface wind analyses (Trenberth *et al.*, 1990). The monthly mean stresses based on twice daily wind analyses from 1980-1989 have been interpolated spatially to the 9 by 11 km model resolution and temporally to daily wind values. Sample wind fields used can be seen in Figure 2, which shows the annual migration of the Azores Subtropical High from the south in the winter (e.g., Figure 2a) to its most northern extent in the summer (e.g., Figure 2d). The atmospheric pressure pattern for November (not shown) and December (Figure 2a) depicts a low to the north and the Azores High to the south. This results in a wind divergence with weakly poleward winds north of $\sim 40^\circ\text{N}$ and equatorward winds to the south. During January (not shown) and February (Figure 2b) the divergence in the wind field migrates poleward. By March (not shown) and April (Figure 2c) an equatorward component in the wind field is observed along the entire domain. The strongest equatorward winds are discernible from July (not shown) through August (Figure 2d). In September (not shown) and October (Figure 2e) the winds start to weaken throughout the domain, and divergence in the wind field is observed in the north by October (Figure 2e). By November (not shown) the wind divergence returns to $\sim 40^\circ\text{N}$.

Table 4 summarizes the design of the four experiments. Note that in all the experiments the model is forced from rest with seasonal ECMWF winds. The model is then allowed to reach a quasi-equilibrium state by running each experiment for three years.

In addition, in all the experiments, seasonal temperature and salinity climatological conditions for the upper seven levels from Levitus and Boyer (1994) and Levitus *et al.* (1994) are used to initialize the model, and every third day, to force the model at the western boundary at 17.5°W. The seasonal temperature and salinity-forcing conditions, which are initially assumed to be homogeneous, are shown for one of the seven levels in Figure 3 for the northern (42.5°N) and southern (30°N) boundaries of the model domain. Since the lower three levels do not exhibit much horizontal variation, they are assumed to be constant for each level. The temperature values used for levels 8-10 are 8.52°C, 3.59°C, and 2.09°C. The salinity used for the lower three levels is 34.7.

While the temperatures to the south are warmer than those to the north above 1000 m depth, only the upper level temperature conditions (e.g., Figure 3) show significant seasonal variability with a temperature maximum in September and a temperature minimum in February throughout the whole region. Below ~150m depth (not shown), both the seasonal temperature fluctuations and the temperature gradient weaken, as expected. In contrast, the salinity conditions above 1000 m (e.g., Figure 3), which in the upper levels show less (more) saline water to the north (south), have no significant seasonal cycle.

In Experiments 1 and 2, the effects of the MO on the NCCS are included while keeping the eastern coastal boundary closed (see Figure 1a). The salinity at each level for the MO is input as a constant (annual) value for five grid points at $\sim 36^\circ \text{N}$ every time step with the values given in Table 6 (from Levitus *et al*, 1994).

As Table 4 shows, Experiment 1 examines the response of seasonal wind forcing and the effects of thermohaline gradients on an irregular coastline when the model is run on an f -plane. To isolate the effects of planetary beta, Experiment 2 is run using the same initialization and forcing parameters as in Experiment 1, but on a β -plane.

To more realistically encompass the effects of MO on the NCCS, the eastern coastal boundary is opened at five grid points to mask the Strait of Gibraltar in Experiments 3 and 4 (see Figure 1b). Seasonal values of salinity are forced from the upper five levels for the MO every third day, while salinity values for the lower levels are input as a constant. The seasonal values forced from the upper five levels for one year are shown in Figure 4 (from Levitus *et al*, 1994).

Experiments 3 and 4 are run to isolate the effects of planetary beta on MO in the NCCS. Experiment 3 investigates the behavior of MO when the model is run on an f -plane, while Experiment 4 is run on a β -plane.

III. RESULTS FROM MODEL SIMULATIONS

A. EXPERIMENT 1 – EFFECTS OF f -PLANE ON IRREGULAR COASTLINE GEOMETRY

In Batteen (1989) and Batteen (1997), several experiments were run on an f -plane. In all experiments straight coastline geometry was used, while the model was forced using different types of wind stress. This experiment, Experiment 1, is also run on an f -plane but includes a realistic irregular coastline as well as being forced by seasonal climatological winds, thermohaline forcing at the western boundary, and annual salinities for MO.

1. Spin-up Phase

Initially, the combination of wind forcing and thermohaline gradients results in different oceanic responses depending on the season. As the temperature decreases poleward (Figure 3), there is an increase of density poleward, and the corresponding pressure gradient establishes an onshore geostrophic inflow from the ocean interior. In the winter (e.g. Figure 5a), in the poleward end of the model domain, the large pressure gradient and poleward wind stress result in onshore geostrophic and Ekman flow, and a coastal poleward surface current. Off Morocco, in the equatorward end of the model domain, the smaller pressure gradient and equatorward wind stress result in weak onshore geostrophic flow, offshore Ekman flow, and a coastal equatorward surface current.

The combined effects of an increase in equatorward winds along the entire coastal domain during the peak upwelling season (July through September) and a weakened pressure gradient, lead to substantial strengthening of equatorward flow. This flow remains close to the west coast of Iberia and Morocco and meanders in a slight anticyclonic manner as it bisects the Gulf of Cadiz (e.g. Figure 5b). A large quasi-permanent cyclonic eddy, extending to ~1000 m depth (e.g. Figure 5c), forms in the eastern half of the Gulf of Cadiz to the north and east of the anticyclonic equatorward flow (e.g. Figure 5b). The weakening (strengthening) of onshore (offshore) flow results in upwelled water replacing the coastal waters along the west coasts of Iberia and Africa. The coldest water is found near coastal promontories (e.g., off Cape Ghir and Cape Beddouzza in Figure 5d).

A typical cross-section (Figure 6a) of the currents shows a relatively strong coastal equatorward jet extending to ~1000 m depth. The surface current lies within ~30 km of the coast, and has core velocities of ~35-40 cm/s. There is a deep (~2800 m depth) poleward undercurrent, also within ~30 km of the coast, below the equatorward jet, with a core velocity of ~6 cm/s.

By fall, a typical cross-section of the currents in the poleward end of the model domain north of ~41°N (e.g. Figure 6b) shows that the equatorward coastal jet (~30 km from the coast) continues to maintain intensity, with core velocities of ~40 cm/s. In addition, at ~2200 m depth, the poleward undercurrent lies within ~30 km of the coast and has a core velocity of ~10 cm/s. Instead of the expected return of a surface poleward flow in the northern portion of the model domain in response to the return to poleward

wind stress in the region, the surface equatorward coastal jet continues to dominate the entire model domain from north to south.

A typical cross-section of salinity near Cabo de Sao Vicente (e.g. Figure 7) shows a salinity maximum ~ 35.71 at ~ 1200 m depth associated with annual forcing of salinity for MO. A salinity minimum of 35.53 , discernible at ~ 600 m depth, is associated with the equatorward coastal jet (not shown).

2. Quasi-equilibrium Phase

A continuation of the model run for Experiment 1 shows that the system has reached quasi-steady state by the end of year 2 (not shown). Using years 2 and 3 of the longer experimental run, the model shows further intensification of the coastal equatorward jet with time and no differences in oceanic responses based on the season. The cyclonic eddy in the Gulf of Cadiz migrates and is incorporated into the mean equatorward flow, while an anticyclonic eddy develops in its wake (e.g., Figure 8a). As the strength of the equatorward jet increases, the anticyclonic meander of the equatorward flow seen earlier is replaced by a more north-south orientated flow (Figure 8b). During years 2 and 3, there are periodic events in which the anticyclonic eddy in the Gulf of Cadiz is forced south by the equatorward jet out of the Gulf and into the mean equatorward flow of the jet. During each of these instances, a new anticyclonic eddy forms in the same region of the Gulf of Cadiz as the anticyclonic eddy seen earlier (e.g. Figure 8c).

In summer, (e.g. Figure 9), upwelling is visible along the west coast of Iberia and along the coast of Morocco, reaching a maximum in October. Areas of enhanced upwelling occur near prominent capes to the north (e.g., off Cabo da Roca in Figure 9) and off Morocco.

A typical cross-section of the currents during the fall and winter (e.g. Figure 10a) shows the strong coastal equatorward jet extending to ~1100 m depth. The surface current is within ~40 km of the coast and has core velocities of ~70-80 cm/s. The poleward undercurrent at ~2800 m depth is within ~70 km of the coast, with a core velocity in excess of ~10 cm/s. A typical cross section of currents in the poleward end of the model domain north of ~41°N (e.g., Figure 10b) shows a surface equatorward jet close to the shore instead of the expected surface poleward flow in response to the poleward wind stress.

A typical cross-section of temperature during year 3 (e.g. Figure 11a), shows temperature patterns consistent with upwelling between ~200 and ~1200 m depths in response to the continuous and deep equatorward jet. By year 3, the coastal jet acts as a thermal boundary, separating warm waters offshore of the equatorward jet from cooler waters along the coast and in the Gulf of Cadiz. For example, Figure 11b shows that a typical temperature for October west of the equatorward jet is ~22° C, while a typical temperature to the east of the jet is ~18° C (excluding coastal upwelling areas).

The coastal jet behaves as a similar boundary for salinity, separating fresher waters offshore of the equatorward jet from saltier waters along the coast and in the Gulf of Cadiz. For example, Figure 12 shows that a typical salinity for October, at 600 m

depth, west of the equatorward jet is less than ~ 35.55 while a typical salinity to the east of the jet is greater than ~ 35.65 . In addition, a typical cross-section of salinity off Cabo de Sao Vicente (e.g. Figure 13) shows a salinity maximum of ~ 35.71 , associated with annual salinity forcing for MO, inshore of the deep equatorward coastal jet at ~ 650 m depth, and a salinity minimum of ~ 35.53 offshore of the jet at around the same depth.

3. Discussion

Many of the results of this f -plane experiment for the NCCS are consistent with previous f -plane, seasonally wind-driven experiments (e.g., Batteen, 1989 and Batteen, 1997), which used straight coastline geometry for the California Current System. For example, in this experiment and in previous cases, the seasonal climatological wind field intensifies the surface equatorward current and deepens and weakens the poleward undercurrent. As a result, there are no strong vertical and horizontal shears in the upper layers between the surface equatorward and the subsurface poleward currents. Consequently, no meanders, filaments or eddies develop along the coast in the vicinity of the equatorward jet.

An exception to the lack of mesoscale activity occurs in the Gulf of Cadiz, which is a large embayment and a unique feature of the NCCS. The sharp angle in the coastline at Cabo de Sao Vicente, the large extent of the embayment, and the increasing momentum of the deep equatorward jet, cause the equatorward flow to bypass most of the Gulf of Cadiz. The Gulf of Cadiz becomes a spawning region for predominantly

anticyclonic mesoscale activity. (The cyclonic eddy that forms in the northeastern part of the Gulf of Cadiz (e.g., Figure 5b) can be attributed to the onshore pressure gradient and poleward flow that occurs before the equatorward jet intensifies.) The series of anticyclonic eddies that periodically develop before being caught up in the equatorward flow during the quasi-equilibrium phase are due to eastward (westward) flow along the northern (southern) coasts of the Gulf and equatorward flow on the west coast of the Gulf, resulting in formation of anticyclonic eddies in the Gulf of Cadiz (e.g. Figure 9c).

The widths of the coastal jet and undercurrent are approximately confined to within the first internal Rossby radius of deformation of the coast along Iberia and Morocco, in concurrence with the expected behavior of eastern boundary currents on an f -plane (Gill, 1982). This radius is ~ 30 km for the model domain, as calculated by the method of Feliks (1985). In addition, the equatorward coastal jet and poleward undercurrent development in Experiment 1 agree well with the f -plane wind forcing results of McCreary *et al.* (1987) and McCreary (1981).

Upwelling along the coast near the surface occurs during the classic upwelling season, but offshore flow of the cooler upwelled surface waters is limited, remaining inshore of the intense, non-meandering, coastal equatorward surface flow. The intensity of the equatorward flow at depth results in year-round upwelling of deep waters offshore, on the eastern side of the jet axis. A subsequent "cold-side" develops, encompassing all waters east of the equatorward jet.

As the seasons change, different oceanic responses do not occur after the initial stage of the spin-up phase due to the continuing strength of the equatorward jet. Surface

poleward flow in the northern end of the model domain does not return in winter, as expected in response to both poleward wind stress in the region and geostrophic inflow toward the coast from the ocean interior due to the offshore pressure gradient.

B. EXPERIMENT 2 – ROLE OF BETA-PLANE

In Experiment 2, the model was run on a β -plane with the same realistic irregular coastline, seasonal climatological winds, thermohaline forcing at the western boundary, and annual salinities for MO as in Experiment 1. The results of Experiment 2 isolate the important role that the beta effect plays, in the presence of seasonal climatological winds and thermohaline gradients, in setting-up more realistic coastal currents that subsequently become unstable.

1. Spin-up Phase

Different oceanic responses occur depending on the season. In winter, the large pressure gradient and poleward wind stress at the poleward end of the model domain result in onshore geostrophic and Ekman flow. As the flow approaches the coast, it turns and forms a poleward surface current. A typical cross-section of the currents in the poleward end of the model domain (e.g. Figure 14) shows that the poleward surface current exists within 100 km of the coast and has a subsurface core velocity of ~ 6 cm/s.

When the Azores High migrates north in the spring, the intensifying winds cause equatorward flow over the entire coastal domain. The weaker pressure gradient and stronger equatorward wind stress at the equatorward end of the model domain result in weak onshore geostrophic flow and strong offshore Ekman flow.

As expected, upwelling first occurs in the south where the stronger winds exist (not shown). In addition to the west coast of Morocco, upwelling is enhanced near prominent capes to the north on the west coast (e.g., off Cabo da Roca in Figure 15). In Experiment 1, the region of enhanced upwelling was confined to the south off Morocco (e.g., Figure 5d). A comparison of the temperatures of the coldest coastal waters during the peak upwelling season shows that the upwelled waters in Experiment 2 are $\sim 1\text{--}2^\circ\text{K}$ cooler than in the f -plane experiment (Experiment 1) (e.g., compare Figures 15 and 5d). In addition, the offshore extent of the upwelled waters at the surface is much wider in Experiment 2.

A typical cross-section (e.g., Figure 16) of the currents shows that there is a surface coastal equatorward jet that extends to ~ 180 m depth near the coast and ~ 800 m depth offshore. The surface current is within ~ 100 km of the coast and has core velocities of $\sim 20\text{--}25$ cm/s. Below the equatorward current is a subsurface poleward undercurrent within ~ 50 km of the coast which has a core velocity of ~ 5 cm/s at 1200m. In contrast to the results on an f -plane in Experiment 1, the core of the poleward undercurrent is shallower, while the core of the equatorward current has weaker velocities (e.g., compare Figures 16 and 6a).

In Experiment 1, there was no development of filaments and, except in the Gulf of Cadiz, there was also no mesoscale activity. In contrast, Experiment 2 shows the formation of meanders, eddies, and filaments developing along the realistic irregular coastline (e.g., see the presence of meanders and eddies in Figure 17). The meanders preferentially develop in the vicinity of capes which subsequently intensify to develop predominantly cold cyclonic core eddies, which in time coalesce with other cyclonic eddies to form larger cyclonic eddies on the order of ~100-300 km diameter.

In the fall, near the end of the upwelling season, (e.g., Figure 17), the equatorward surface flow has taken the form of a meandering jet embedded with predominantly cyclonic eddies. The meandering jet generally flows along the west coasts of Iberia and Morocco and traverses the perimeter of the Gulf of Cadiz. While the equatorward jet in Experiment 1 bisected the Gulf of Cadiz in an anticyclonic manner to the south and was associated with the development of a cyclonic eddy in the northern end of the Gulf of Cadiz, the meandering jet in Experiment 2 induces anticyclonic flow at the surface over the entire Gulf of Cadiz (e.g., compare Figure 17 of Experiment 2 with Figure 5b of Experiment 1).

Of particular note is the development of an anticyclonic eddy at ~1200 m depth off the southwestern coast of Portugal near the end of year 1 (e.g., Figure 18a). A cross-section of salinity at 37.50°N, in the vicinity of the anticyclonic eddy (e.g., Figure 18b) shows a salty core of ~ 35.73 psu at ~1200 m depth, which is associated with the subsurface poleward spreading of MO. The deep origin, salty signature, depth and anticyclonic rotation of the eddy west of Cabo de Sao Vicente, is consistent with

observations of Meddies in this region (e.g., Richardson and Tychensky, 1998). Maintaining its salty property, the anticyclonic eddy (Meddy) subsequently propagates to the west away from the coast (not shown) with speeds of ~ 2 km/day, consistent with available observations (e.g., Richardson and Tychensky, 1998). The development and subsequent westward propagation of this unique NCCS feature was not observed in the results on an f -plane (Experiment 1).

2. Quasi-equilibrium Phase

Longer run times (~ 3 years) of the model simulation show that many of the features associated with a classical eastern boundary current recur seasonally. For example, a surface poleward current develops during the winter in the northern end of the model domain (e.g., Figure 19a), upwelling of cooler waters along the coast extends offshore in the form of cyclonic eddies and narrow filaments (e.g., Figure 19b), and a subsurface poleward current beneath the meandering equatorward jet is maintained (e.g., Figure 19c). In addition, typical cross-sections of the surface equatorward and subsurface poleward currents along the coast (e.g., Figures 19c and 19d) show considerable horizontal and vertical shear in the upper layer currents.

To determine the type of instability that could generate the meander, eddy, and filament features, more detailed analysis was performed. Barotropic instability can result from horizontal shear in the currents, while baroclinic instability can result from vertical shear in the currents. Horizontal maps of the upper layer mean kinetic energy (MKE) and

eddy kinetic energy (EKE) are time averaged for each month during the upwelling season and are used to indicate locations of barotropic and baroclinic instability. Typical MKE and EKE results during the upwelling season (e.g., Figures 20a and 20b) show that high values of MKE and EKE are found all along the coastal and offshore axes of the meandering jet in the regions of eddy and filament development. (e.g., compare Figures 20a and 20b to Figure 19b). A comparison of Figures 20a and 20b shows that maximum values of MKE and EKE occur in the same region. This is consistent with the results of Batteen (1997), which showed that eddies are generated from instabilities of the mean equatorward current and the poleward undercurrent via barotropic and/or baroclinic instability processes. Similar horizontal maps of energetics for Experiment 1 (Figures 20c and 20d) show that high values of MKE or EKE are confined inshore of $\sim 12^\circ \text{W}$ due to the lack of offshore movement which the beta effect produces. This suggests that limited or no barotropic and/or baroclinic instabilities can exist when the model is run on an f -plane.

During year three, the Meddies generated earlier in the model run continue to propagate to the west and south at $\sim 2 \text{ km/day}$ (not shown). Figure 21a shows three Meddies labeled as "A", "B" and "C". The Meddies have deep-water origins at $\sim 1200 \text{ m}$ depth off southwest Portugal. Cross-sections of meridional velocity (Figure 21b) and temperature (Figure 21c) associated with Meddy "A" illustrate the anticyclonic rotation of the Meddy. The corresponding cross-section of salinity (Figure 21d) shows the relatively salty signature of the Meddy at $\sim 1200 \text{ m}$ depth which it retains as it propagates westward (e.g., see the high salinity cores at $\sim 11.5^\circ \text{W}$ and between 15°W and 16°W in

Figure 21d). Unlike Experiment 2, no Meddy development off Cabo de Sao Vincente was observed in Experiment 1. Also, no westward propagation of any anticyclonic or cyclonic eddies occurred in Experiment 1.

3. Discussion

To help illustrate the importance of Coriolis parameterization (specifically the role of planetary beta), in the presence of alongshore and cross-shore varying wind fields and thermohaline gradients, in developing realistic EBC and unique NCCS features, the following summary of Experiment 2 results is provided:

- Responsiveness to seasonal oceanic changes (e.g., development of a poleward surface current).
- Realistic locations, depths, and velocities of coastal currents.
- Realistic offshore extent of upwelling patterns with enhanced upwelling in the vicinity of capes.
- Upper layer barotropic and baroclinic instability.
- Typical EBC mesoscale activity (i.e. eddies, meandering jet, filaments).
- Poleward movement of MO, Meddy generation, and subsurface westward propagation of Meddies.

Since none of these features were present in the results of Experiment 1, it can be concluded that their existence is related to the beta effect.

The beta effect allows the existence of freely propagating planetary waves, i.e., Rossby waves (Gill, 1982). The offshore propagation of these waves contributes to the generation of an alongshore pressure gradient field, which aids the development of a realistic undercurrent along the eastern boundary. In addition, the offshore extent of the surface equatorward current (e.g., Figure 19c) was due to the beta effect. This is consistent with the results of McCreary *et al.*, 1987, which showed that, due to the beta effect, the surface coastal jet does not necessarily have to be confined to within a Rossby radius of deformation of the coast. As a result, the beta effect changes both the vertical and horizontal structures of the currents.

In particular, as the core of the undercurrent (which is initially beneath the equatorward jet) intensifies, it shoals and displaces the equatorward jet offshore (e.g., compare Figures 16 and 19c). Strong vertical and horizontal shears in the upper layers between the equatorward jet and the undercurrent result (e.g. see Figures 19c and 19d), and meanders, upwelling filaments, and eddies subsequently develop in the baroclinically and barotropically unstable coastal environment. Note that neither vertical nor horizontal shears existed between the deep and intense equatorward jet and the even deeper poleward undercurrent in Experiment 1 (*f*-plane). As a result, the equatorward jet was unmodified by the poleward subsurface flow, and no meanders, filaments nor eddies developed in Experiment 1.

The beta effect also played an important role in the unique development and westward propagation of Meddies from the MO in the NCCS. It is suggested that the Meddies are generated by the basic instability of the equatorward coastal jet and the

poleward undercurrent. The major difference between Meddies and the previously discussed eddies is that the Meddies are generated at depth rather than near the surface. The relatively salty MO core of the undercurrent below ~500 m depth, which makes water in the core saltier than water above or below it, could lead to a local baroclinic instability process, resulting in the generation of Meddies. This scenario is consistent with the results of Kase *et al.*, (1989), who observed eddies in the MO off Iberia similar to the Meddy off Cabo de Sao Vicente in Figure 18a and postulated that baroclinic instabilities generated by the undercurrent could lead to the generation of Meddies.

The development of the Meddy off Cabo de Sao Vicente in Figure 18a is also consistent with another Meddy generation theory. Pichevin and Nof (1996) suggested that a Meddy generation mechanism can occur when the MO curves back on itself west of Cabo de Sao Vicente producing a flow-force that cannot be balanced without growth and shedding of eddies. The beta effect plays an important role in the Meddy generation model of Pichevin and Nof (1996) because it arrests the growth of Meddies and removes them from their generation region. (In contrast, f -plane experiments by Pichevin and Nof (1996) develop a constantly growing coastal eddy at the tip of Cabo de Sao Vicente.)

In Experiment 2, the beta effect acted as a necessary force in promoting the generation and growth of Meddies and causing their removal from the source region. Generation and growth were promoted by local baroclinic instabilities in the MO and by the MO curving back on itself in a region of relatively weak coastal currents. Removal from the Cabo de Sao Vicente generation region was a result of the free offshore propagation of planetary waves, in the vicinity of the relatively benign coastal currents.

In contrast to both Experiment 2 and the f -plane experiment of Pichevin and Nof (1996), Meddy generation was not simulated in Experiment 1 due to the domination of the intense equatorward jet through the potential Meddy generation region. In addition, the waters with a salty MO signature in Experiment 1, instead of freely propagating offshore, were confined to the Gulf of Cadiz and the narrow region between the equatorward jet and west facing coastlines (e.g., see Figure 12).

To more realistically investigate the effects of MO on the NCCS, two additional experiments (Experiments 3 and 4) were run using seasonal values of salinity for the MO (see Figure 4). In addition, the Strait of Gibraltar was opened (see Figure 1b) to allow for the free exchange of water with the Mediterranean Sea.

Results for the f -plane case (Experiment 3), showed similar effects as the f -plane case (Experiment 1), i.e., the intense equatorward jet dominated the entire NCCS region and stifled the development of upper layer mesoscale activity and Meddies. Experiment 4, run on a β -plane, also produced results similar to the β -plane case (Experiment 2) in the upper layers. Since it more realistically incorporated the influences of MO at depth along with the realistic opening of the Strait of Gibraltar, it will be compared with observations.

C. COMPARISON WITH OBSERVATIONS

It is useful to qualitatively compare Experiment 4 model simulation results with observational data because, of all the experiments, it most realistically depicts the classical and unique features of the NCCS. Since this experiment is an idealized process-oriented study and not a model hindcast, we cannot make direct comparisons with data; however we can investigate whether the phenomenological model behavior is qualitatively similar to observational data in the NCCS. Overall, the model behavior of this experiment's complex flow regime highlights the mesoscale features of the NCCS with relatively close similarities to field observations in both the upper and lower layers.

In previous studies, major EBC features produced by the PE model were similar to observations of mesoscale activity in the upper layers (e.g. see Batteen, 2000). In similar fashion, Experiment 4 captures these classical EBC features. The mean equatorward surface flow of ~10-30 cm/s throughout the model domain is consistent with Wooster and Reid (1963) and observations by DMAH/TC (1988). The poleward flow along Iberia developed in the model is in conformity with hydrographic survey data from 1986 (Haynes and Barton, 1990), and the poleward surface flow depicted in the model is in accord with infrared satellite images and in situ hydrographic data from Frouin *et al.*, (1990).

The upwelling patterns and cold filaments in Experiment 4 were consistent with high resolution satellite SST observations of these features off Cape Ghir, Cape Beddouzza and southwestern Portugal (e.g., Van Camp *et al.*, 1991), and off western

Portugal (Foulkard *et al.*, 1997). In addition, the results of Experiment 4 show termination of filaments in cyclonic and anticyclonic pairs of eddies as observed in satellite observations (e.g., Van Camp *et al.*, 1991 and Hagen *et al.*, 1996).

In the lower layers, the behavior of MO as it flows along the southern coast of Iberia in the Gulf of Cadiz and around Cabo de Sao Vicente in two distinct cores is well documented (e.g. Ambar and Howe, 1979; Ambar, 1982; Fiuza, 1982; Zenk and Armi, 1990; Iorga and Lozier, 1999). CTD stations near Cabo de Sao Vicente by Daniault *et al.*, (1994) show upper core and lower core high salinity maxima and support this two core phenomenon. Typical cross-sections of salinity in Experiment 4 near Cabo de Sao Vicente show similar high salinity values associated with the poleward and westward spreading of MO at ~800 and ~1200 m depth (e.g., Figure 22). In addition, typical cross-sections of salinity throughout the model domain are relatively consistent with the assembled database of the North Atlantic Ocean from the National Ocean Data Center by Lozier *et al.* (1995) that traces the salinity signature of MO throughout the NCCS region.

In Experiment 4, the salty characteristics and structure of Meddy "A" in Figures 23a through 23e are consistent with recent observations of Meddies in the Canary Basin (e.g. Prater and Sanford, 1994; Richardson and Tychensky, 1998; Stammer *et al.*, 1991). Rotation speeds of between ~10-20 cm/s (e.g., Figures 23a, 23b, and 23e) and the elliptical orientation along a northeast to southwest line in the lower part of the Meddy (e.g., Figure 23e) are consistent with observations by Prater and Sanford (1994). Propagation speeds and propagation paths of Meddies in Experiment 4 agree with observations by Richardson and Tychensky (1998). Anticyclonic motion near the surface

above Meddy "A" in Experiment 4 (not shown) is in agreement with observations of Meddies made by Stammer *et al.* (1991) which compared a Geosat signal with the hydrographic survey data of Kase *et al.* (1989) in the NCCS region.

In the model simulations, the influences of the beta effect and the associated offshore movement of planetary Rossby waves resulted in accurate depiction of observed mesoscale features of the NCCS. Using Geosat altimeter data, Tokmakian and Chancellor (1993) observed baroclinic Rossby waves between $\sim 30^{\circ}\text{N}$ and 40°N in the vicinity of the NCCS that appeared to originate off the African coast.

IV. SUMMARY

The objective of this study was to use a multilevel PE model to investigate the role of planetary beta on classical as well as unique features in the predominantly wind-driven NCCS. Toward this end, four numerical experiments were run with varying Coriolis parameterizations (f -plane or β -plane). The first two experiments used a closed boundary and annual salinity forcing for MO. The latter two experiments used an open Mediterranean Sea at the Strait of Gibraltar and seasonal salinity forcing for MO to permit a more accurate investigation of the role of the beta effect on subsurface spreading of MO and Meddies.

In a similar fashion to classical EBC systems, both experiments run on a β -plane (Experiments 2 and 4) produced an offshore surface equatorward meandering jet, realistic surface and subsurface poleward currents, upwelling, meanders, eddies, and filaments. In addition, these experiments depicted unique NCCS features including geographical separation of the of the Gulf of Cadiz region from the west coast upwelling regimes, anticyclonic mesoscale activity in the upper layers of the Gulf of Cadiz, poleward spreading of MO, and the development and propagation of Meddies from the Cabo de Sao Vicente generation region.

To isolate the role of the beta effect, the results of the f -plane runs (Experiments 1 and 3) were compared to the β -plane runs (Experiments 2 and 4). Results on an f -plane showed the occurrence of coastal upwelling and the eventual appearance of anticyclonic mesoscale activity in the Gulf of Cadiz, but the continuously strengthening equatorward

jet prevented other classical mesoscale features associated with upwelling systems from occurring. Specifically, upwelling was confined to the immediate coastal regions, a seasonal surface poleward current did not occur in the north, the subsurface poleward flow was forced to great depths, barotropic and baroclinic instabilities were relatively non-existent, and meanders, filaments, and eddies did not develop. At depth, the deep equatorward jet prevented unique NCCS features from occurring, including the typical westward and poleward spreading of MO and the development of Meddies. In addition, cold upwelled water and salty MO were restricted to the region east of the equatorward jet and in the Gulf of Cadiz.

The additional effects of seasonally forcing MO and opening the eastern boundary at the Strait of Gibraltar in Experiment 4 more realistically depicted the poleward spreading of MO and produced sub-mesoscale coherent vortices (SCVs) off Cabo de Sao Vicente with more typical Meddy characteristics. Specifically, Meddies in Experiment 4 were shed regularly from the classic generation region (in numbers consistent with available observations), and with rotation velocities, high salinities, and temperature patterns consistent with various Meddy observations.

Meddies produced near Cabo de Sao Vicente in the β -plane experiments supported recent theories on Meddy generation. In particular, the generation mechanisms of Meddies appeared to be due to baroclinic instabilities in the undercurrent (saltier MO cores than the water above or below) as suggested by Kase *et al.*, 1989. In addition, the Meddies also appeared to be generated due to the curvature of the MO back on itself (i.e.,

the flow force could not be balanced without generating and shedding anticyclonic eddies), as suggested by Pichevin and Nof (1996).

A comparison of currents, upwelling, meanders, eddies, jets, filaments, MO, and Meddies generated by the model in Experiment 4 with available observations showed that the model successfully simulated the location, size, and velocity of these features when run on a β -plane. In particular, the β -plane results of the complex upper layer and subsurface flow regimes of Experiment 4 showed that the incorporation of the beta effect resulted in an accurate depiction of observed mesoscale activity, and highlighted major classical EBC and unique NCCS mesoscale features.

THIS PAGE INTENTIONALLY LEFT BLANK

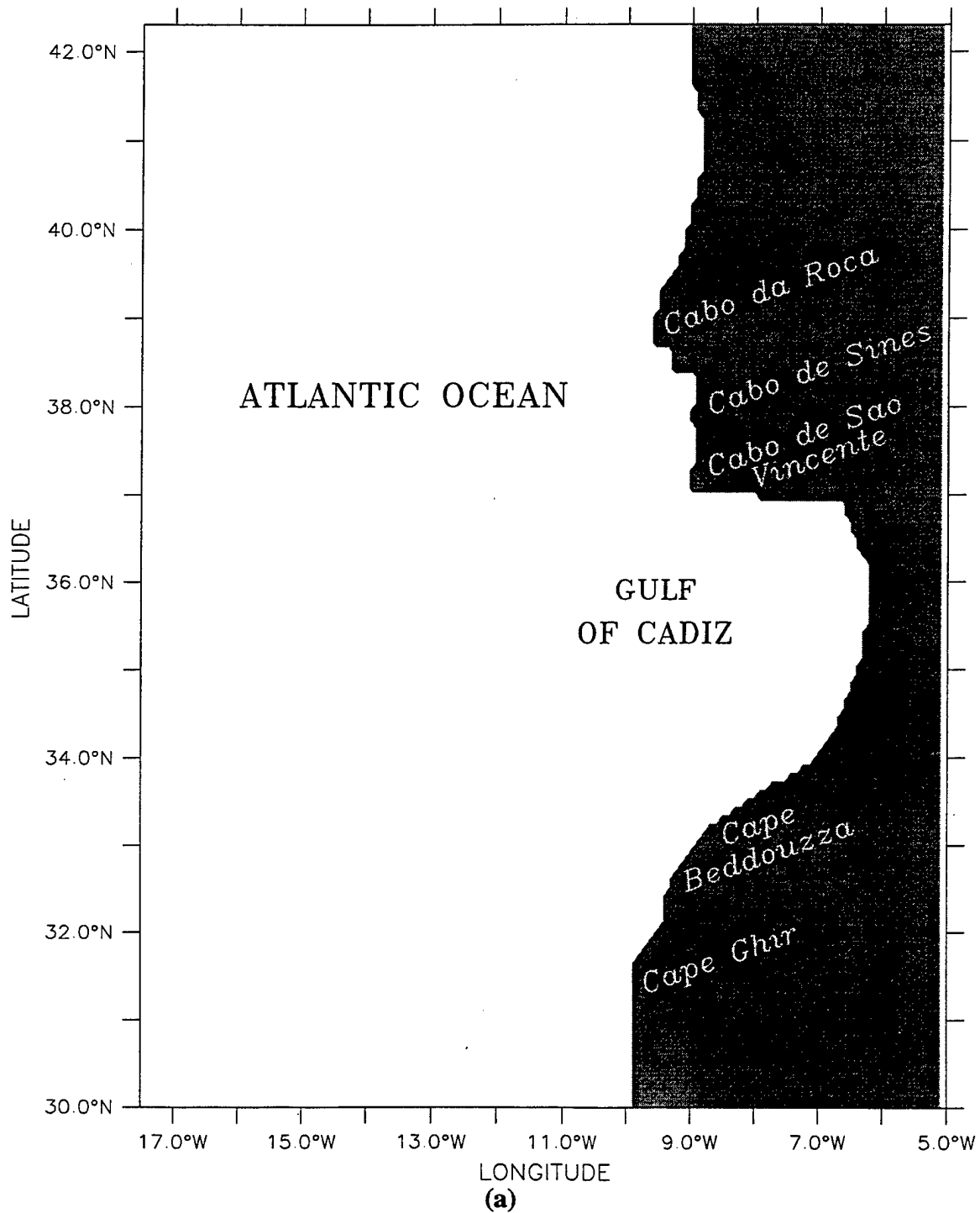
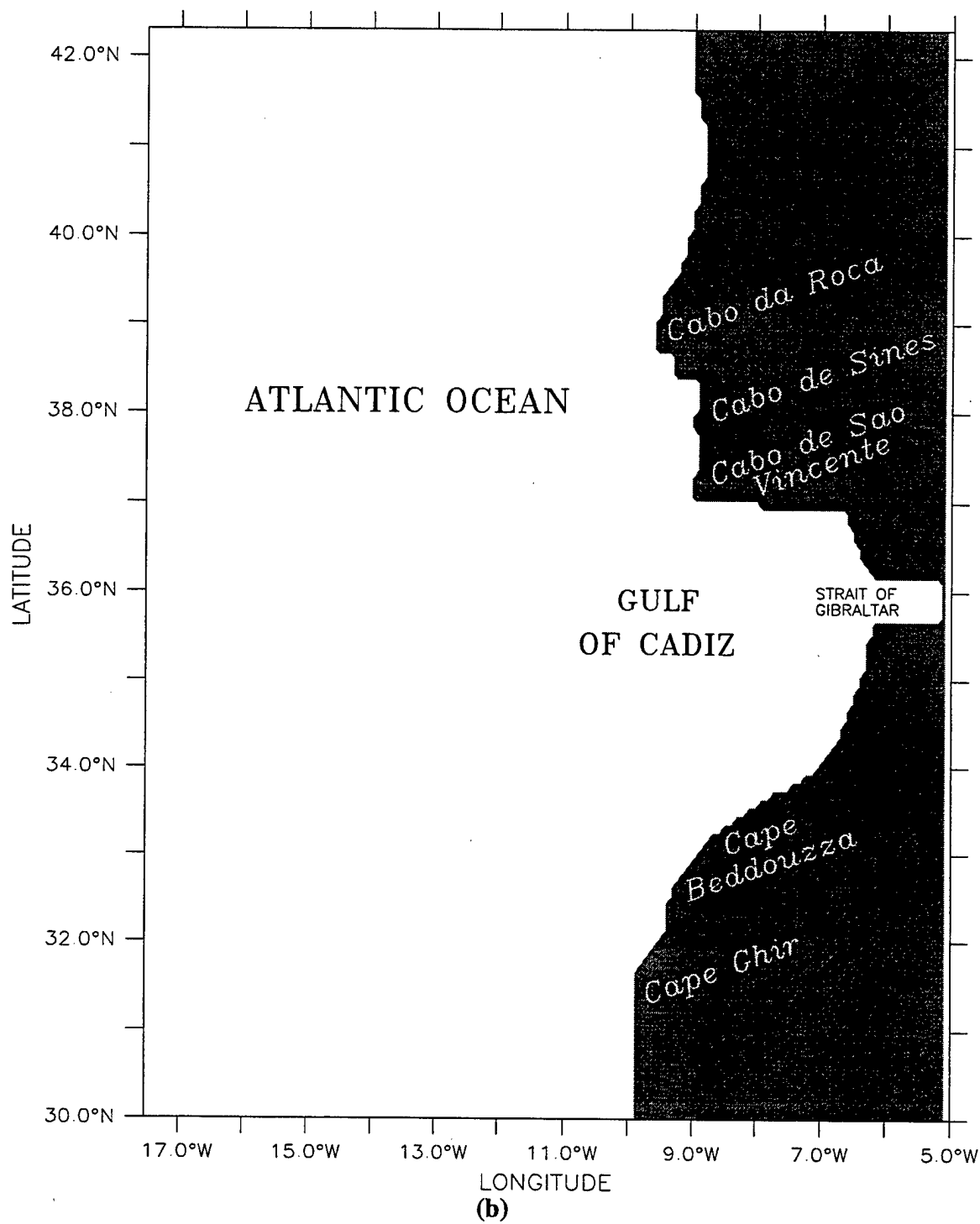


Figure 1. The model domain for the northern Canary Current System (NCCS) is bounded by 30°N to 42.5°N, 5°W to 17.5°W. The cross-shore (alongshore) resolution is 9 km (11 km). Geographical locations and prominent features are labeled. Model domain in (a) has a closed boundary along the entire coast, and in (b) has been modified at 5 grid points at the eastern boundary to open the Mediterranean Sea at the Strait of Gibraltar.



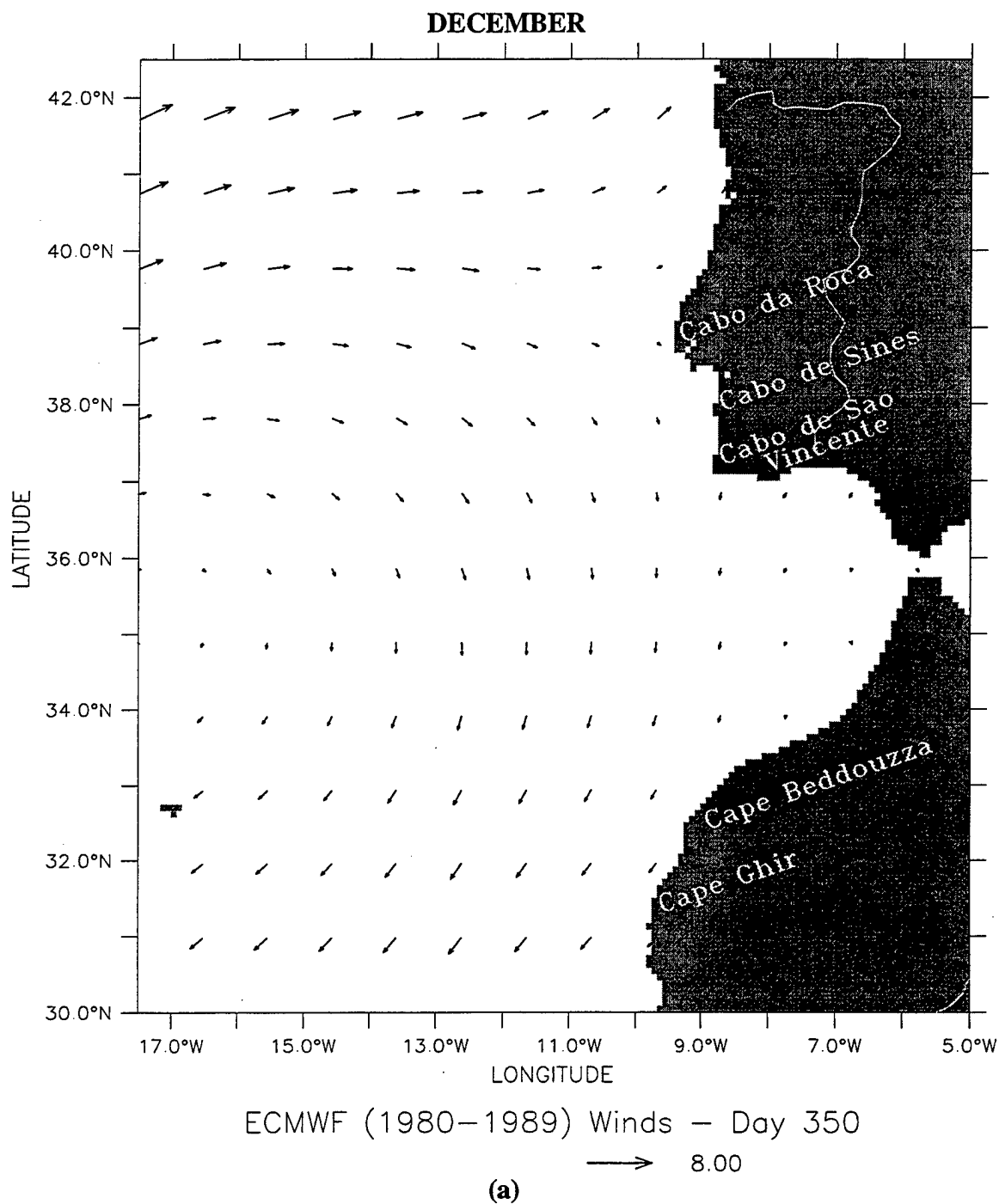
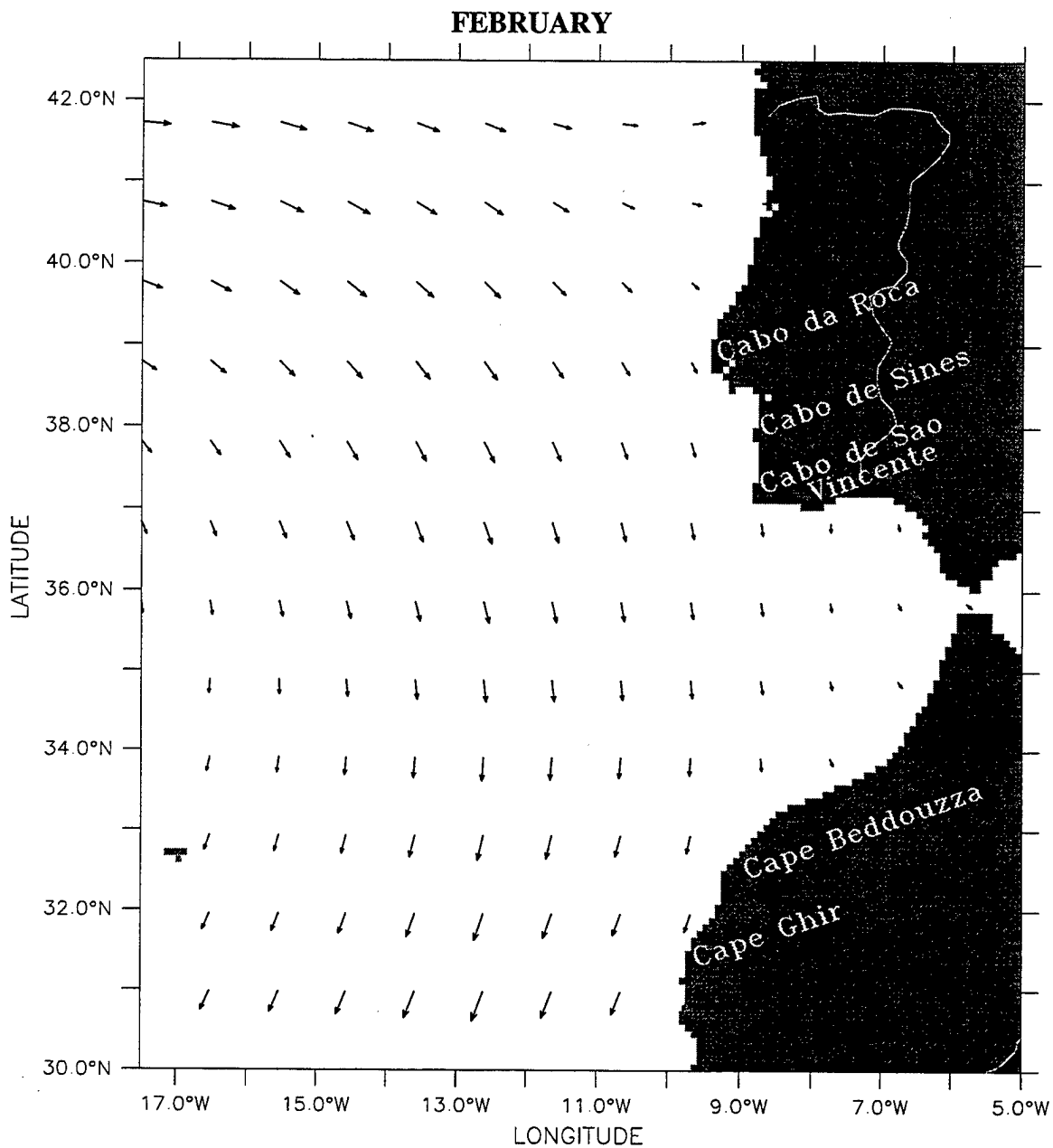


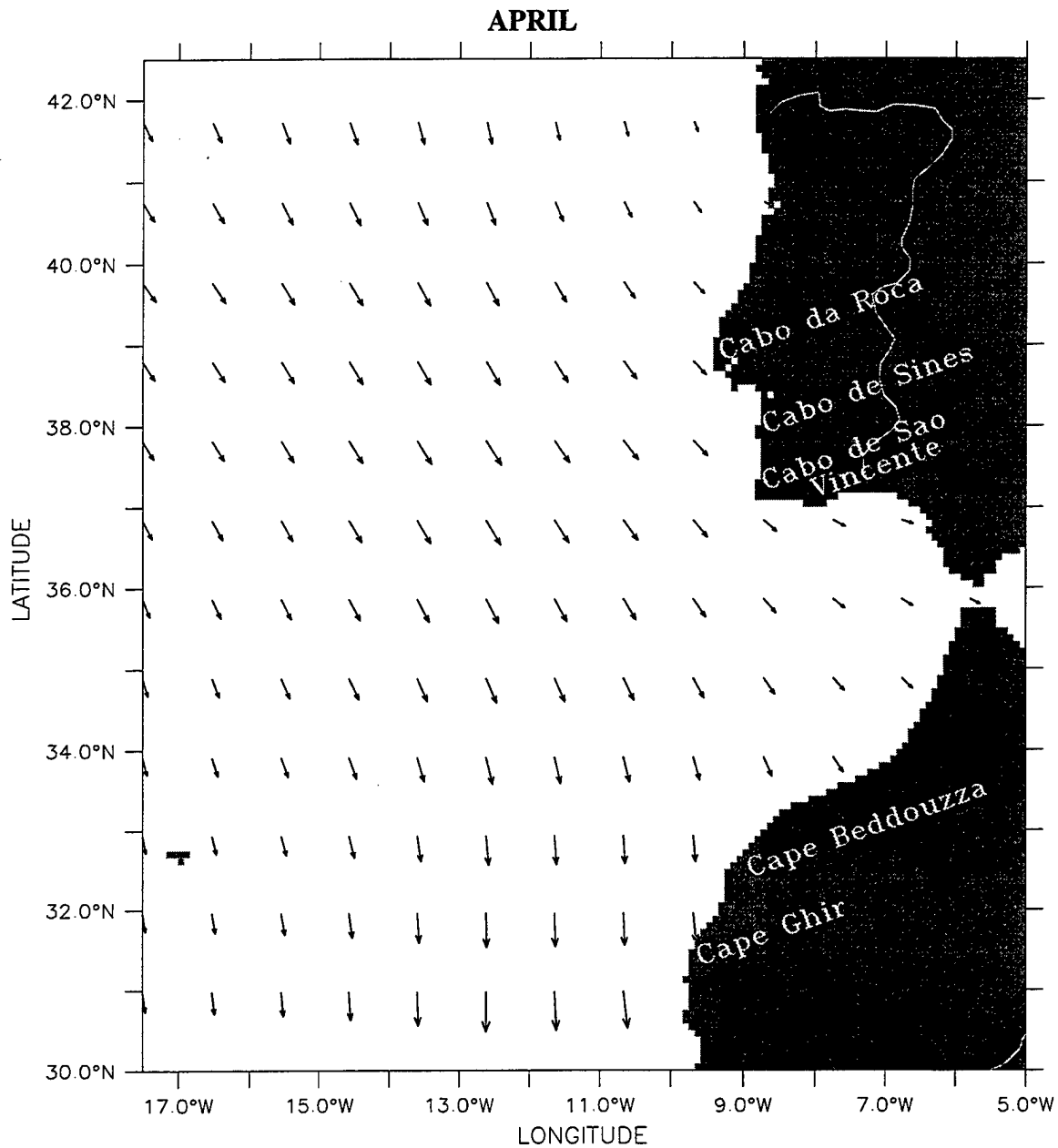
Figure 2. Climatological (1980-1989) ECMWF winds in m/s for: (a) December, (b) February, (c) April, (d) August, and (e) October. Maximum wind vector is 8 m/s.



ECMWF (1980-1989) Winds — Day 46

→ 8.00

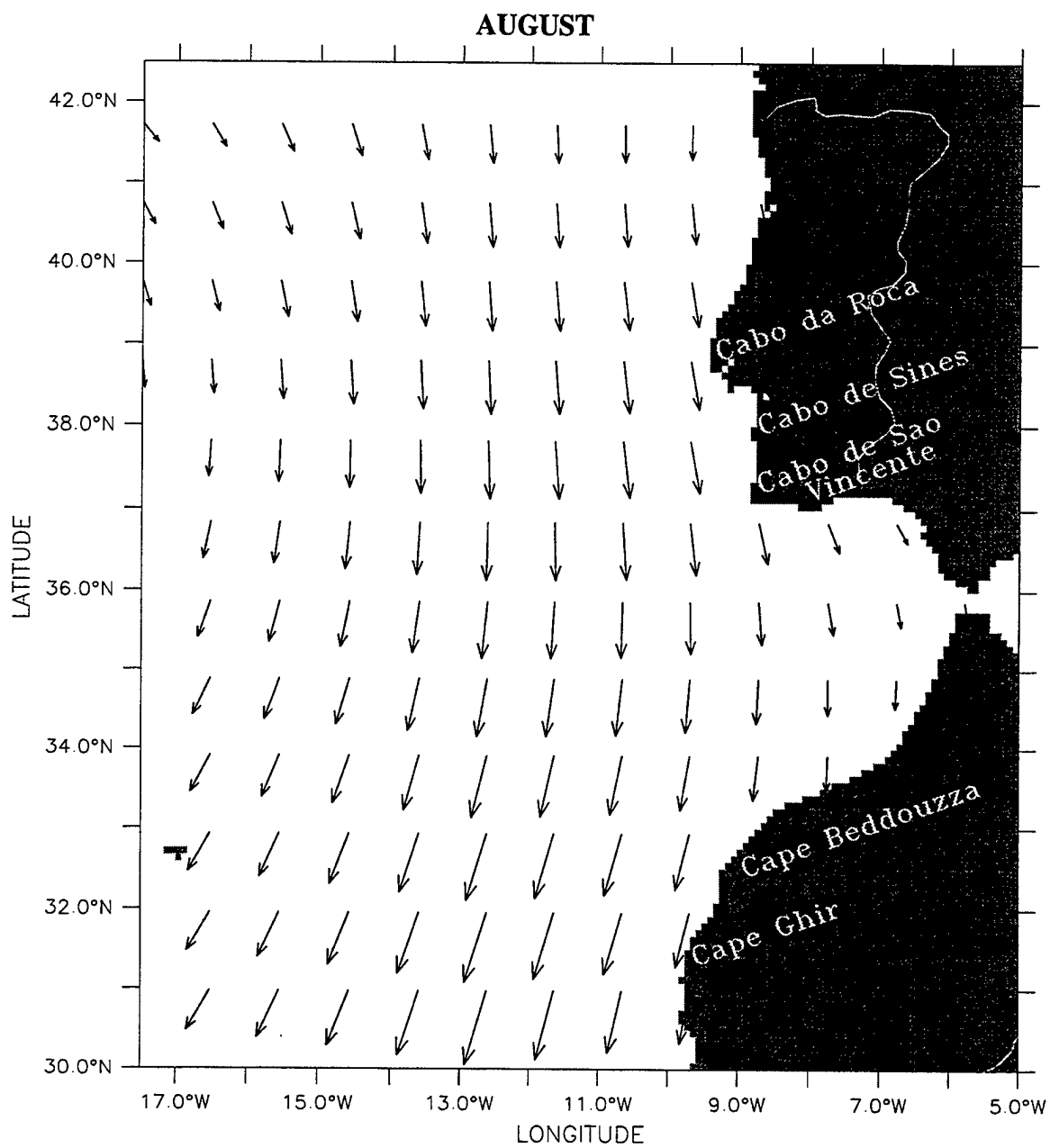
(b)



ECMWF (1980–1989) Winds – Day 105

→ 8.00

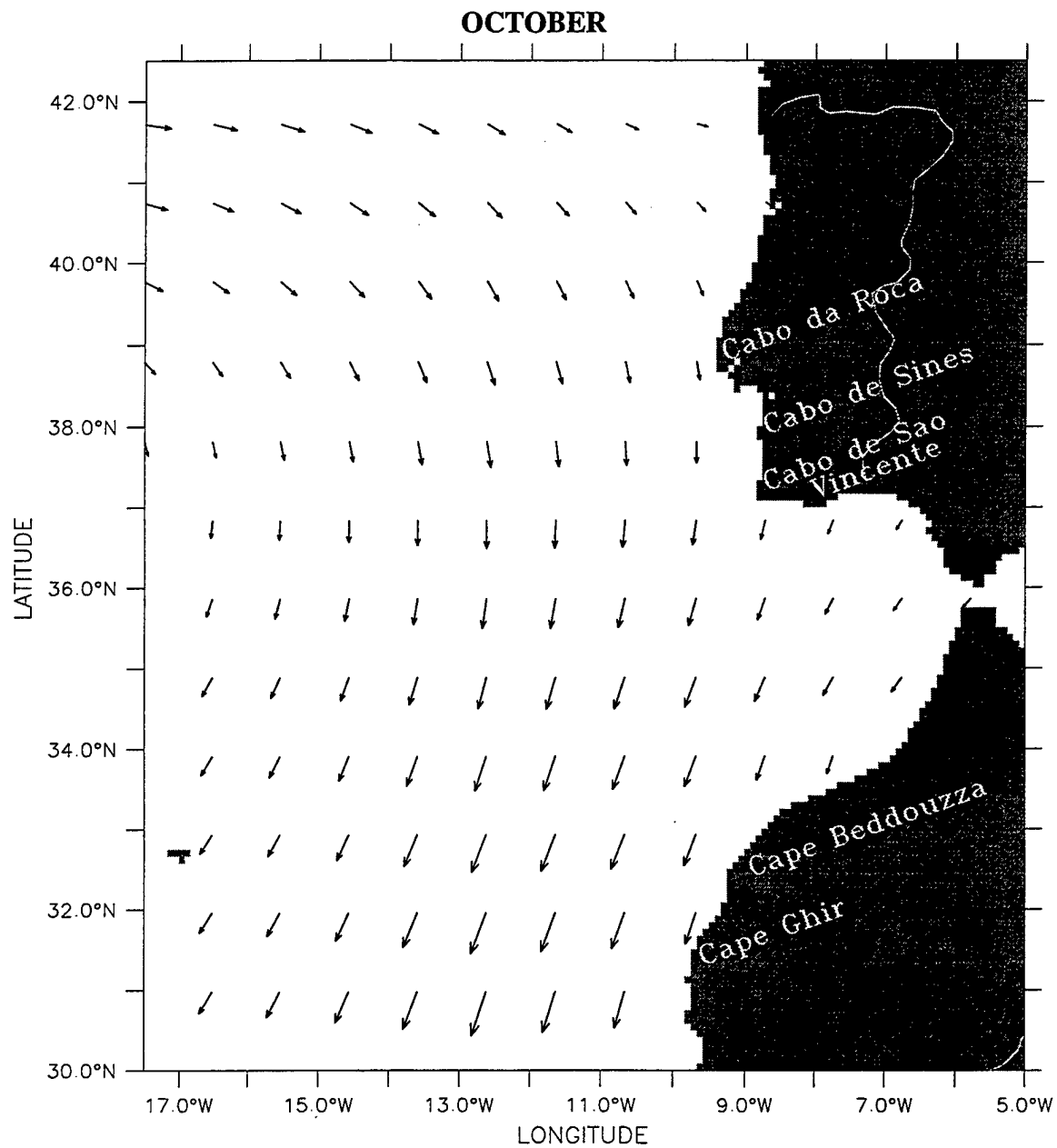
(c)



ECMWF (1980-1989) Winds — Day 227

→ 8.00

(d)



ECMWF (1980-1989) Winds - Day 285

→ 8.00

(e)

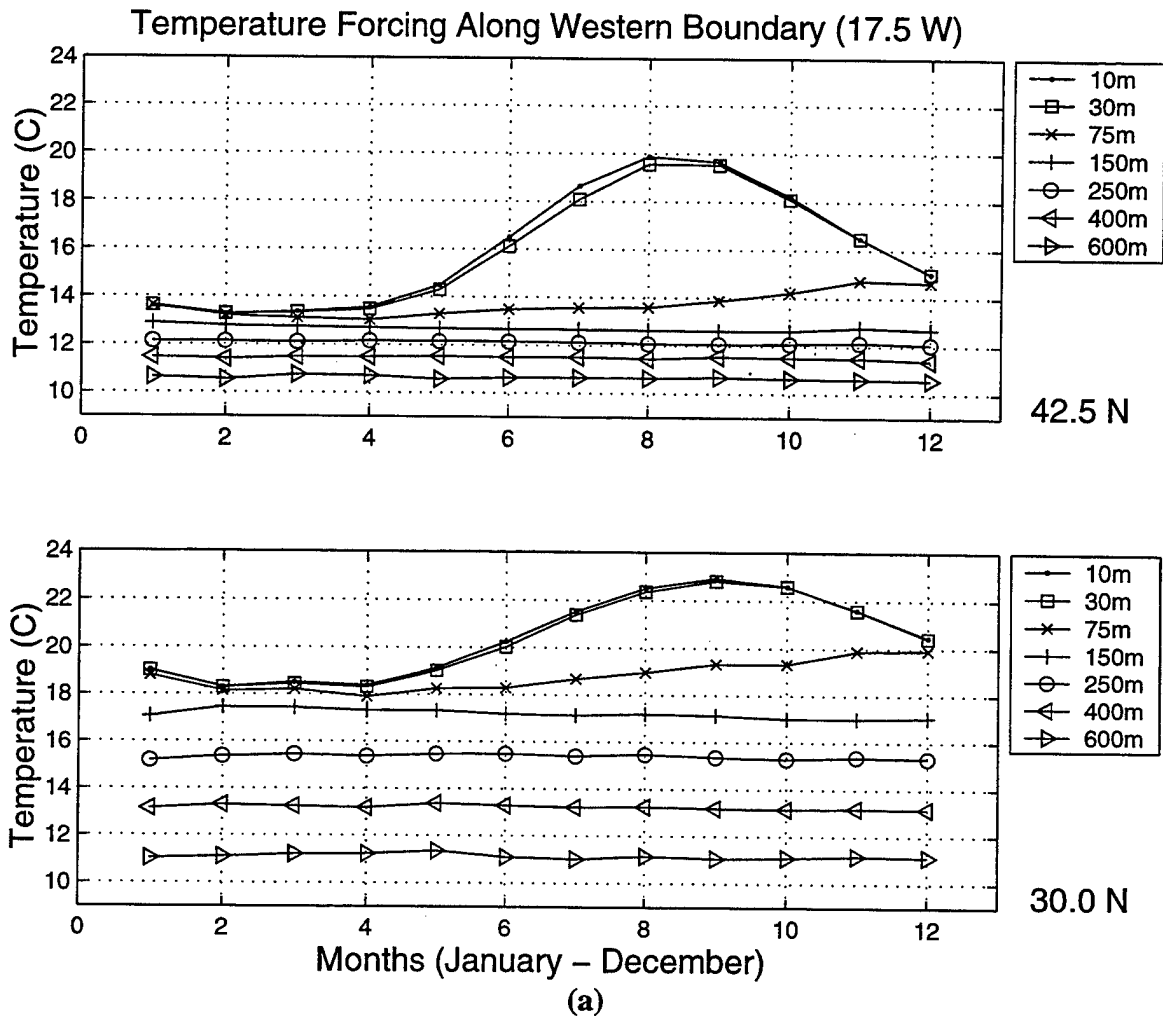
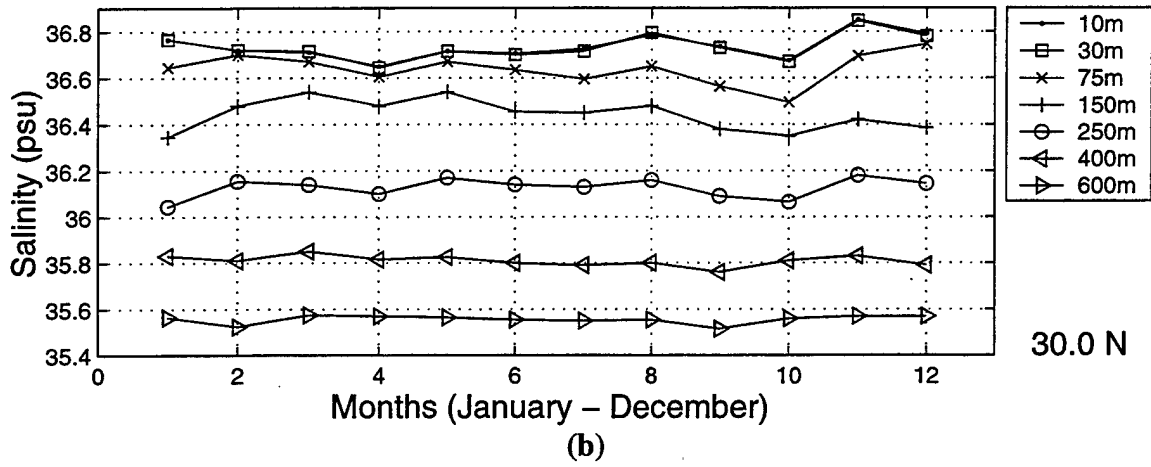
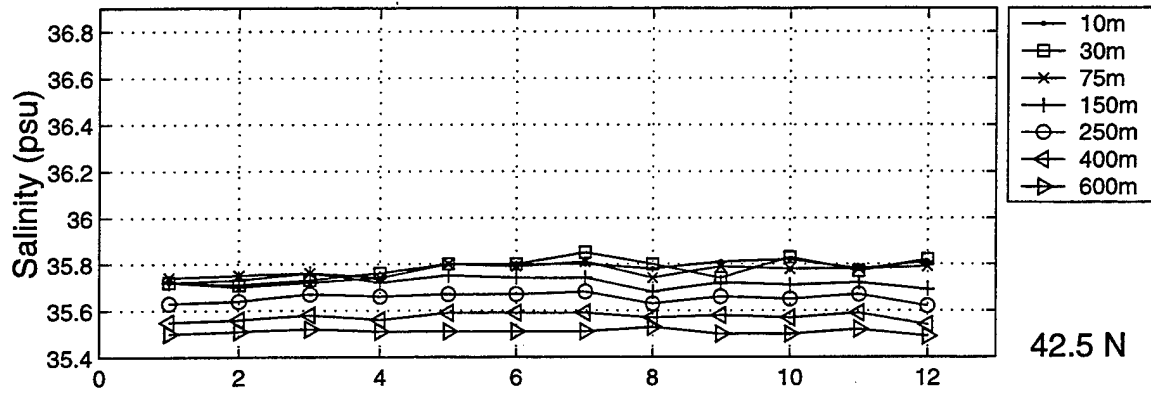


Figure 3. Plot of Levitus climatological fields used as seasonal forcing along the western boundary (17.5°W) at 42.5°N (top) and 30°N (bottom) for (a) temperature and (b) salinity.

Salinity Forcing Along Western Boundary (17.5W)



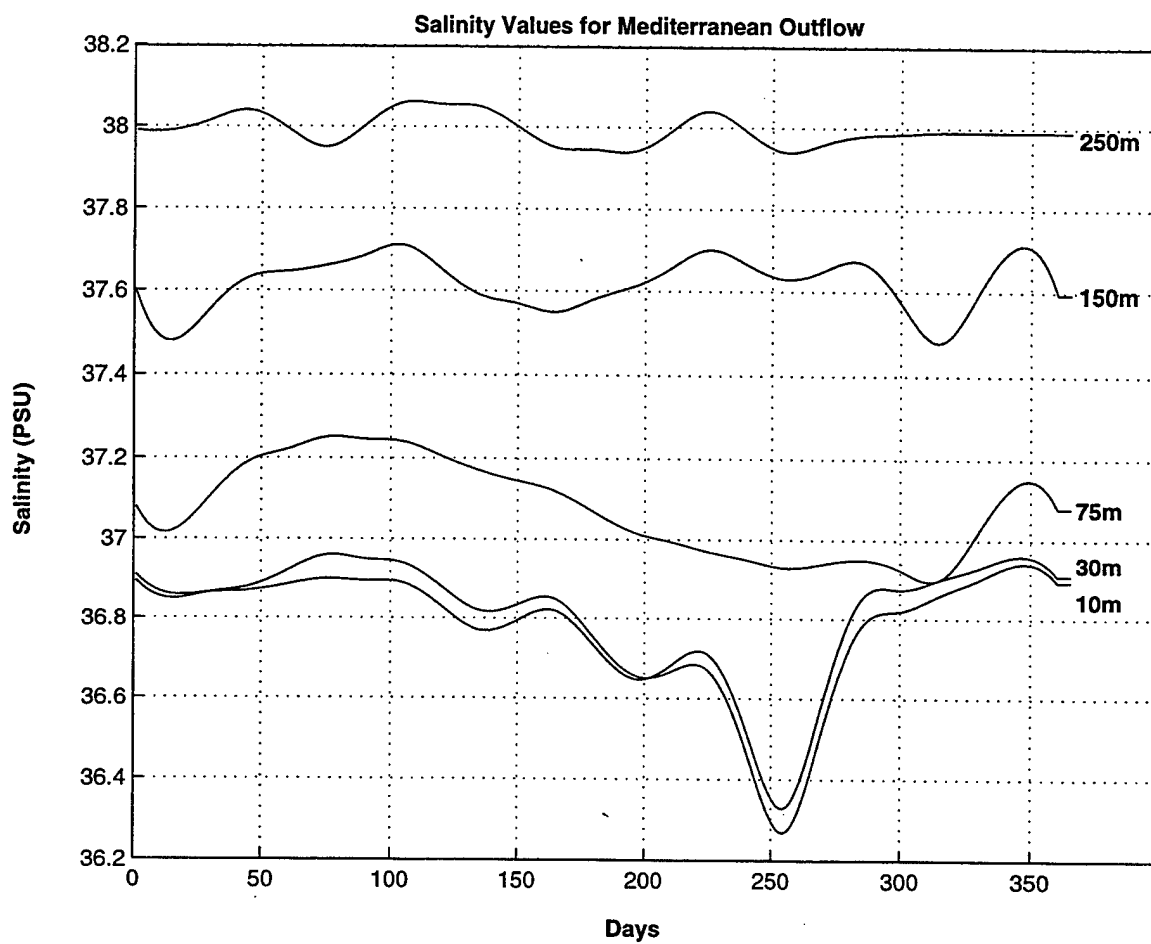
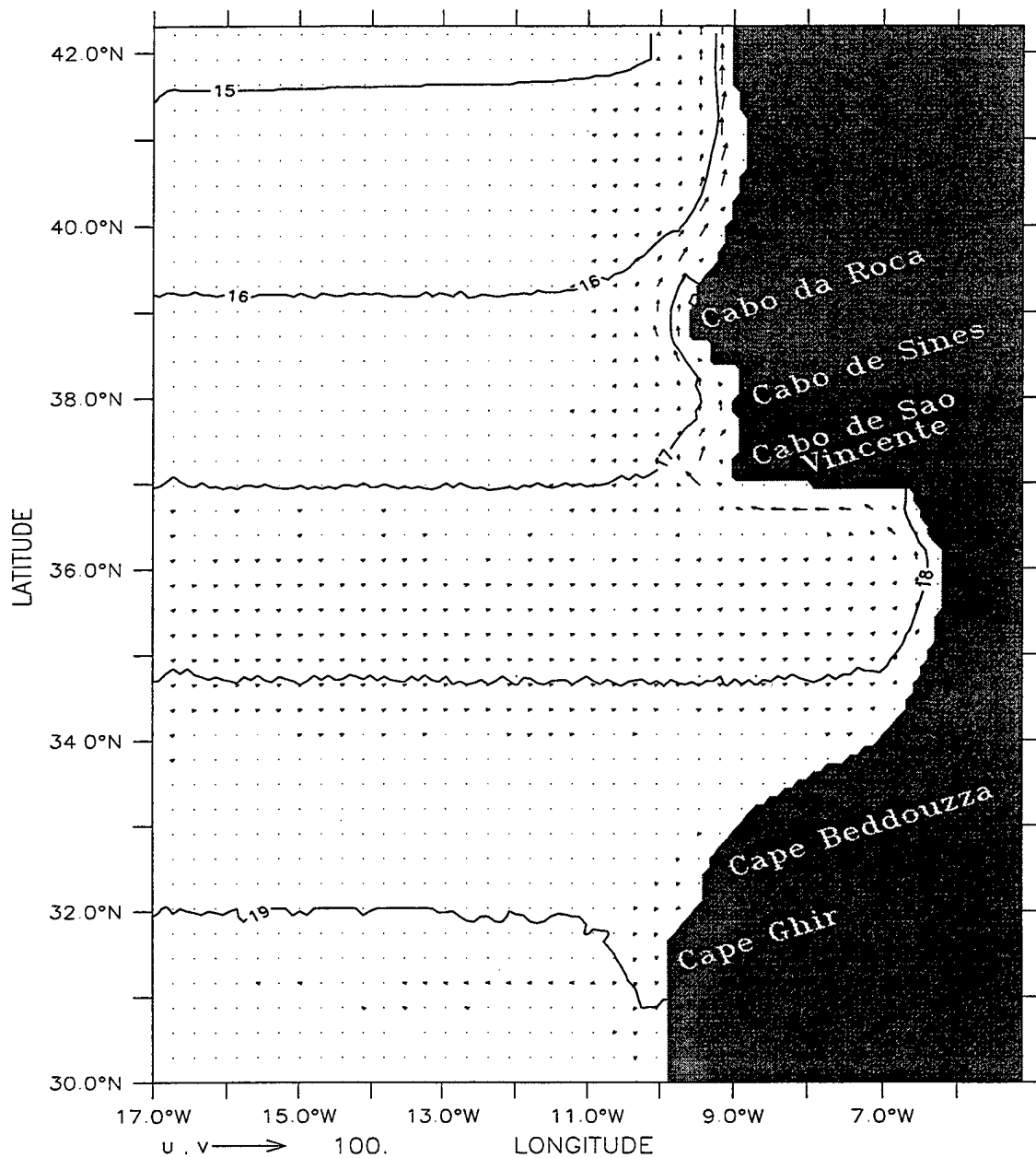


Figure 4. Salinities for Mediterranean Outflow (MO) used as seasonal forcing at the Strait of Gibraltar (from Levitus et al., 1994).

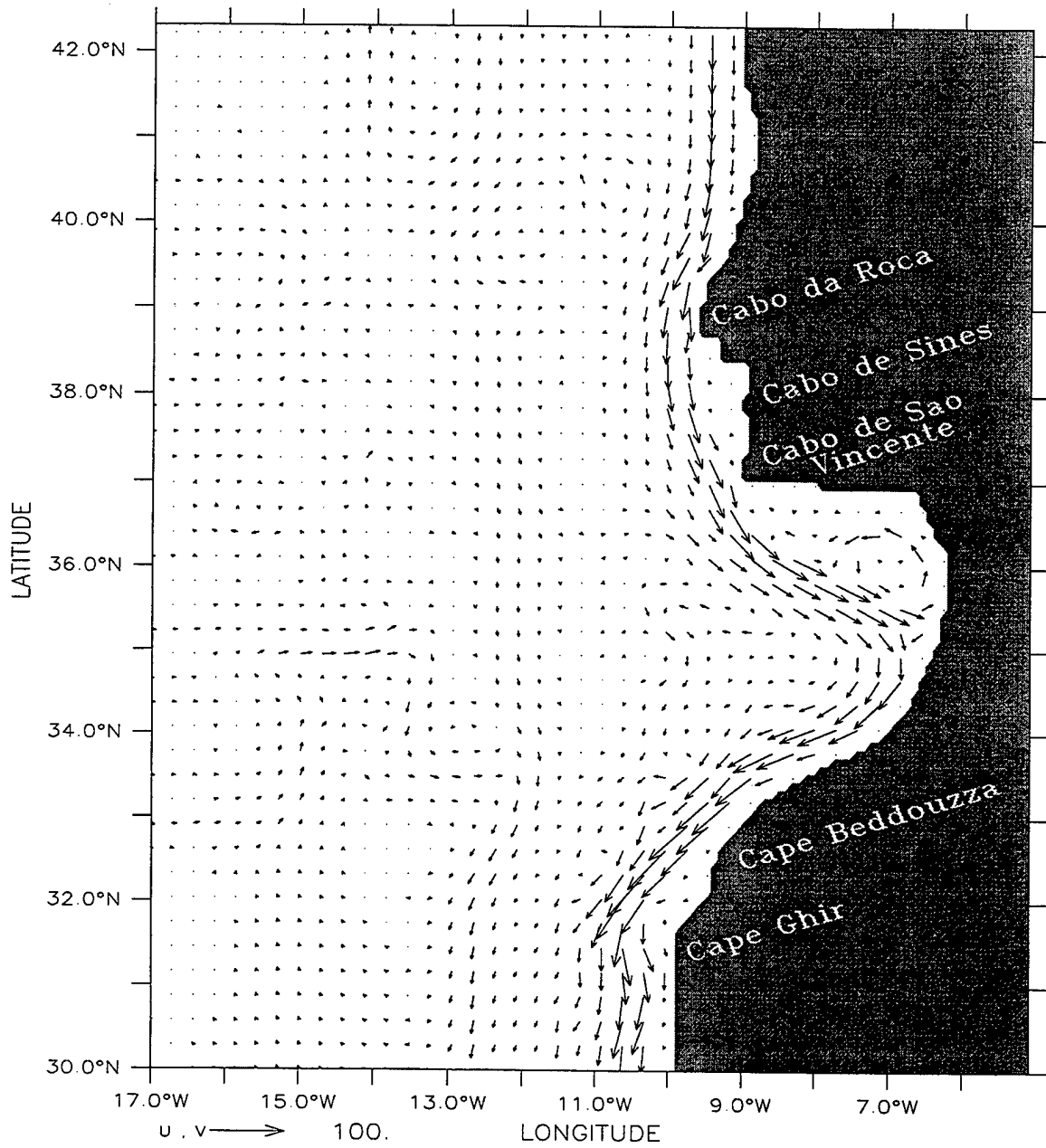
DEPTH (m) : 10
T (DAY) : 27



Temperature (deg C) and Velocity (cm/s)
(a)

Figure 5a. Temperature contours and velocity vectors at 10 m depth for Experiment 1 at day 27. To avoid clutter, velocity vectors are plotted every third gridpoint in the cross-shore and alongshore directions. Contour interval is 1° C. Maximum velocity vector is 100 cm/s.

DEPTH (m) : 10
T (DAY) : 267

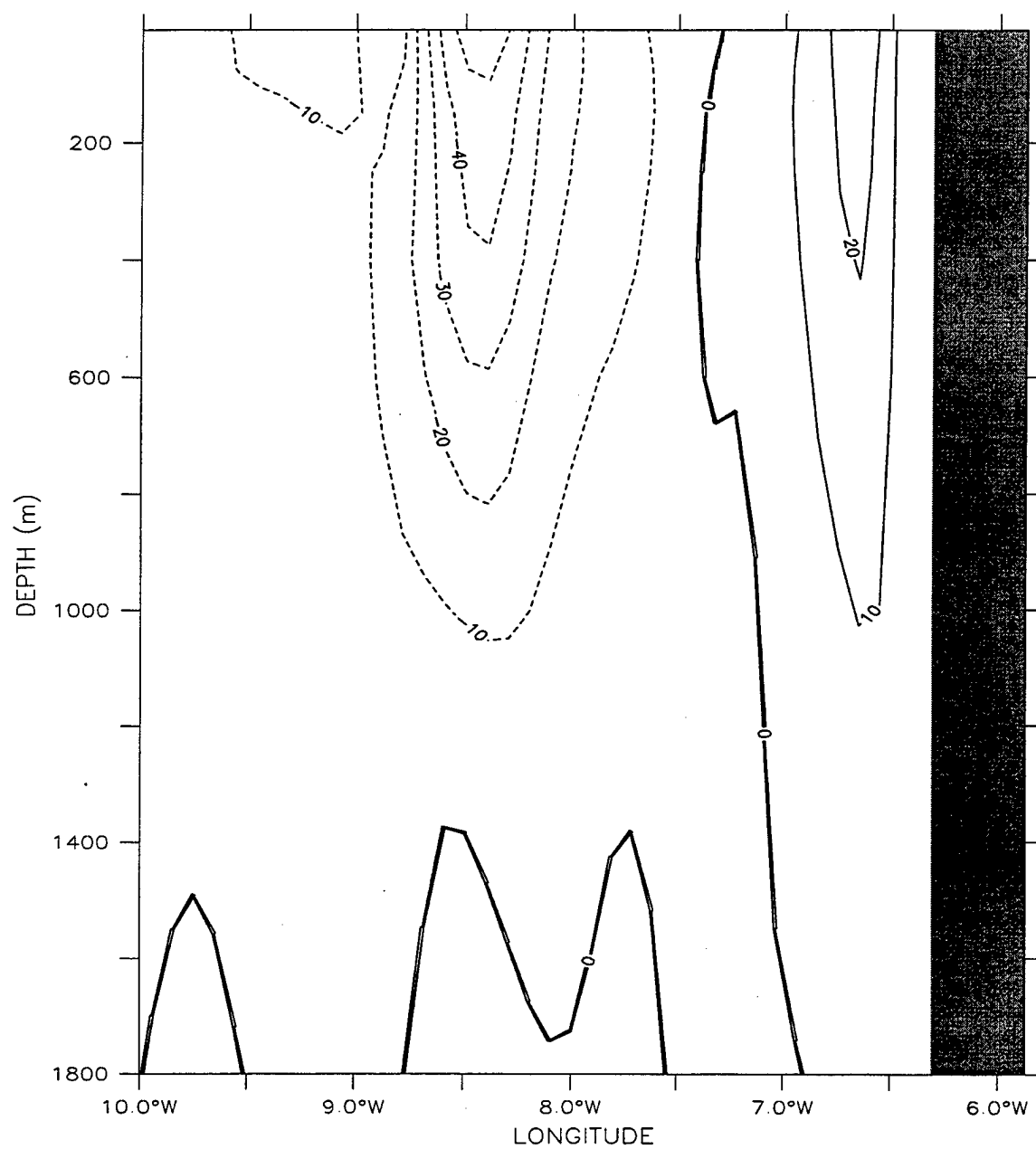


Velocity (cm/s)

(b)

Figure 5b. Velocity vectors at 10 m depth for Experiment 1 at day 267. To avoid clutter, velocity vectors are plotted every third gridpoint in the cross-shore and alongshore directions. Maximum velocity vector is 100 cm/s.

LATITUDE : 35.3N
T (DAY) : 330



Meridional Velocity (cm/s)

(c)

Figure 5c. Cross-shore section of meridional velocity (v) at 35.3°N for Experiment 1 on day 330. Contour interval is 10 cm/s. Equatorward (poleward) flow is denoted by dashed (solid) lines.

DEPTH (m) : 10
T (DAY) : 216

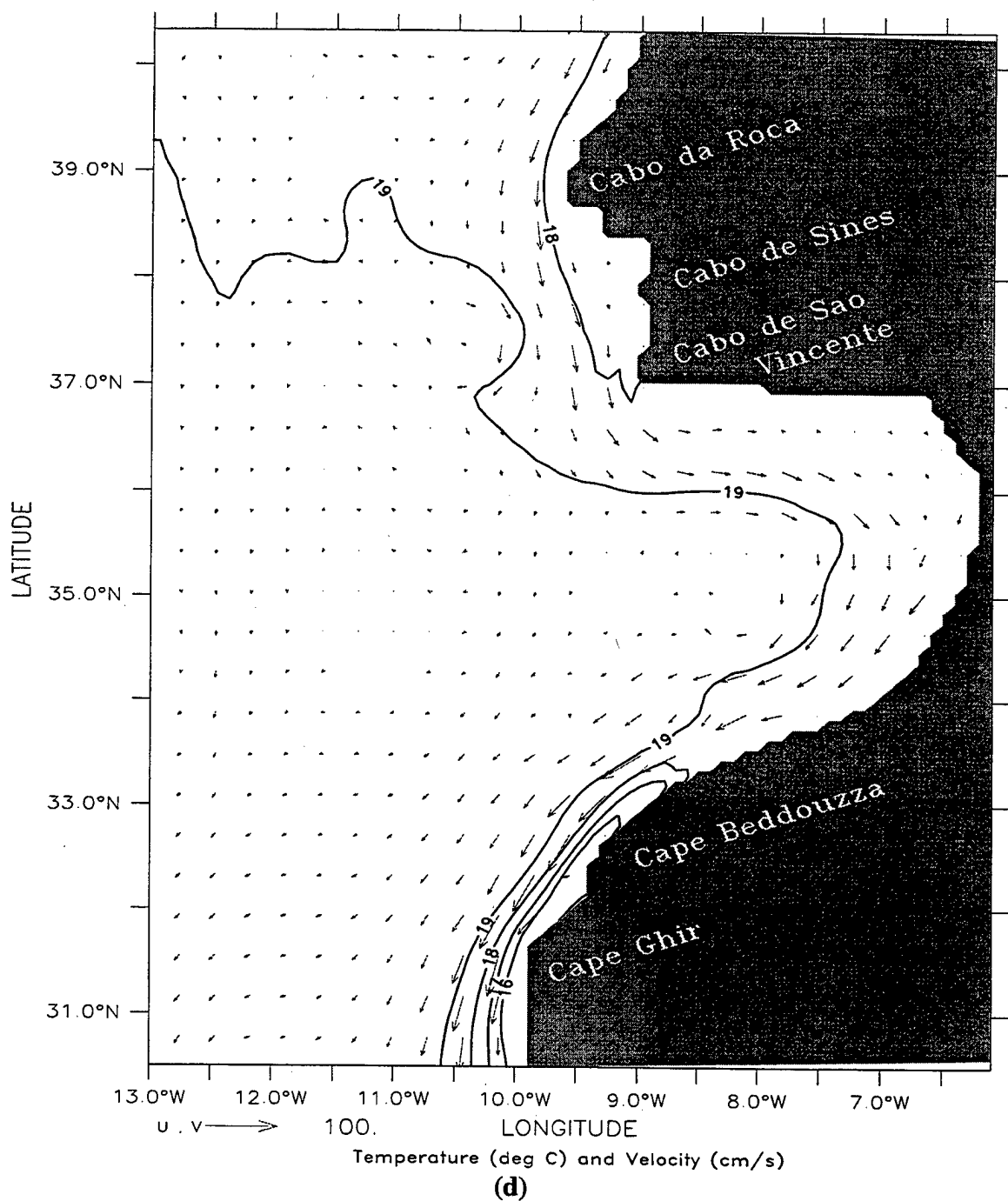
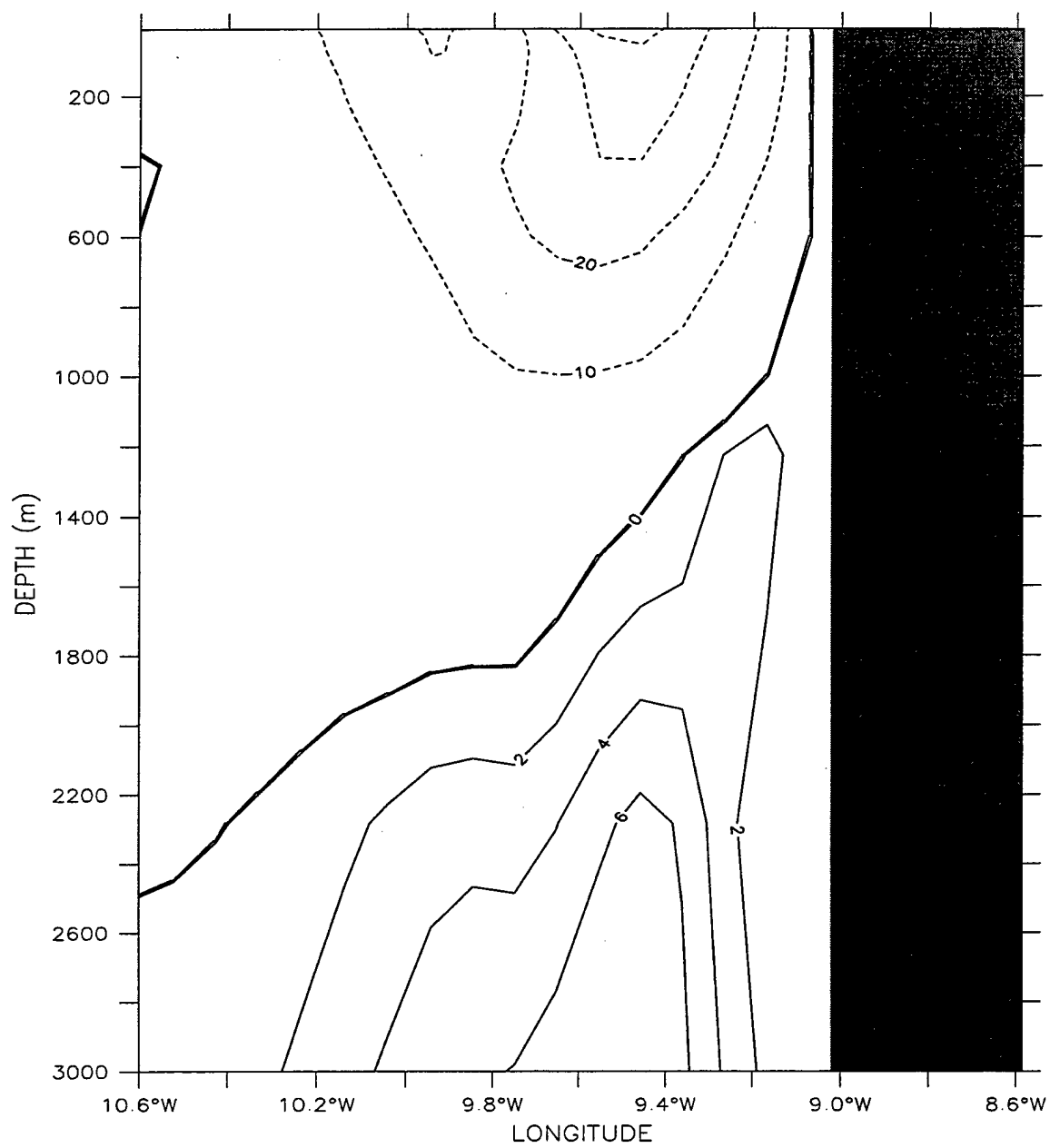


Figure 5d. Temperature contours and velocity vectors at 10 m depth for Experiment 1 at day 216. To avoid clutter, velocity vectors are plotted every third (fourth) gridpoint in the cross-shore (alongshore) direction. Contour interval is 1° C. Maximum velocity vector is 100 cm/s.

LATITUDE : 37.3N
T (DAY) : 231



Meridional Velocity (cm/s)

(a)

Figure 6a. Cross-shore section of meridional velocity (v) at 37.3°N for Experiment 1 on day 231. Contour interval is 10 cm/s for equatorward flow (dashed lines) and 2 cm/s for poleward flow (solid lines).

LATITUDE : 41.5N
T (DAY) : 357

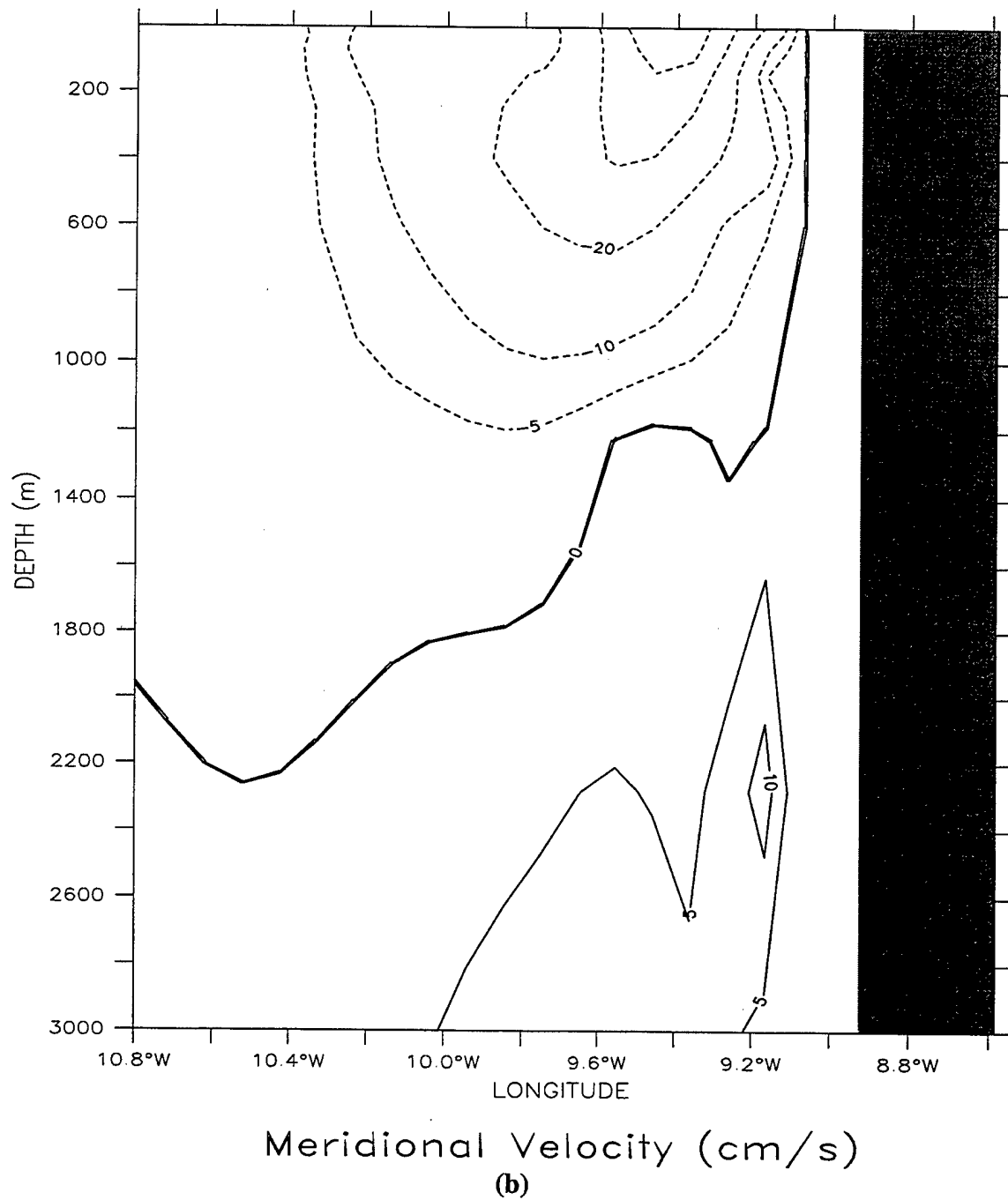


Figure 6b. Cross-shore section of meridional velocity (v) at 41.5°N for Experiment 1 on day 357. Contour interval is 10 cm/s for equatorward flow (dashed lines, with an additional 5 cm/s contour added) and 5 cm/s for poleward flow (solid lines).

LATITUDE : 37.1N
T (DAY) : 273

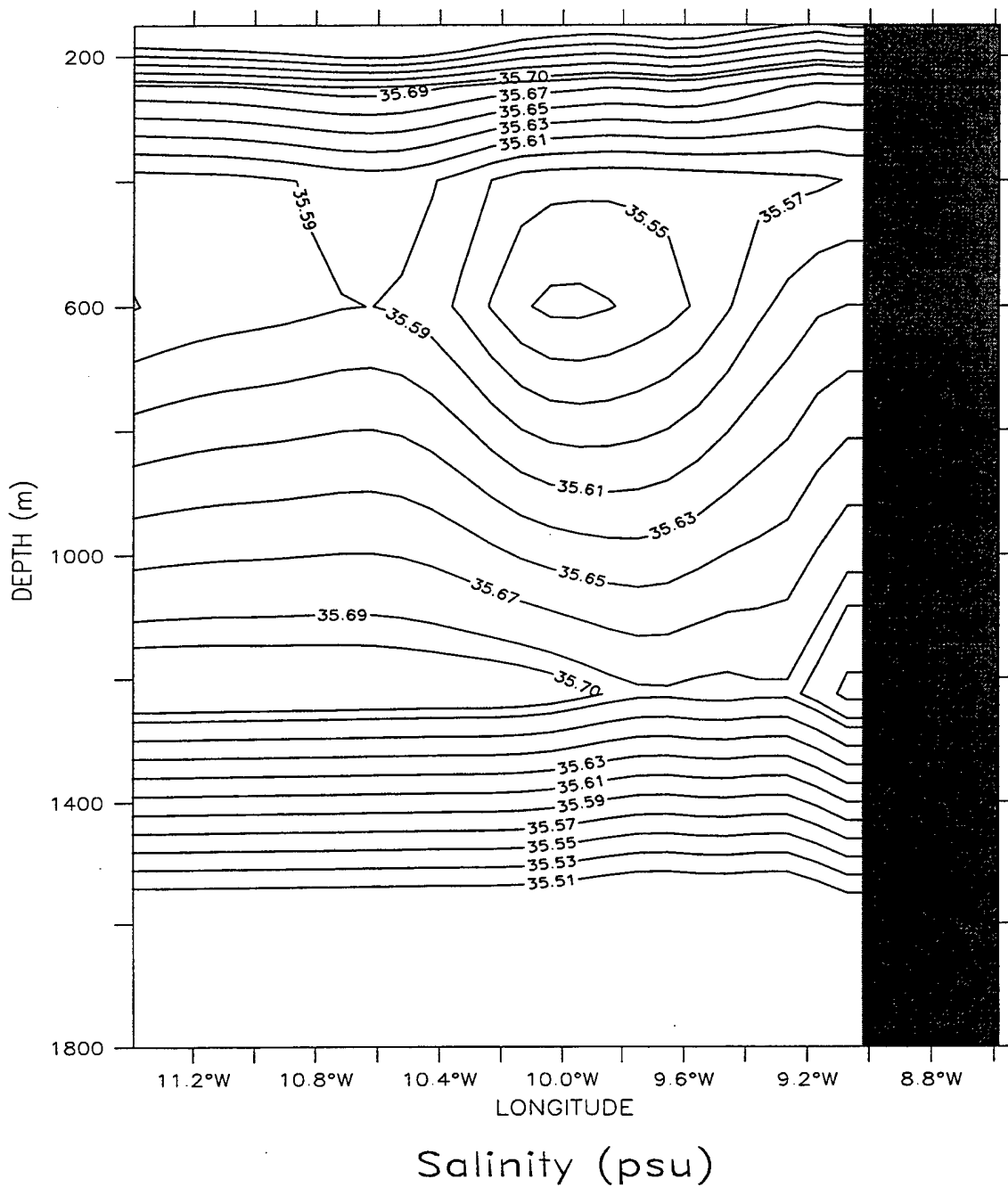


Figure 7. Cross-shore section of salinity for Experiment 1 at 37.1°N on day 273. The contour interval for salinity is 0.01 (0.02) above (below) 35.69 values.

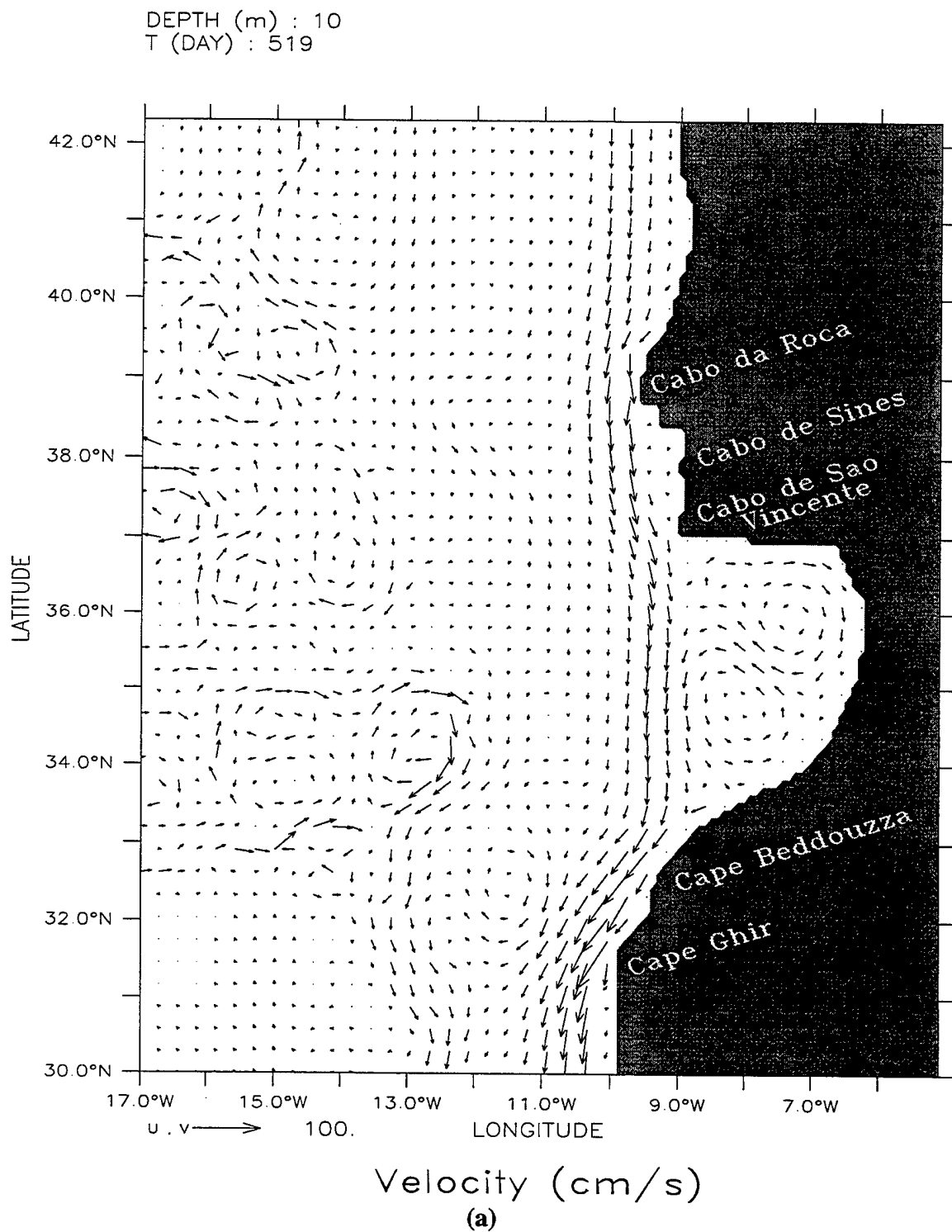
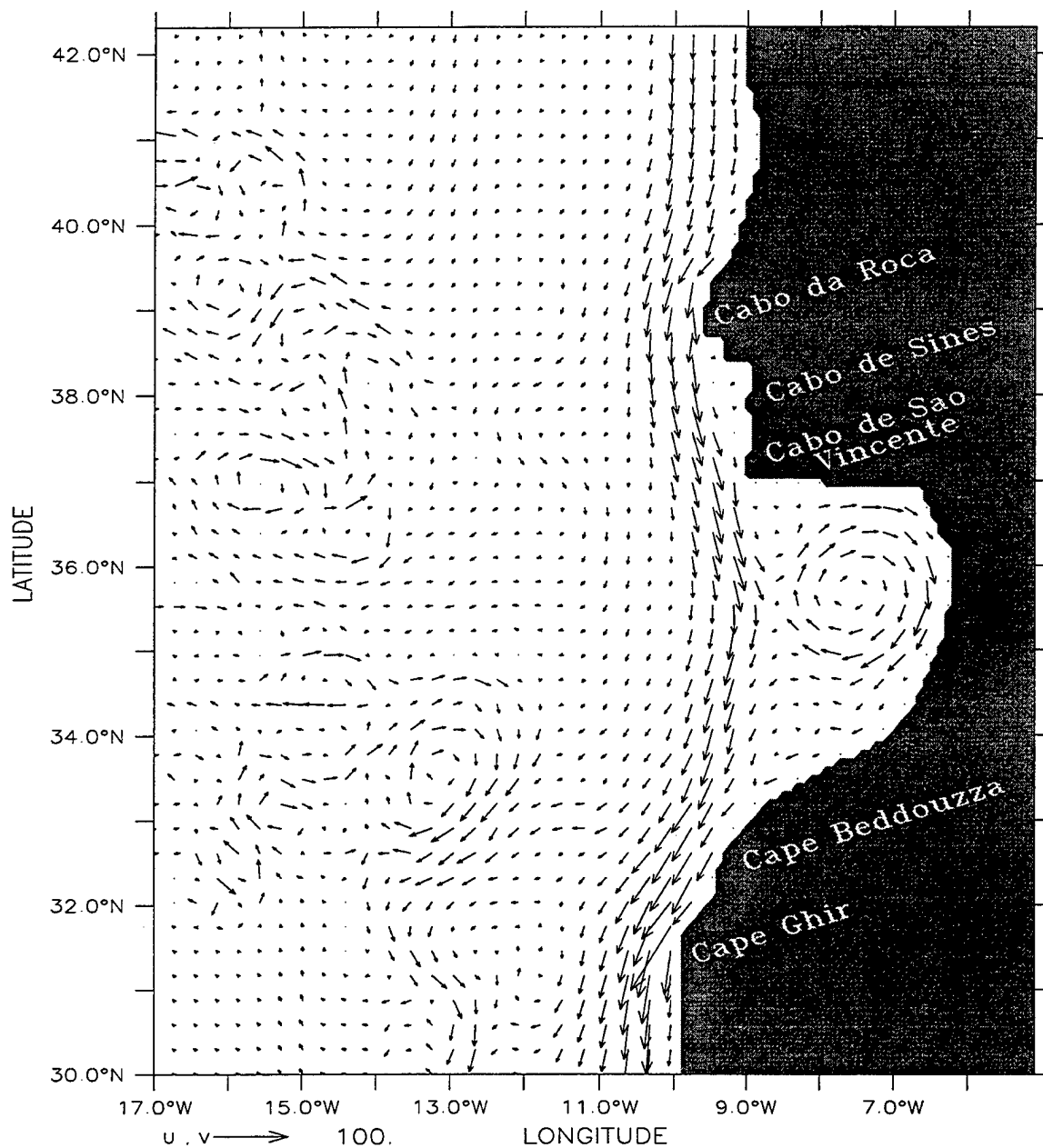


Figure 8a. Velocity vectors at 10 m depth for Experiment 1 on day 519. To avoid clutter, velocity vectors are plotted every third gridpoint in the cross-shore and alongshore directions. Maximum velocity vector is 100 cm/s.

DEPTH (m) : 10
T (DAY) : 561



Velocity (cm/s)

(b)

Figure 8b. Velocity vectors at 10 m depth for Experiment 1 at day 561. To avoid clutter, velocity vectors are plotted every third gridpoint in the cross-shore and alongshore directions. Maximum velocity vector is 100 cm/s.

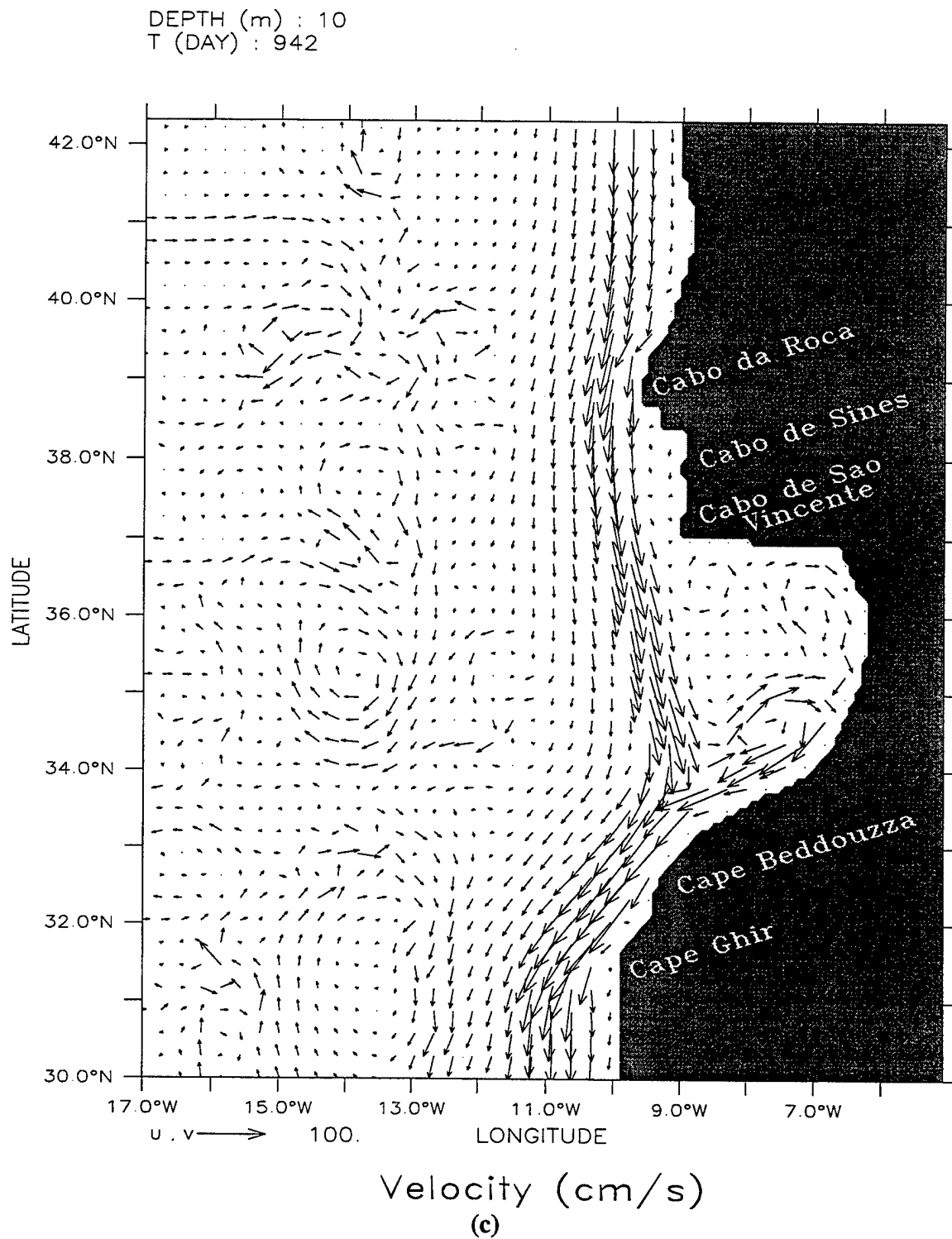


Figure 8c. Velocity vectors at 10 m depth for Experiment 1 at day 942. To avoid clutter, velocity vectors are plotted every third gridpoint in the cross-shore and alongshore directions. Maximum velocity vector is 100 cm/s.

DEPTH (m) : 10
T (DAY) : 999

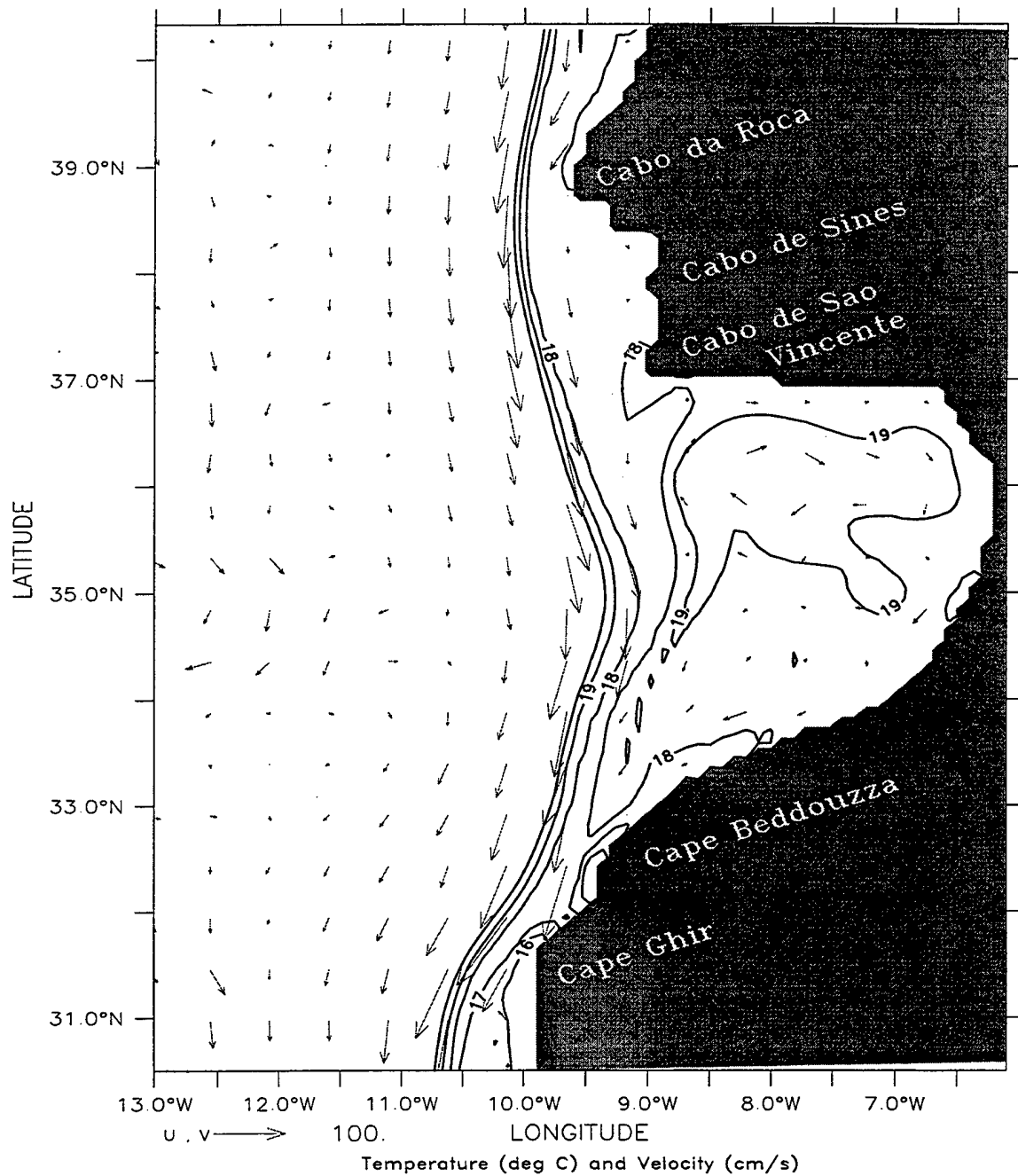


Figure 9. Temperature contours and velocity vectors at 10 m depth for Experiment 1 at day 999. To avoid clutter, velocity vectors are plotted every fifth gridpoint in the cross-shore and alongshore direction. Contour interval is 1° C. Maximum velocity vector is 100 cm/s.

LATITUDE : 39.3N
T (DAY) : 762

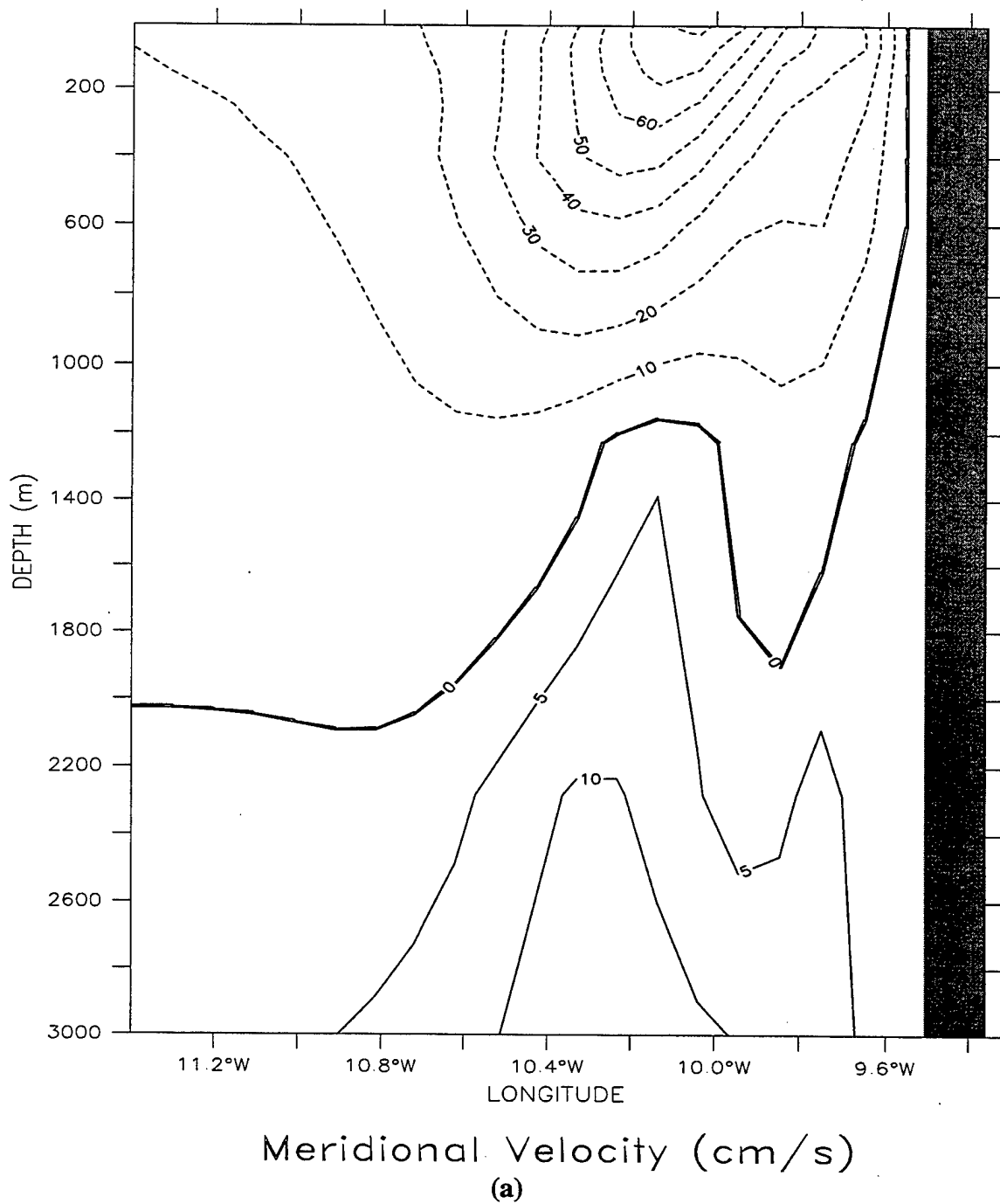
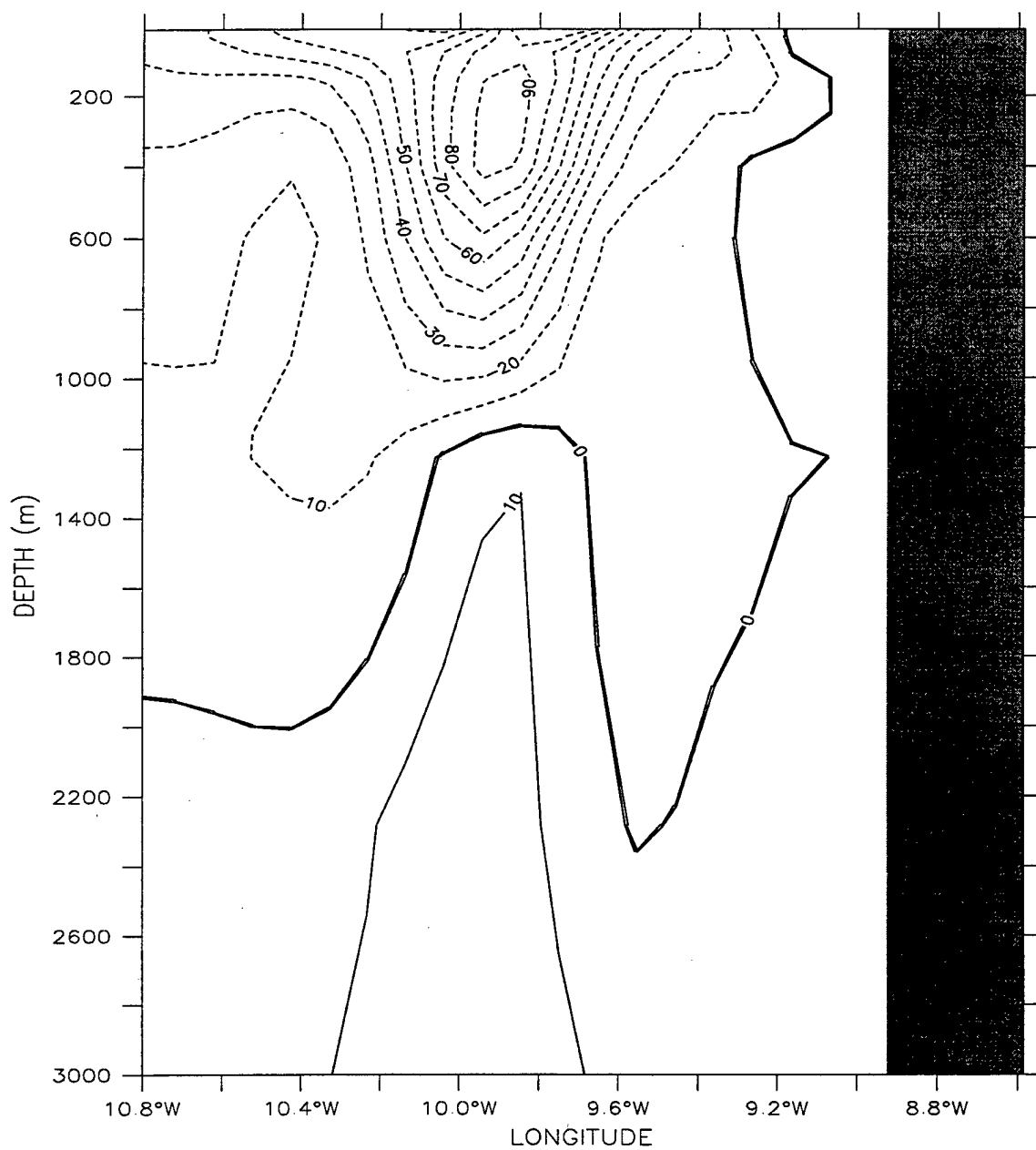


Figure 10a. Cross-shore section of meridional velocity (v) at 39.3°N for Experiment 1 on day 762. Contour interval is 10 cm/s for equatorward flow (dashed lines) and 5 cm/s for poleward flow (solid lines).

LATITUDE : 41.5N
T (DAY) : 1086

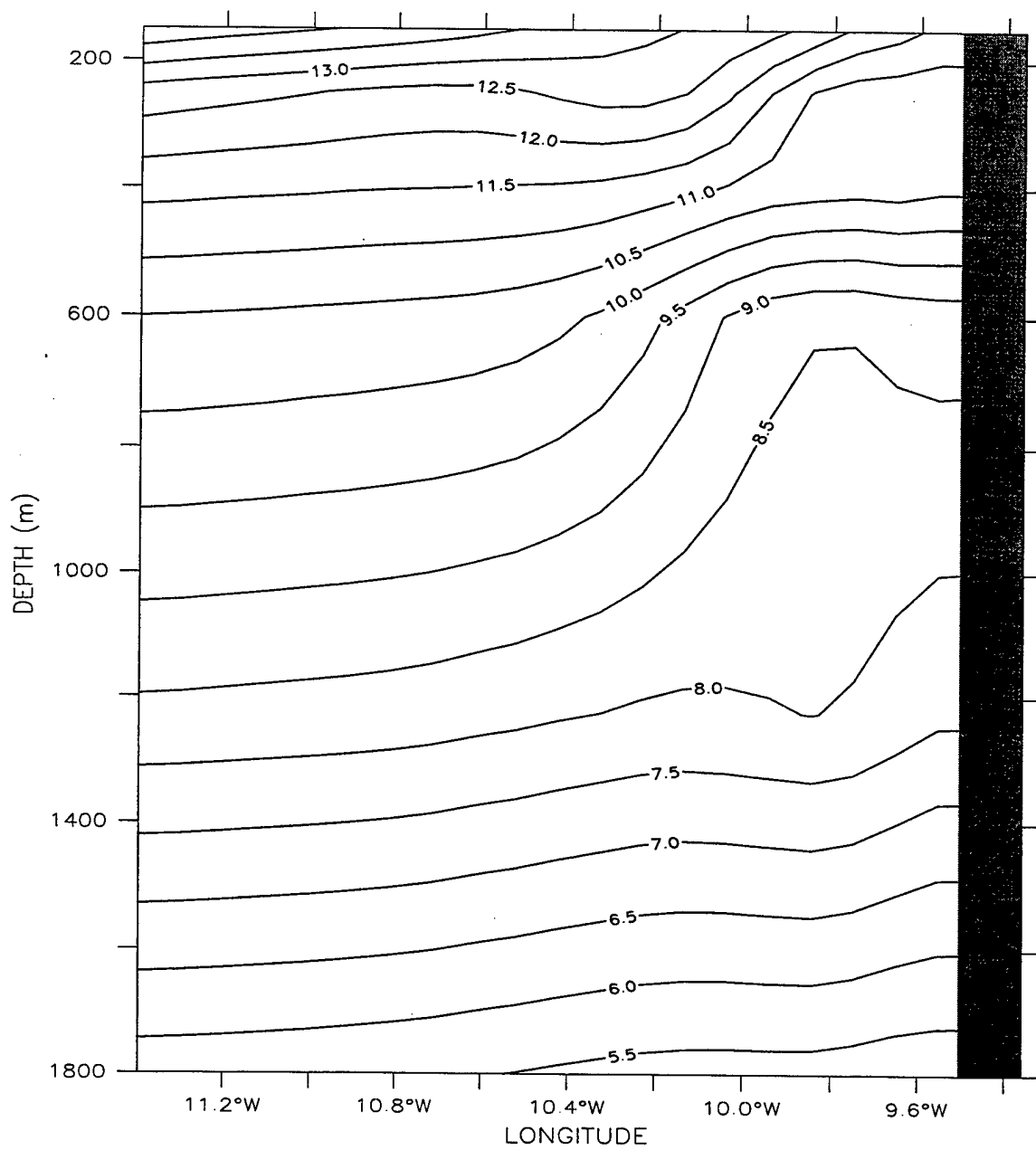


Meridional Velocity (cm/s)

(b)

Figure 10b. Cross-shore section of meridional velocity (v) at 41.5°N for Experiment 1 on day 1086. Contour interval is 10 cm/s for equatorward flow (dashed lines) and poleward flow (solid lines).

LATITUDE : 39.3N
T (DAY) : 828



Temperature (deg C)

(a)

Figure 11a. Cross-shore section of temperature for Experiment 1 at 39.3°N on day 828. The contour interval for temperature is 0.5°C.

DEPTH (m) : 10

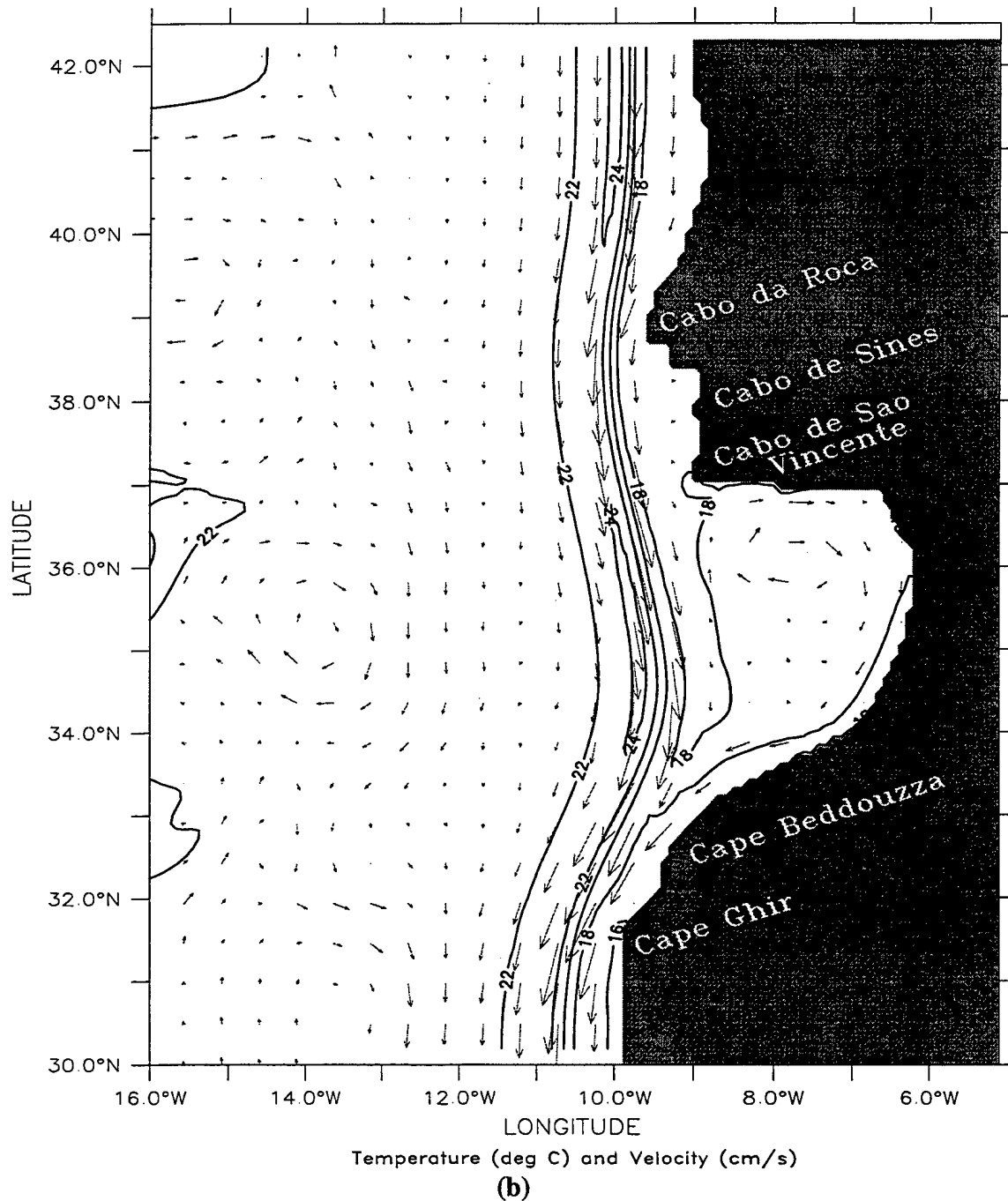


Figure 11b. Time-averaged plot of temperature contours and velocity vectors at 10 m depth for Experiment 1 in the third year for October. To avoid clutter, velocity vectors are plotted every fifth gridpoint in the cross-shore and alongshore directions. Contour interval is 2° C. Maximum velocity vector is 100 cm/s.

DEPTH (m) : 600

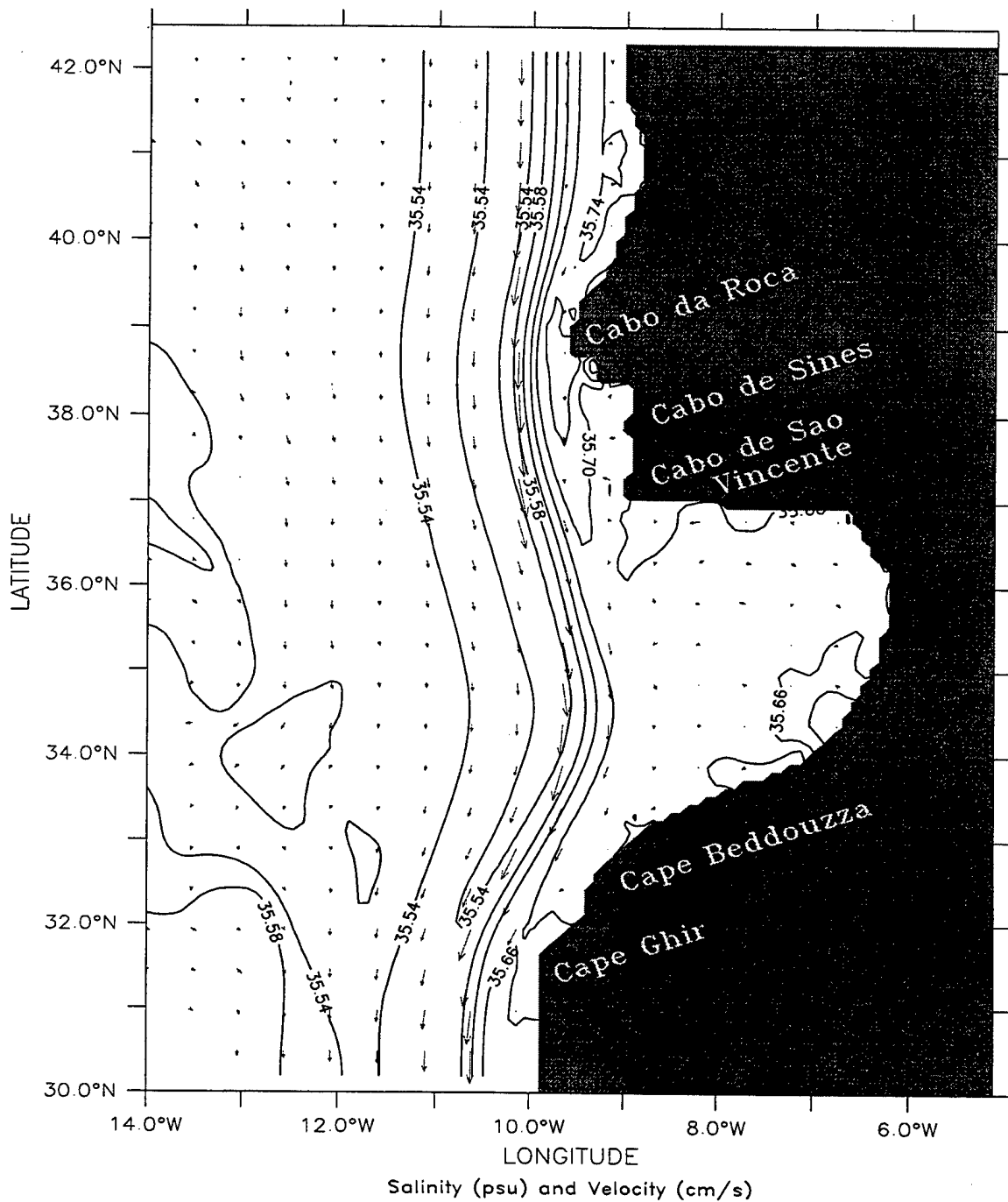


Figure 12. Time-averaged plot of salinity contours and velocity vectors at 600 m depth for Experiment 1 in the third year for October. To avoid clutter, velocity vectors are plotted every sixth gridpoint in the cross-shore and alongshore directions. Contour interval is 0.04. Maximum velocity vector is 100 cm/s.

LATITUDE : 37.1N
T (DAY) : 1002

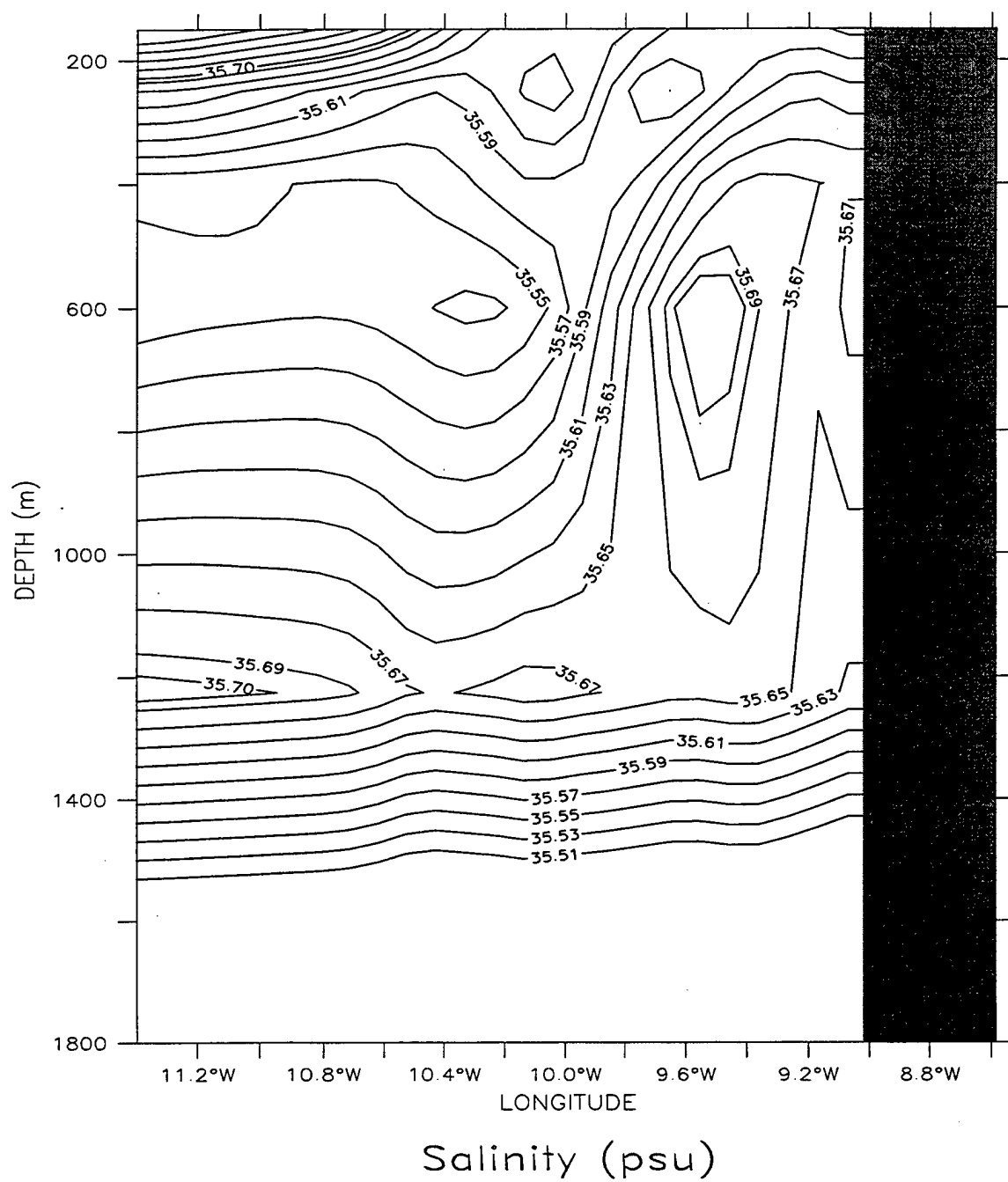


Figure 13. Cross-shore section of salinity for Experiment 1 at 37.1°N on day 1002. The contour interval for salinity is 0.01 (0.02) above (below) 35.69 values.

LATITUDE : 40.3N
T (DAY) : 363

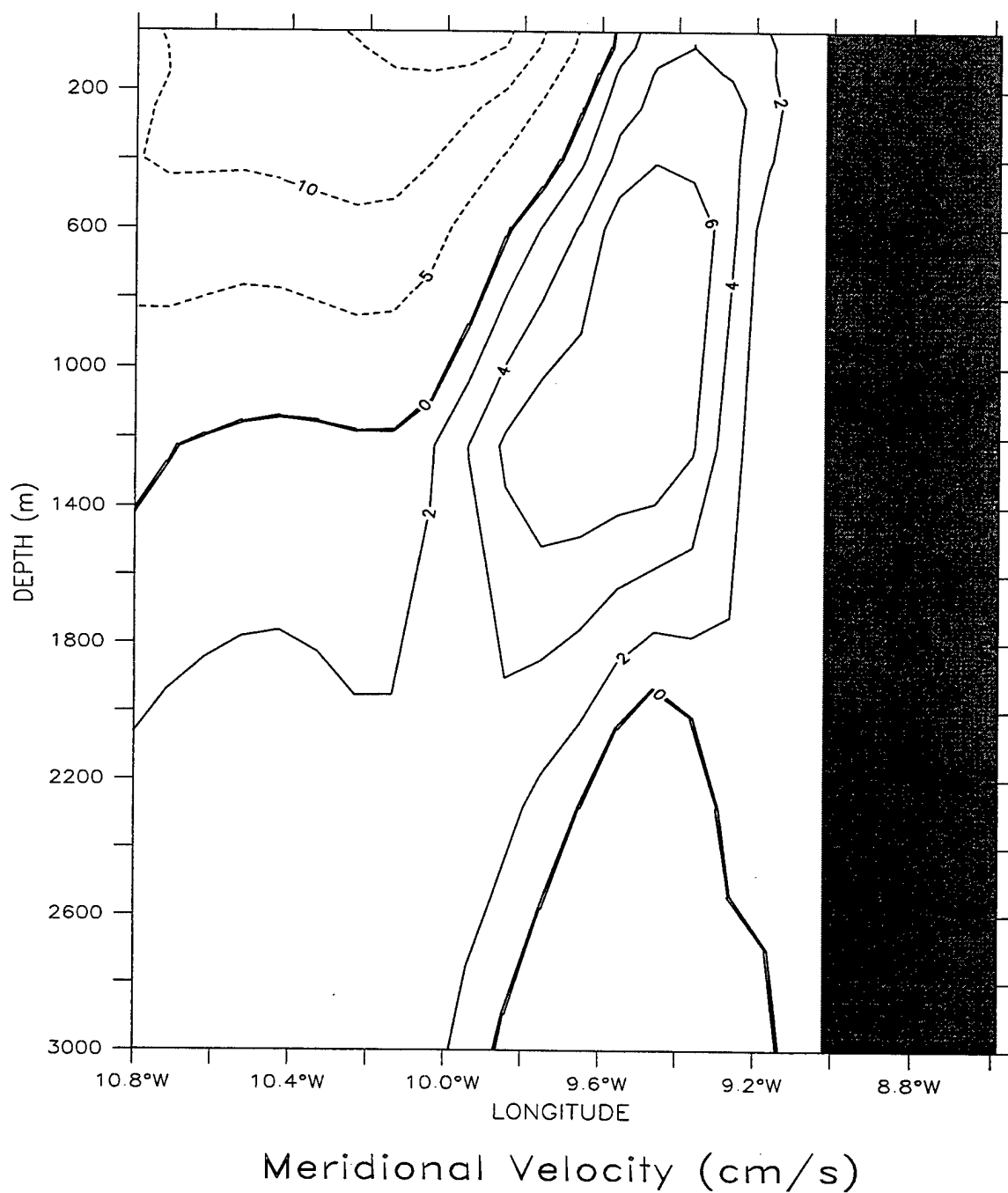


Figure 14. Cross-shore section of meridional velocity (v) at 40.3°N for Experiment 2 on day 363. Contour interval is 10 cm/s for equatorward flow (dashed lines) and 2 cm/s for poleward flow (solid lines).

DEPTH (m) : 10
T (DAY) : 216

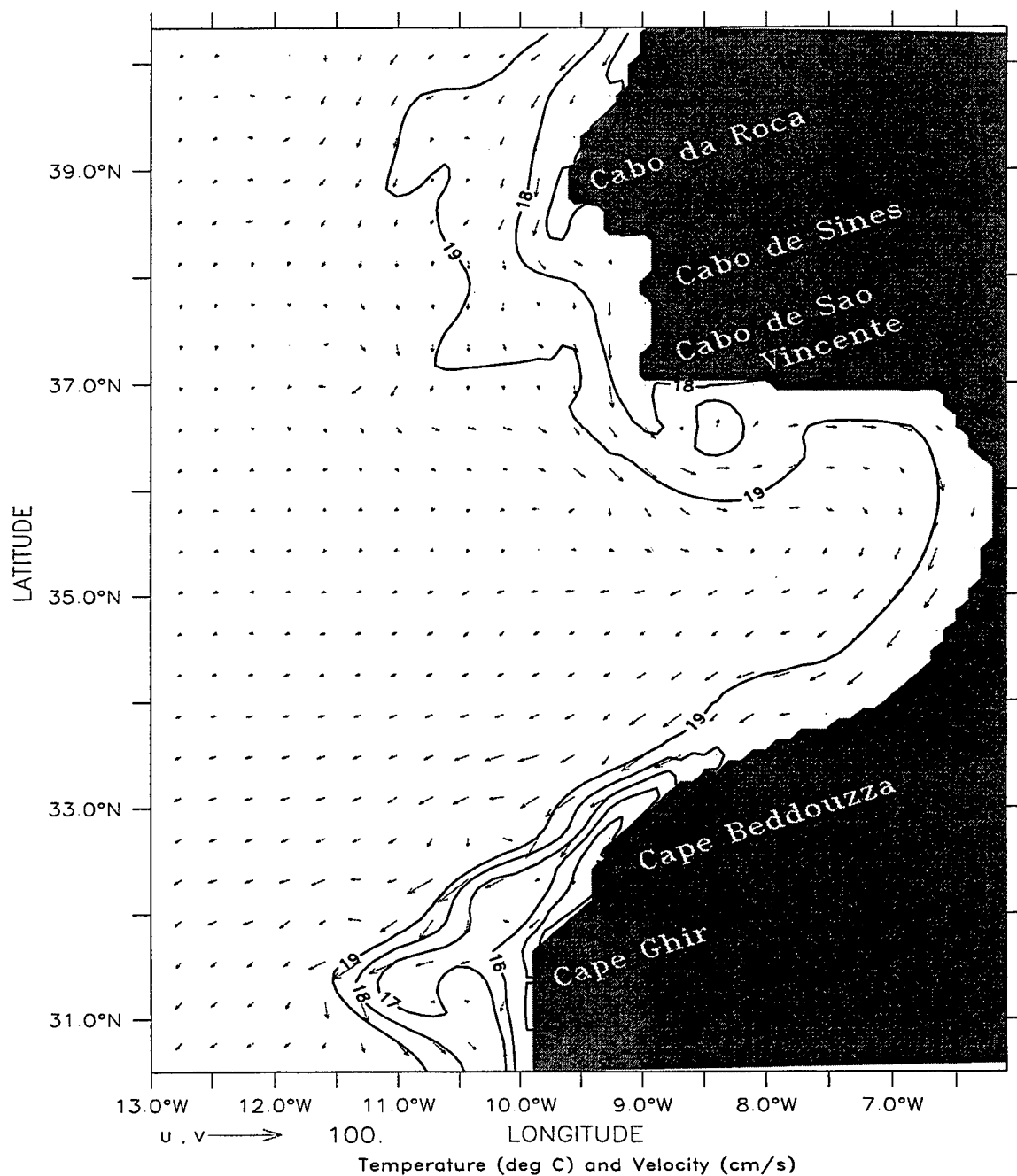


Figure 15. Temperature contours and velocity vectors at 10 m depth for Experiment 2 at day 216. To avoid clutter, velocity vectors are plotted every third (fourth) gridpoint in the cross-shore (alongshore) direction. Contour interval is 1° C. Maximum velocity vector is 100 cm/s.

LATITUDE : 37.3N
T (DAY) : 210

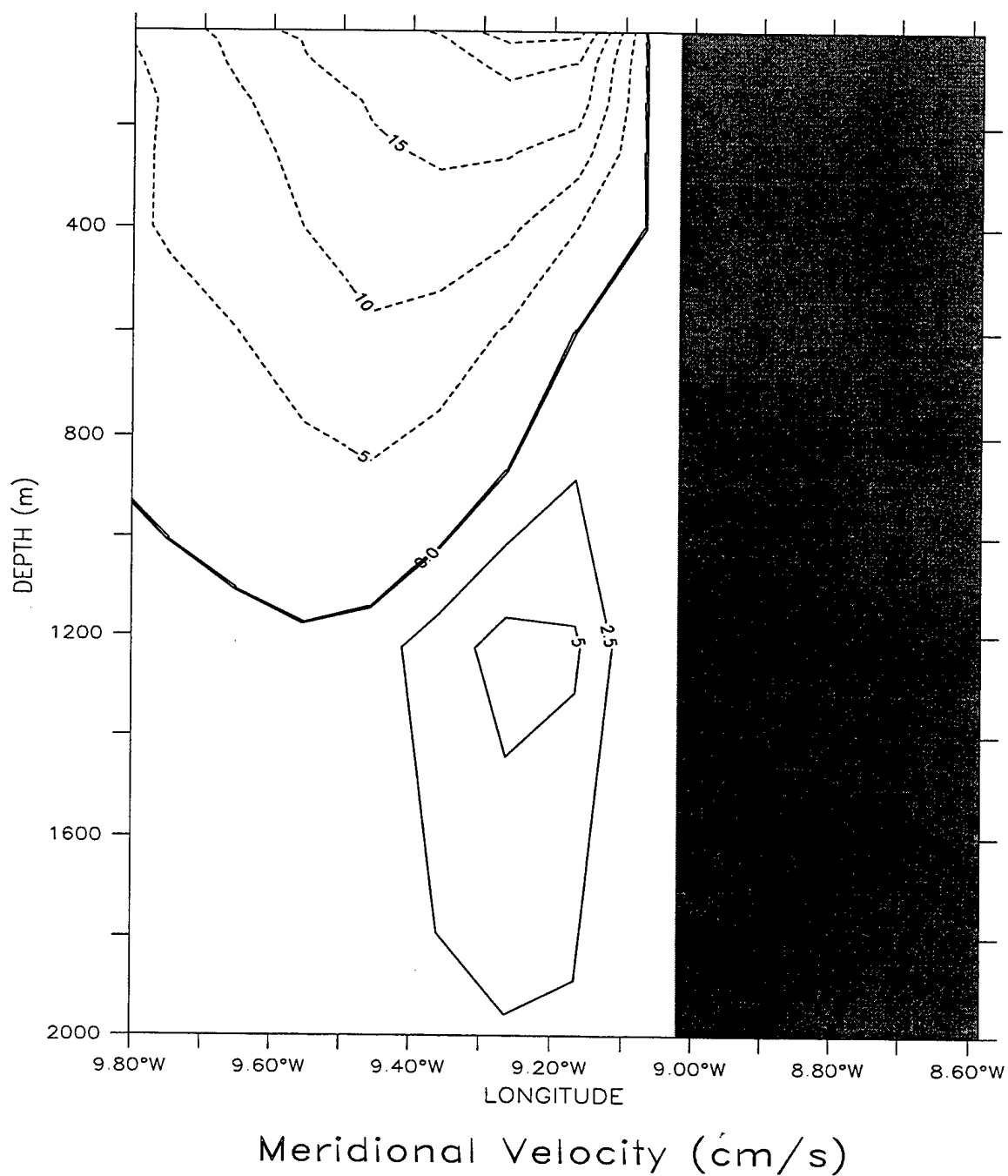


Figure 16. Cross-shore section of meridional velocity (v) at 37.3°N for Experiment 2 on day 210. Contour interval is 5 cm/s for equatorward flow (dashed lines) and 2.5 cm/s for poleward flow (solid lines).

DEPTH (m) : 10
T (DAY) : 300

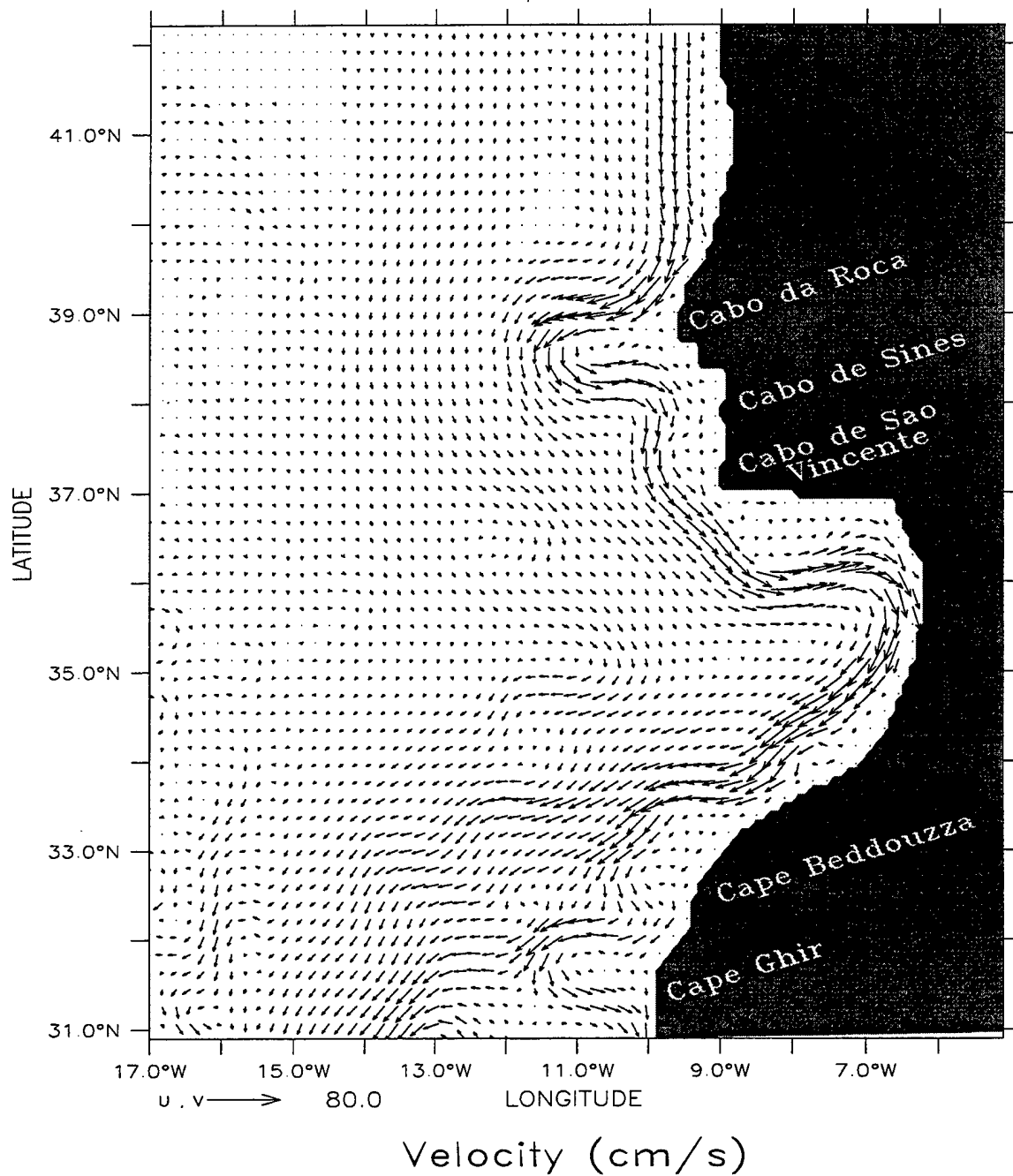


Figure 17. Velocity vectors at 10 m depth for Experiment 2 at day 300. Velocity vectors are plotted every second gridpoint in the cross-shore and alongshore directions. Maximum velocity vector is 80 cm/s.

DEPTH (m) : 1226
T (DAY) : 345

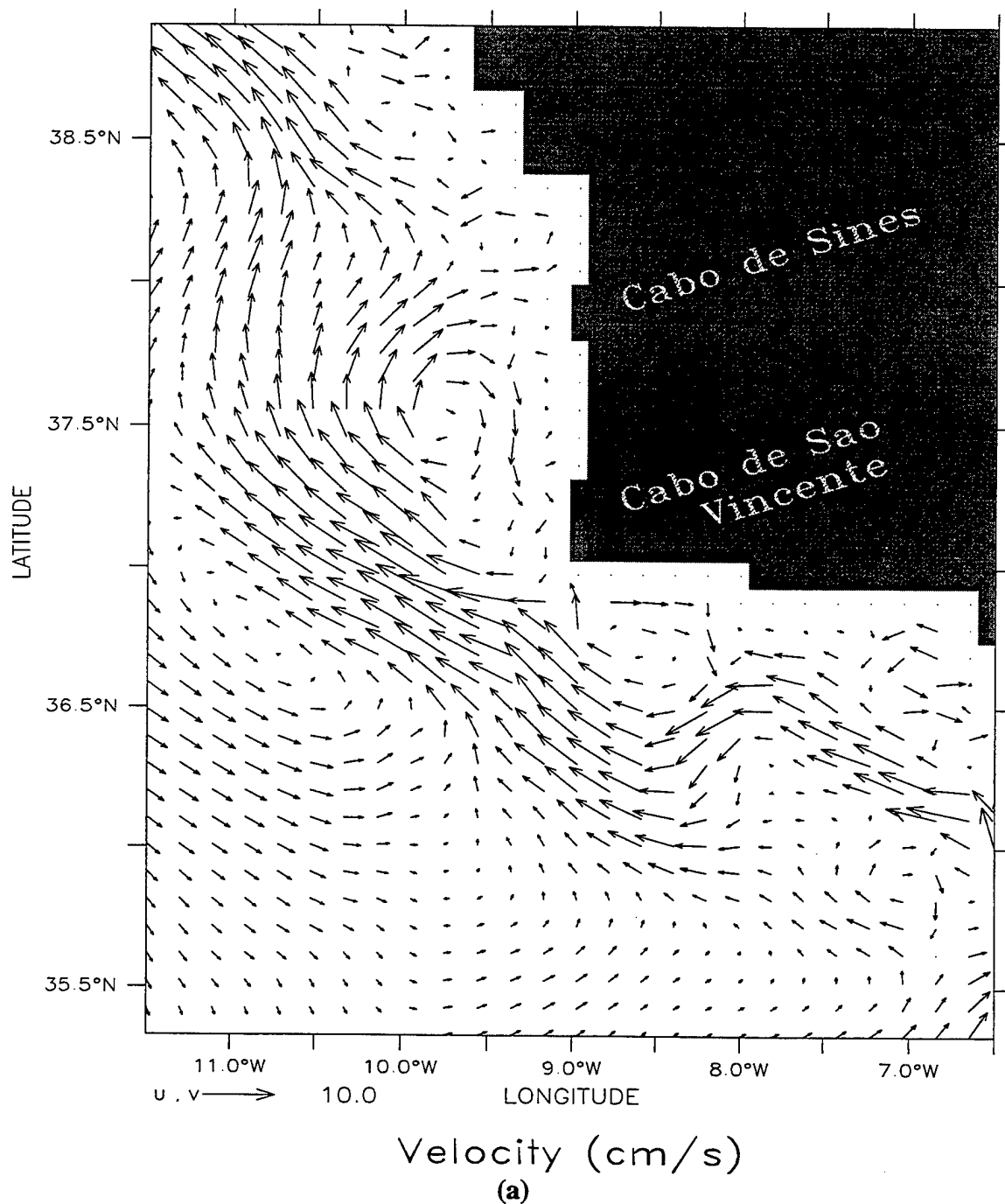
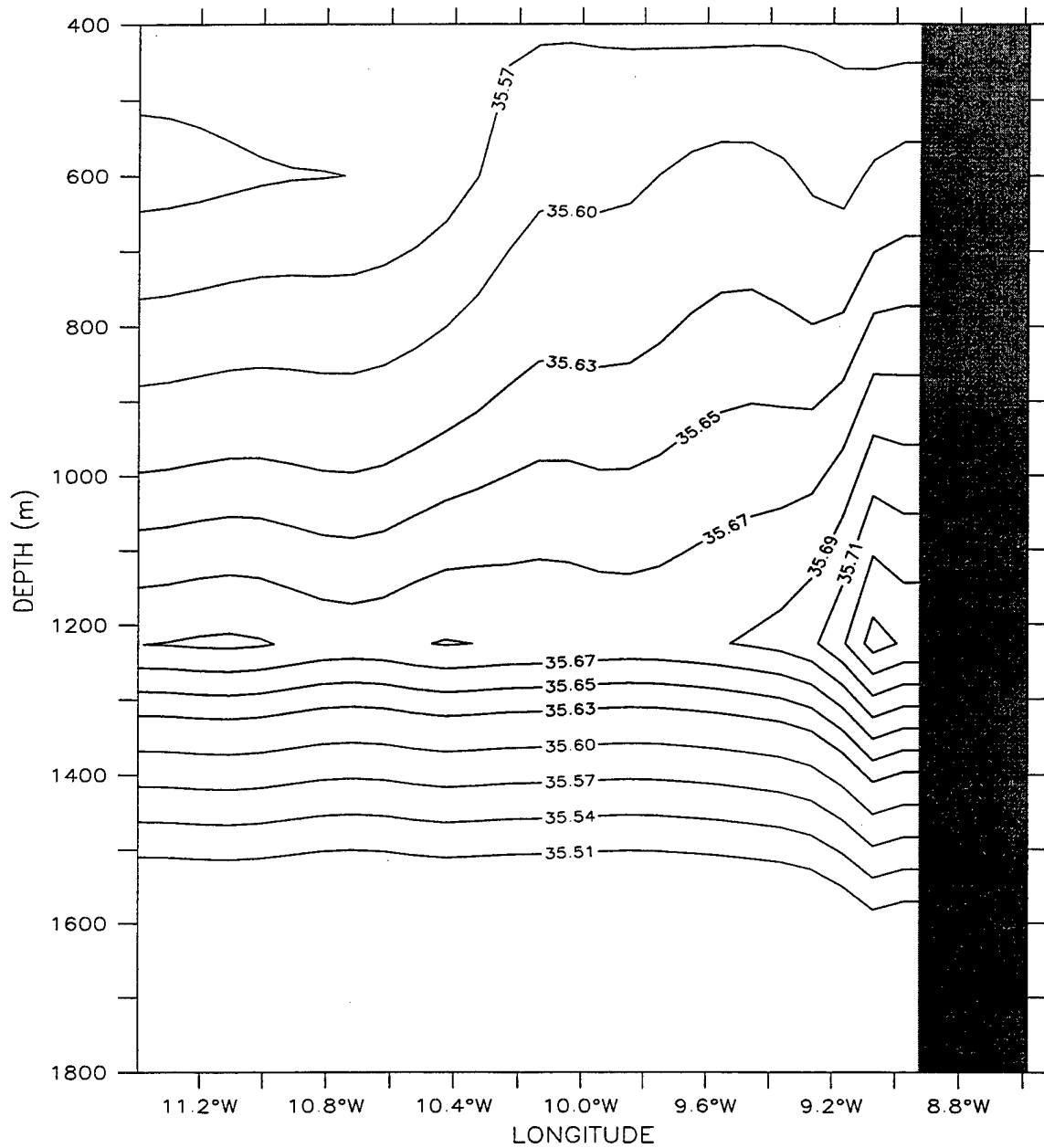


Figure 18a. Velocity vectors at 1226 m depth for Experiment 3 at day 345. Velocity vectors are plotted every second gridpoint in the cross-shore direction and at every gridpoint in the alongshore direction. Maximum velocity vector is 10 cm/s.

LATITUDE : 37.5N
T (DAY) : 273

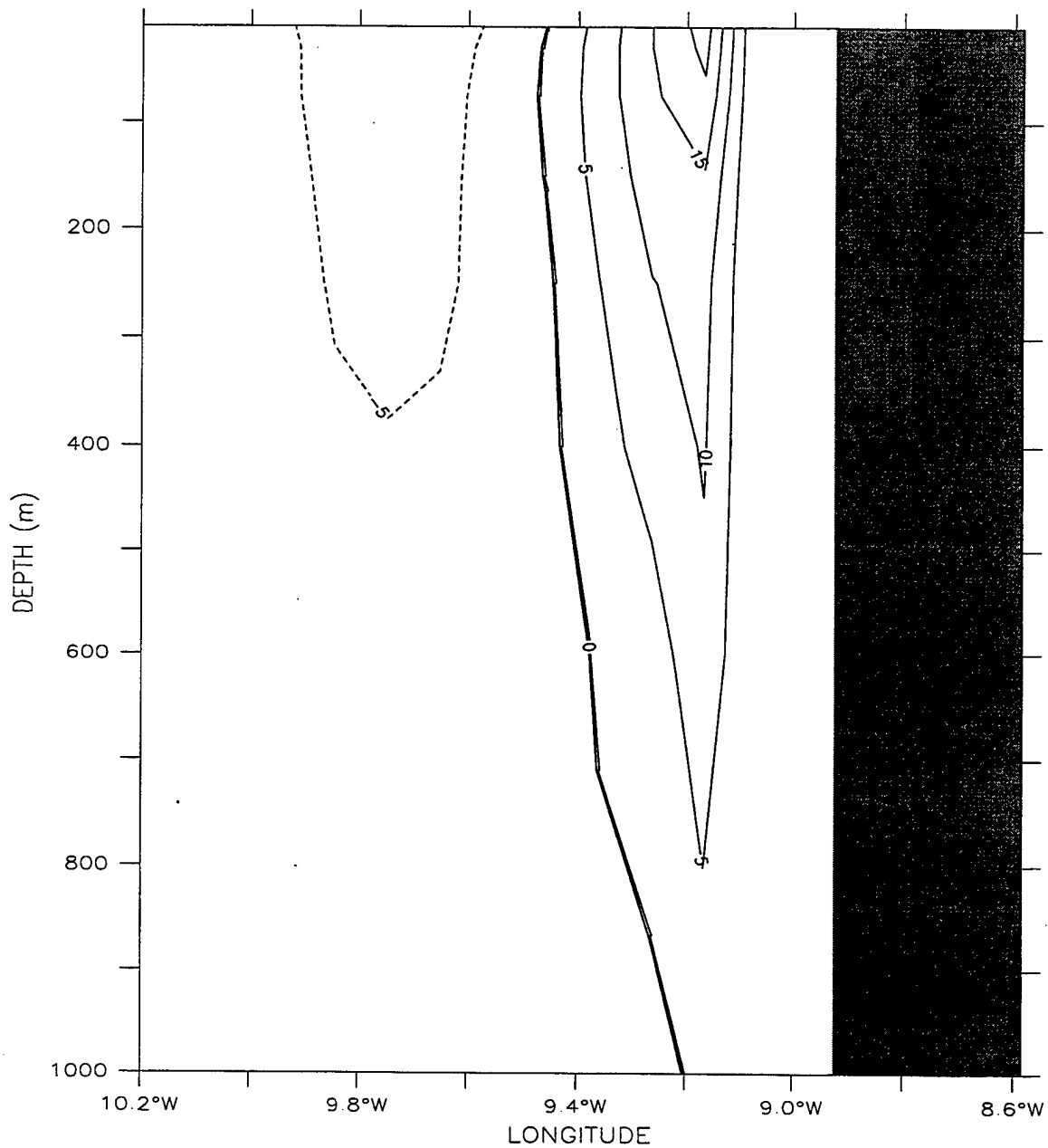


Salinity (psu)

(b)

Figure 18b. Cross-shore section of salinity for Experiment 2 at 37.5°N on day 273. The contour interval for salinity is 0.02 (0.03) above (below) 35.63 values.

LATITUDE : 41.5N
T (DAY) : 1089



Meridional Velocity (cm/s)

(a)

Figure 19a. Cross-shore section of meridional velocity (v) at 41.5°N for Experiment 2 on day 1089. Contour interval is 5 cm/s for equatorward flow (dashed lines) and for poleward flow (solid lines).

DEPTH (m) : 10
T (DAY) : 978

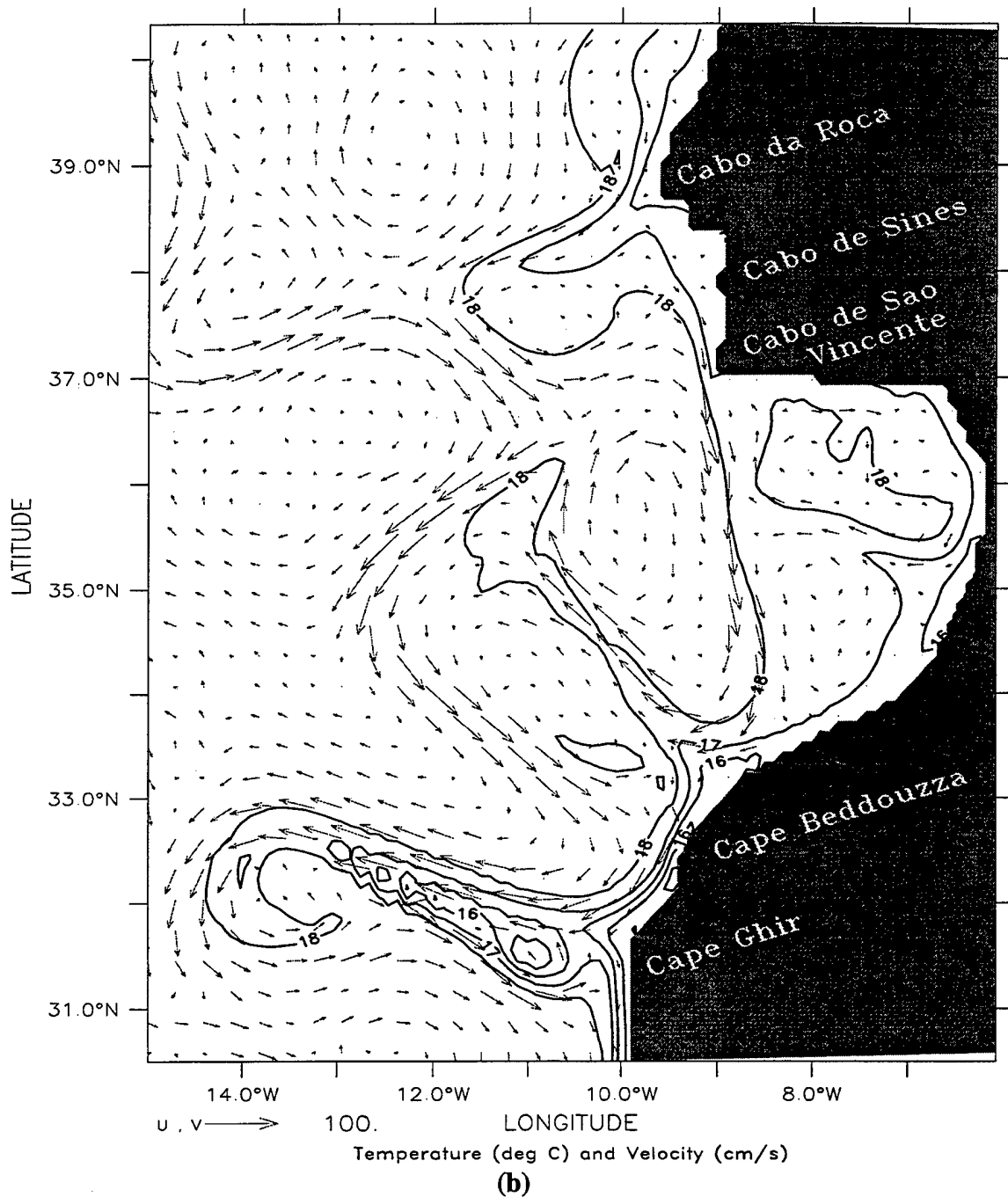
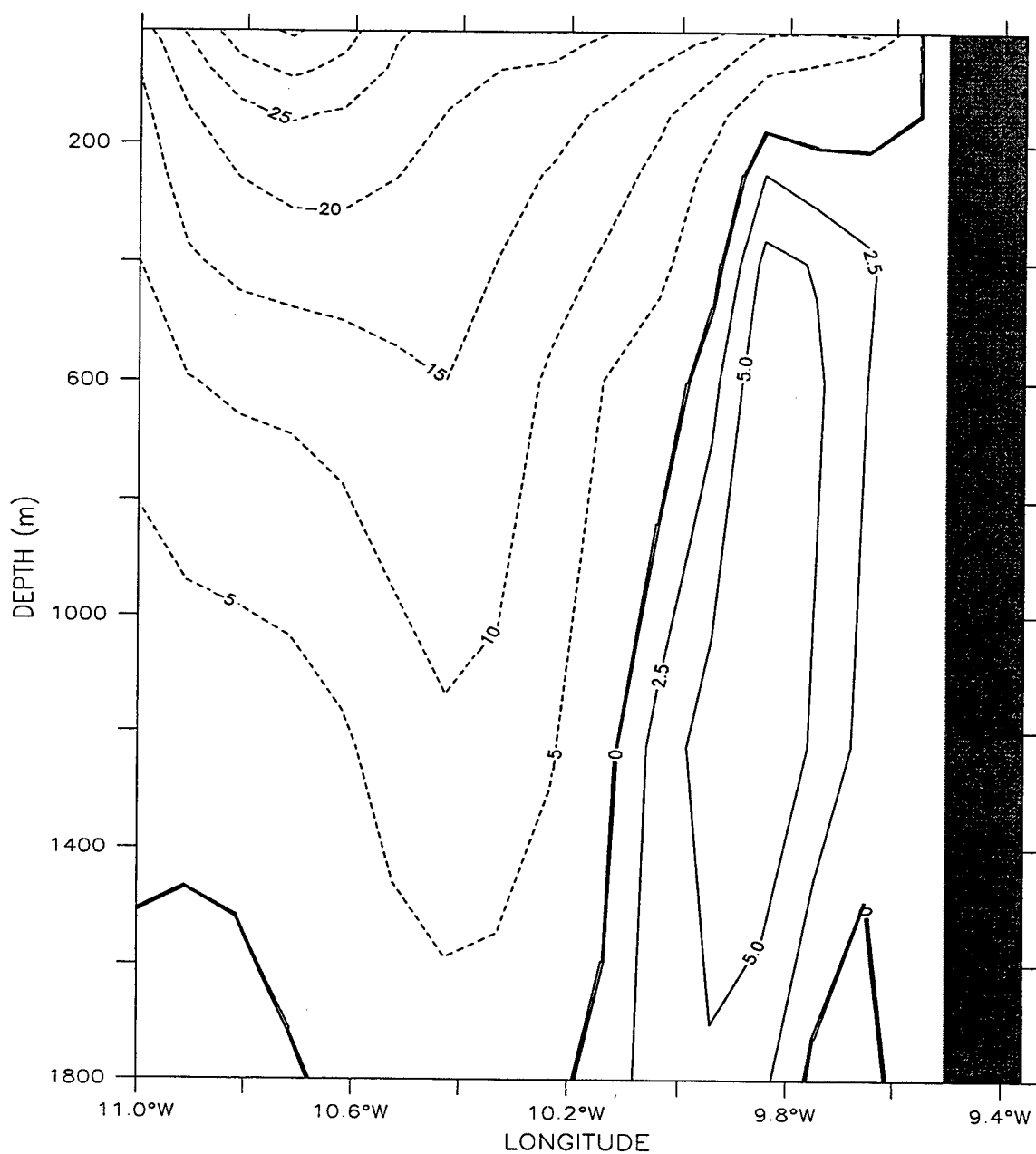


Figure 19b. Temperature contours and velocity vectors at 10 m depth for Experiment 2 at day 978. To avoid clutter, velocity vectors are plotted every third gridpoint in the cross-shore and alongshore directions. Contour interval is 1° C. Maximum velocity vector is 100 cm/s.

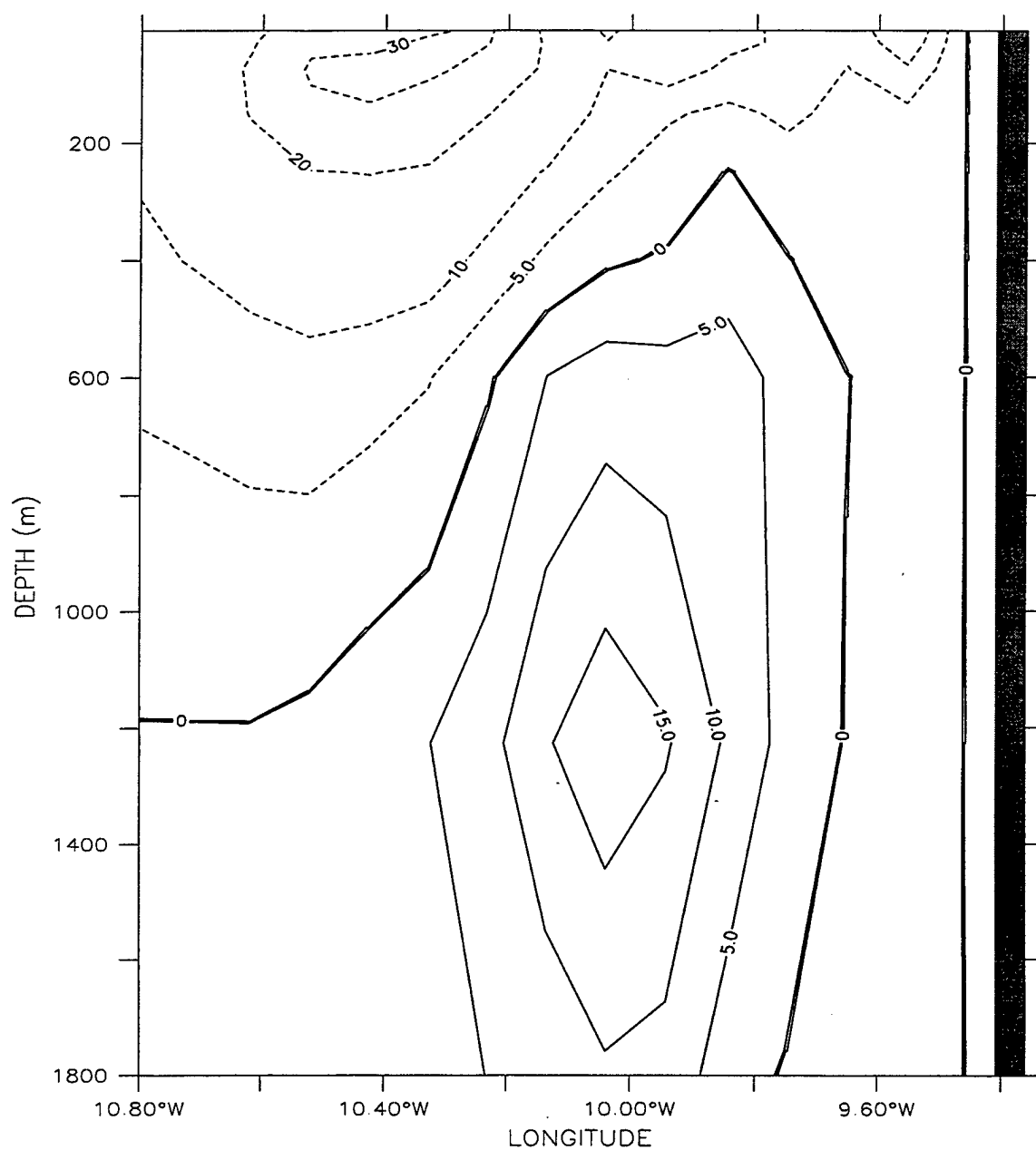
LATITUDE : 39.3N
T (DAY) : 909



Meridional Velocity (cm/s)
(c)

Figure 19c. Cross-shore section of meridional velocity (v) at 39.3°N for Experiment 2 on day 909. Contour interval is 10 cm/s for equatorward flow (dashed lines) and 2.5 cm/s for poleward flow (solid lines).

LATITUDE : 32.3N
T (DAY) : 816



Meridional Velocity (cm/s)
(d)

Figure 19d. Cross-shore section of meridional velocity (v) at 32.3°N for Experiment 2 on day 816. Contour interval is 10 cm/s for equatorward flow (dashed lines, with an additional 5 cm/s contour added) and 5 cm/s for poleward flow (solid lines).

DEPTH (m) : 10

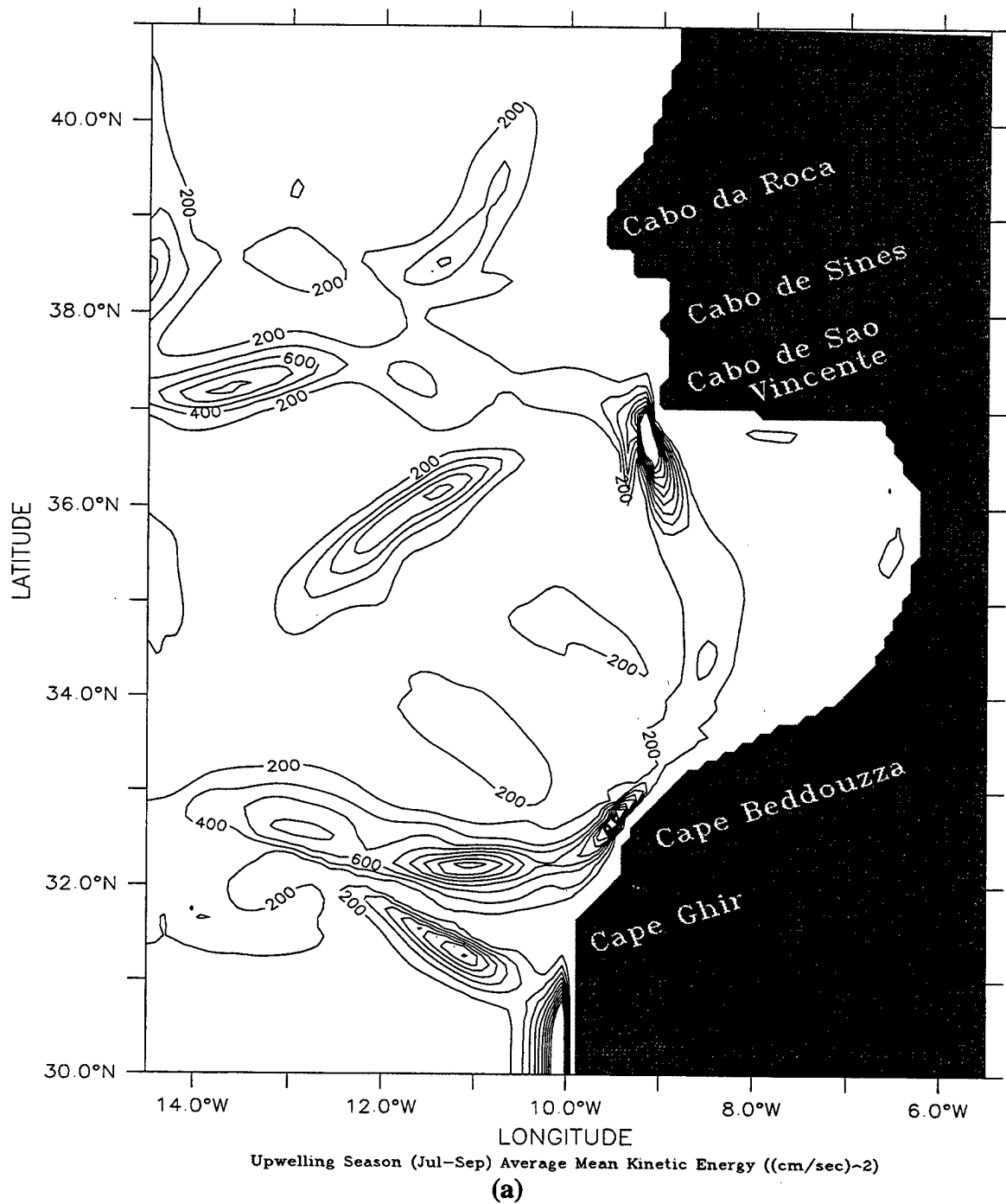


Figure 20a. Horizontal map at 10 m depth of average mean kinetic energy (MKE) for Experiment 2 in the third year of the model simulation, time averaged for July through September. Contour interval is 200 (cm/s)².

DEPTH (m) : 10

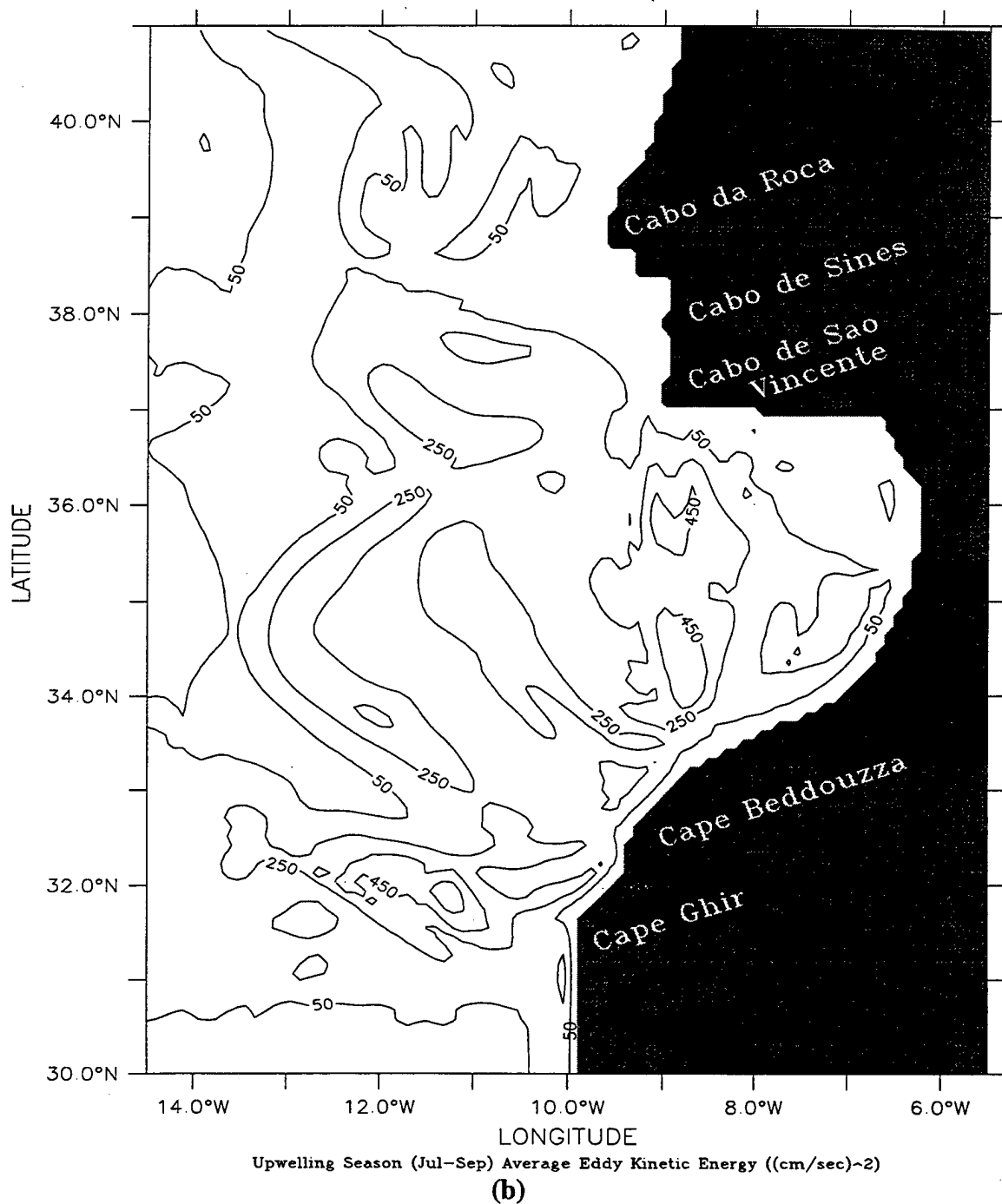


Figure 20b. Horizontal map at 10 m depth of average eddy kinetic energy (EKE) for Experiment 2 in the third year of the model simulation, time averaged for July through September. Contour interval is 200 (cm/s)².

DEPTH (m) : 10

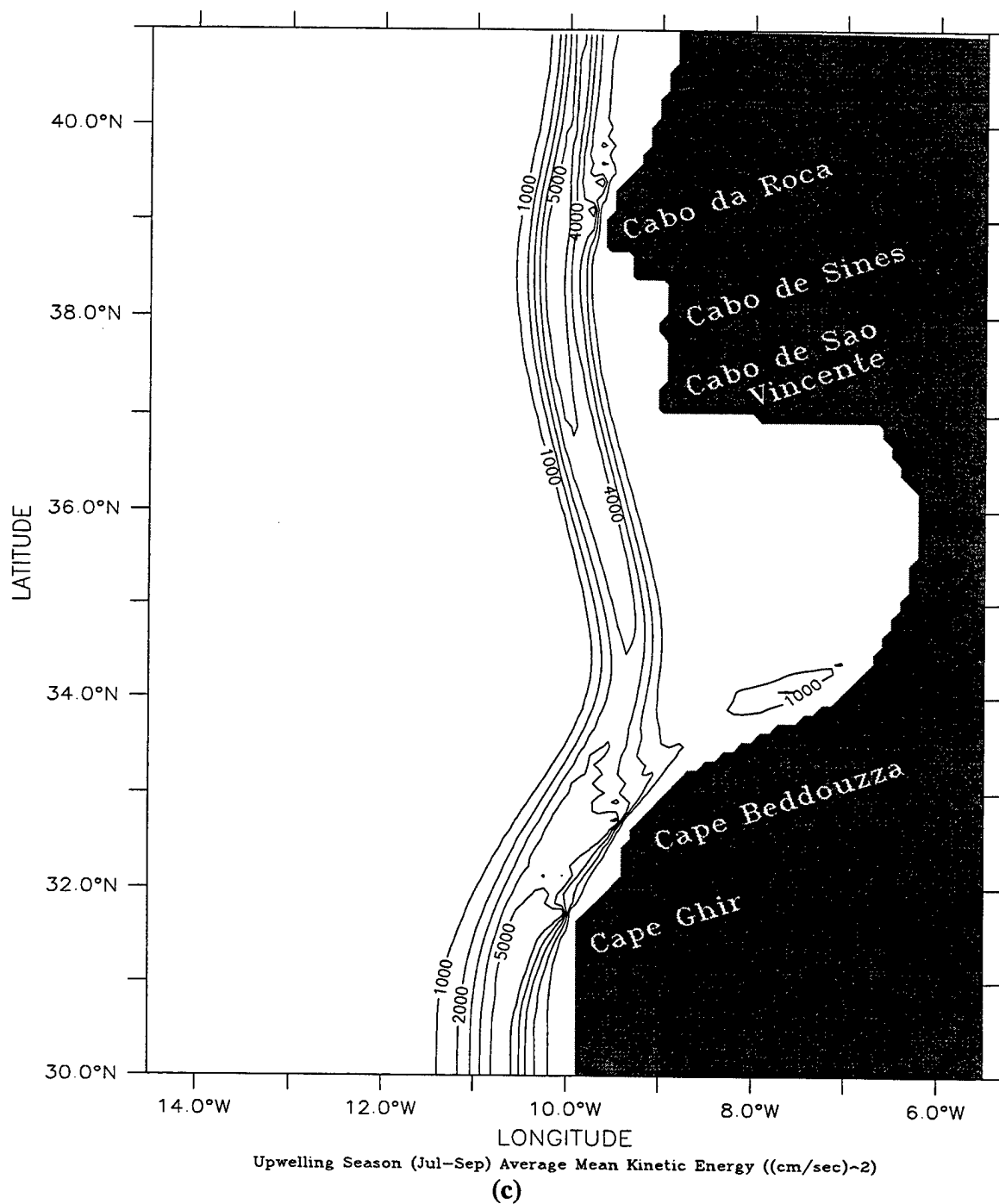


Figure 20c. Horizontal map at 10 m depth of average mean kinetic energy (MKE) for Experiment 1 in the third year of the model simulation, time averaged for July through September. Contour interval is 1000 (cm/s)².

DEPTH (m) : 10

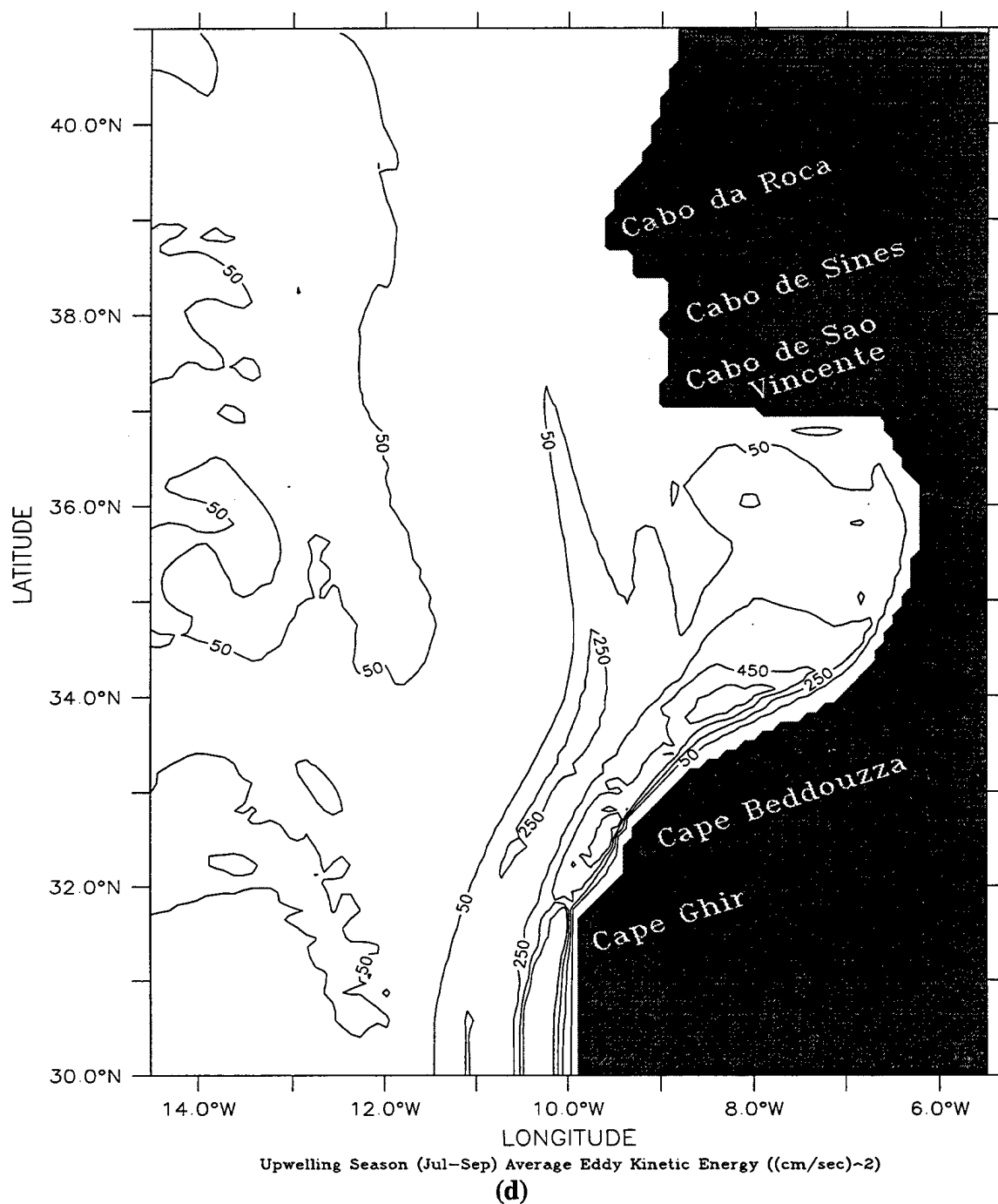


Figure 20d. Horizontal map at 10 m depth of average eddy kinetic energy (EKE) for Experiment 1 in the third year of the model simulation, time averaged for July through September. Contour interval is 200 (cm/s)².

DEPTH (m) : 1226
T (DAY) : 1059

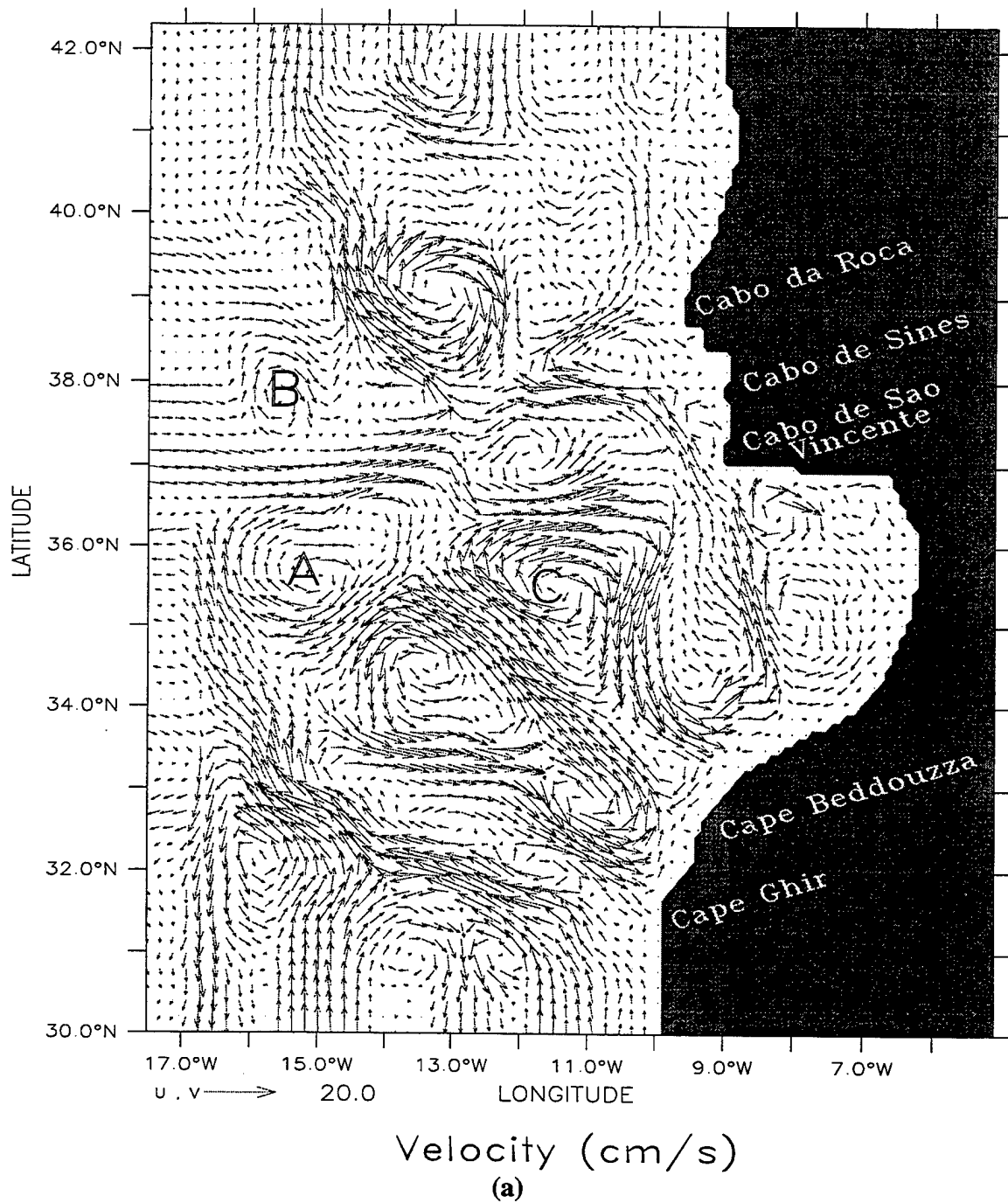
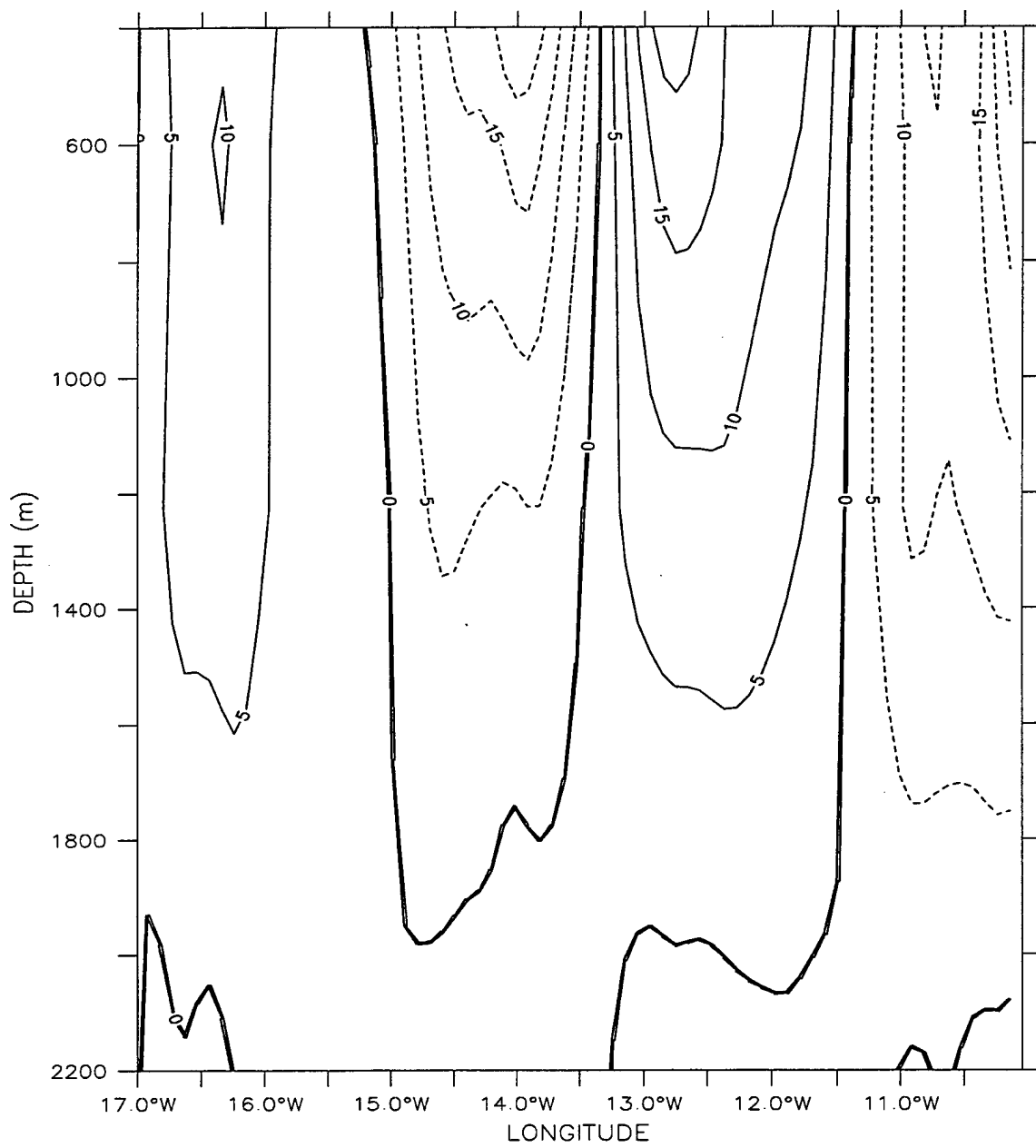


Figure 21a. . Velocity vectors at 1226 m depth for Experiment 2 at day 1059. Velocity vectors are plotted every second gridpoint in the cross-shore and alongshore directions. Maximum velocity vector is 20 cm/s. Meddies are labeled "A", "B", and "C".

LATITUDE : 35.5N
T (DAY) : 1059

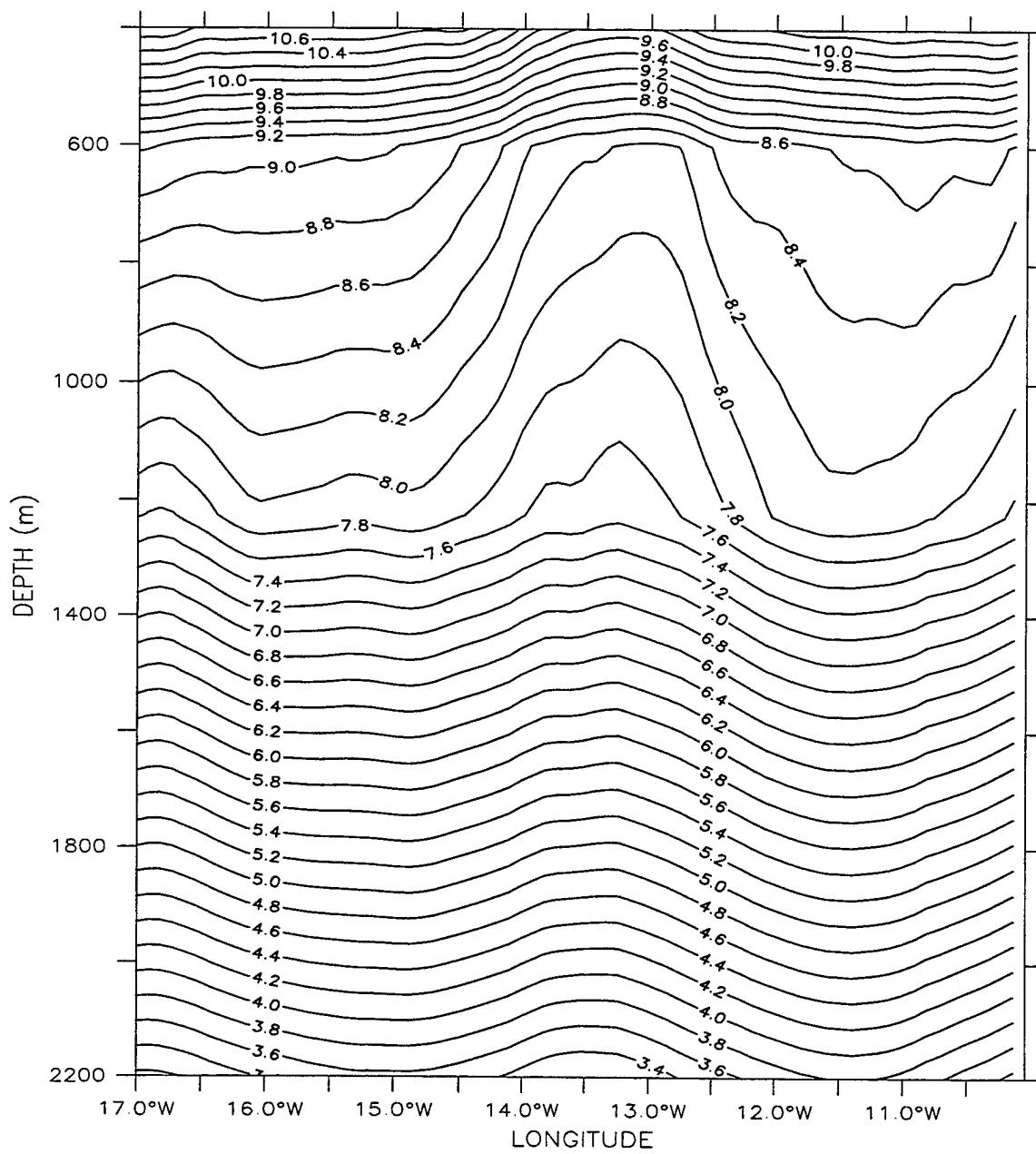


Meridional Velocity (cm/s)

(b)

Figure 21b. Cross-shore section of meridional velocity (v) at 35.5°N for Experiment 2 on day 1059. Contour interval is 5 cm/s for equatorward flow (dashed lines) and poleward flow (solid lines).

LATITUDE : 35.5N
T (DAY) : 1059

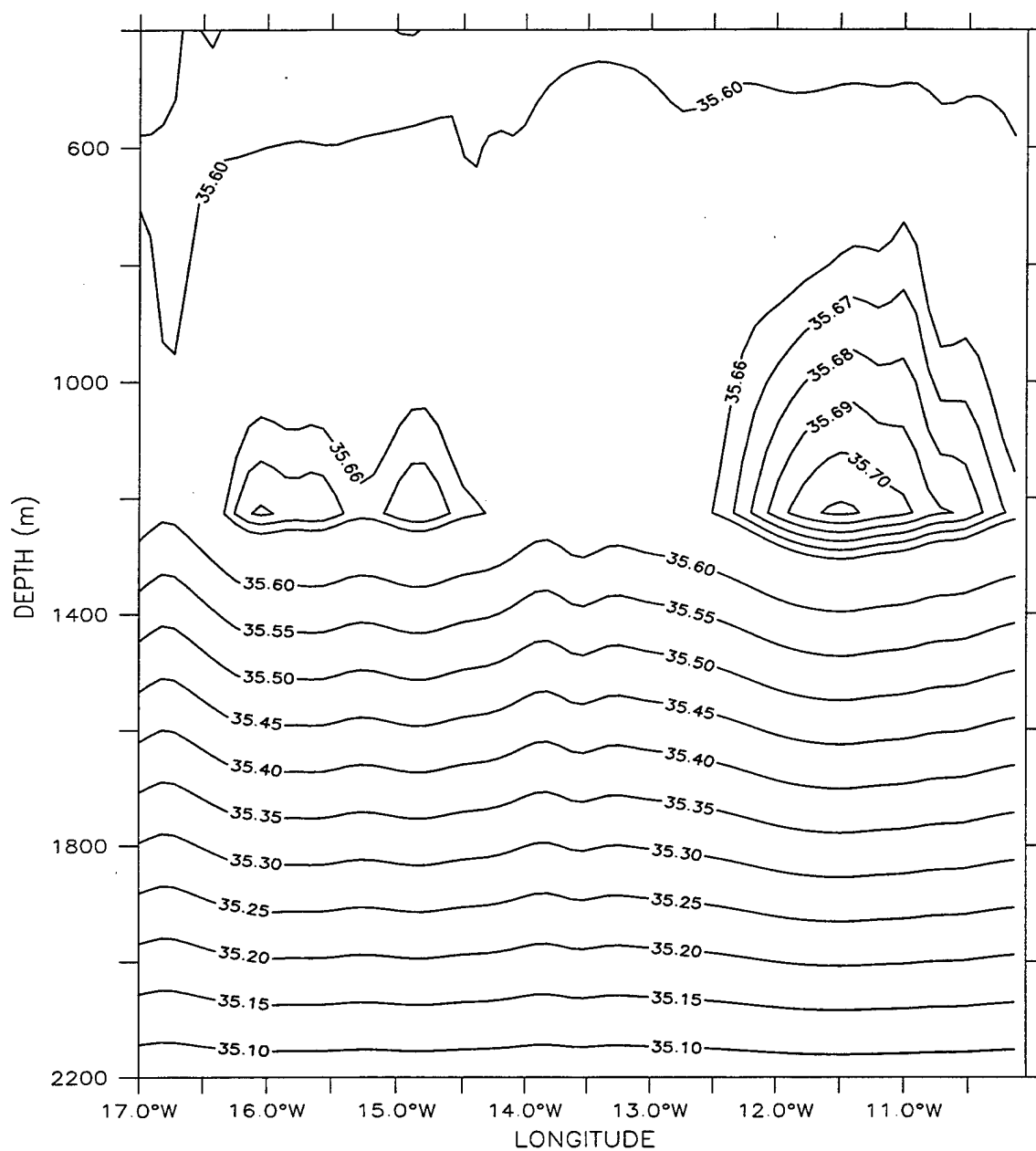


Temperature (deg C)

(c)

Figure 21c. Cross-shore section of temperature for Experiment 2 at 35.5°N on day 1059. The contour interval for temperature is 0.2°C.

LATITUDE : 35.5N
T (DAY) : 1059



(d)

Figure 21d. Cross-shore section of salinity for Experiment 2 at 35.5°N on day 1059. The contour interval for salinity is 0.01 (0.05) above (below) 35.66 (35.60) values.

LATITUDE : 37.1N
T (DAY) : 273

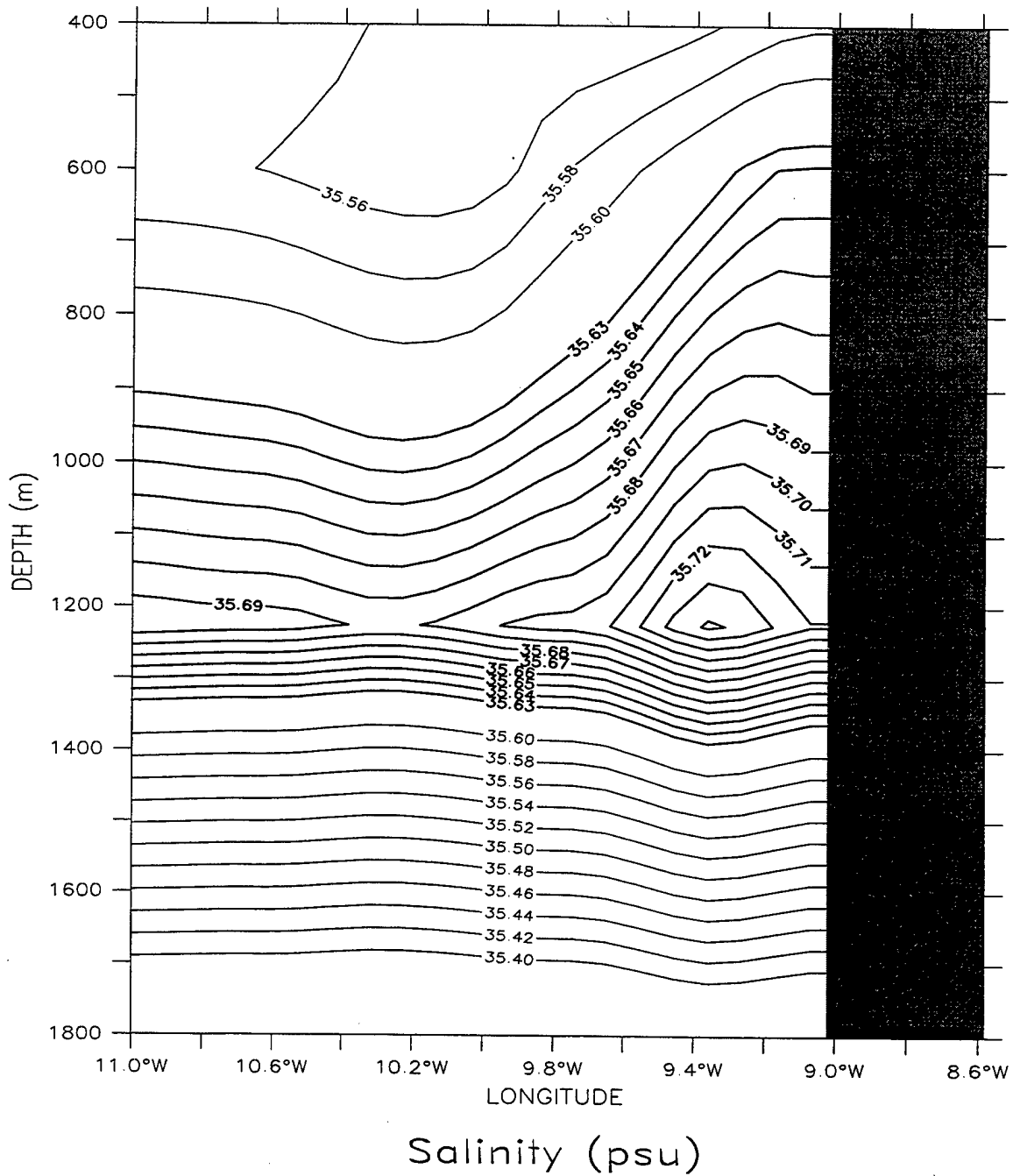


Figure 22. Cross-shore section of salinity for Experiment 4 at 37.1°N on day 273. The contour interval for salinity is 0.01 (0.02) above (below) 35.63 (35.60) values.

DEPTH (m) : 1226
T (DAY) : 1068

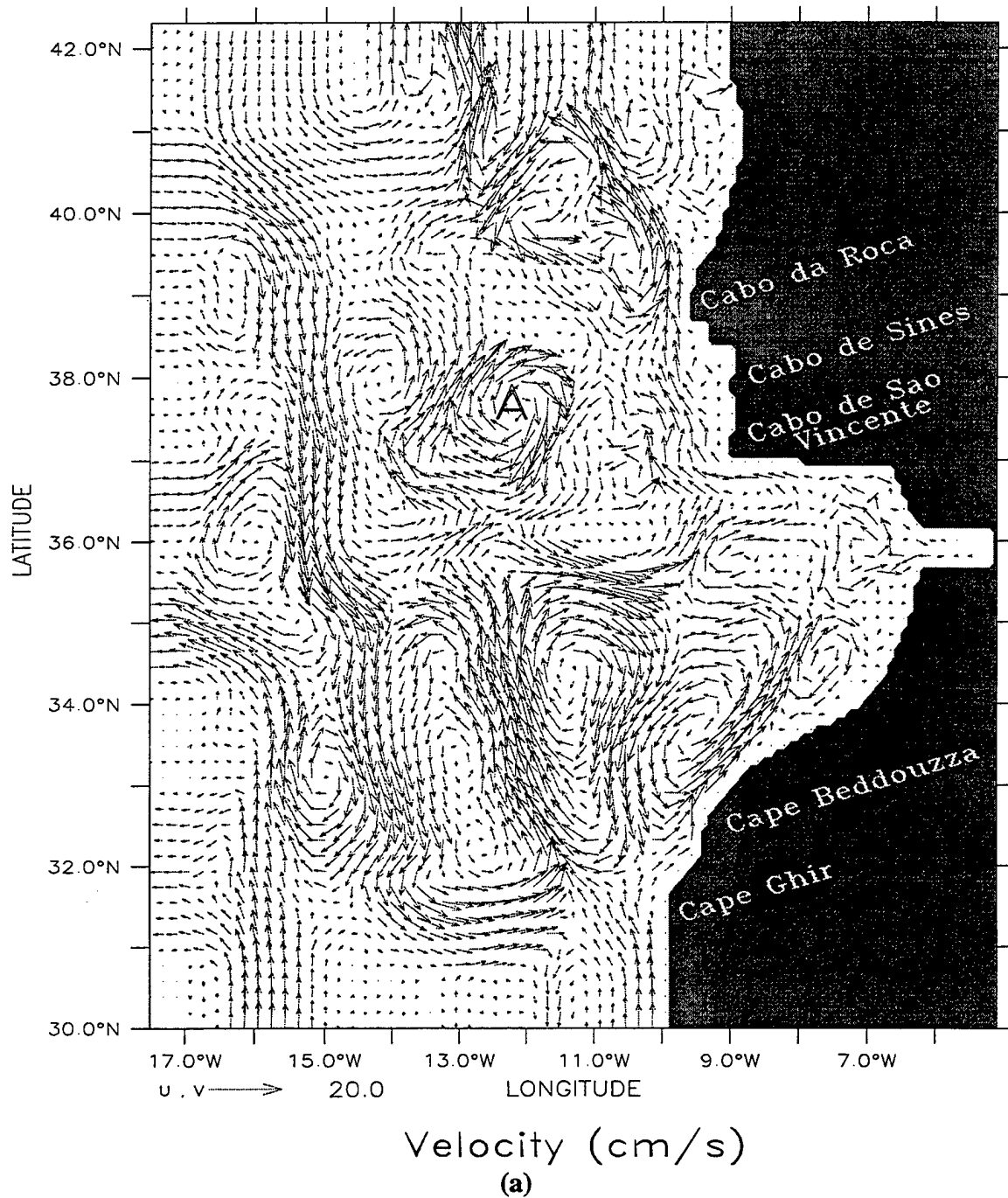
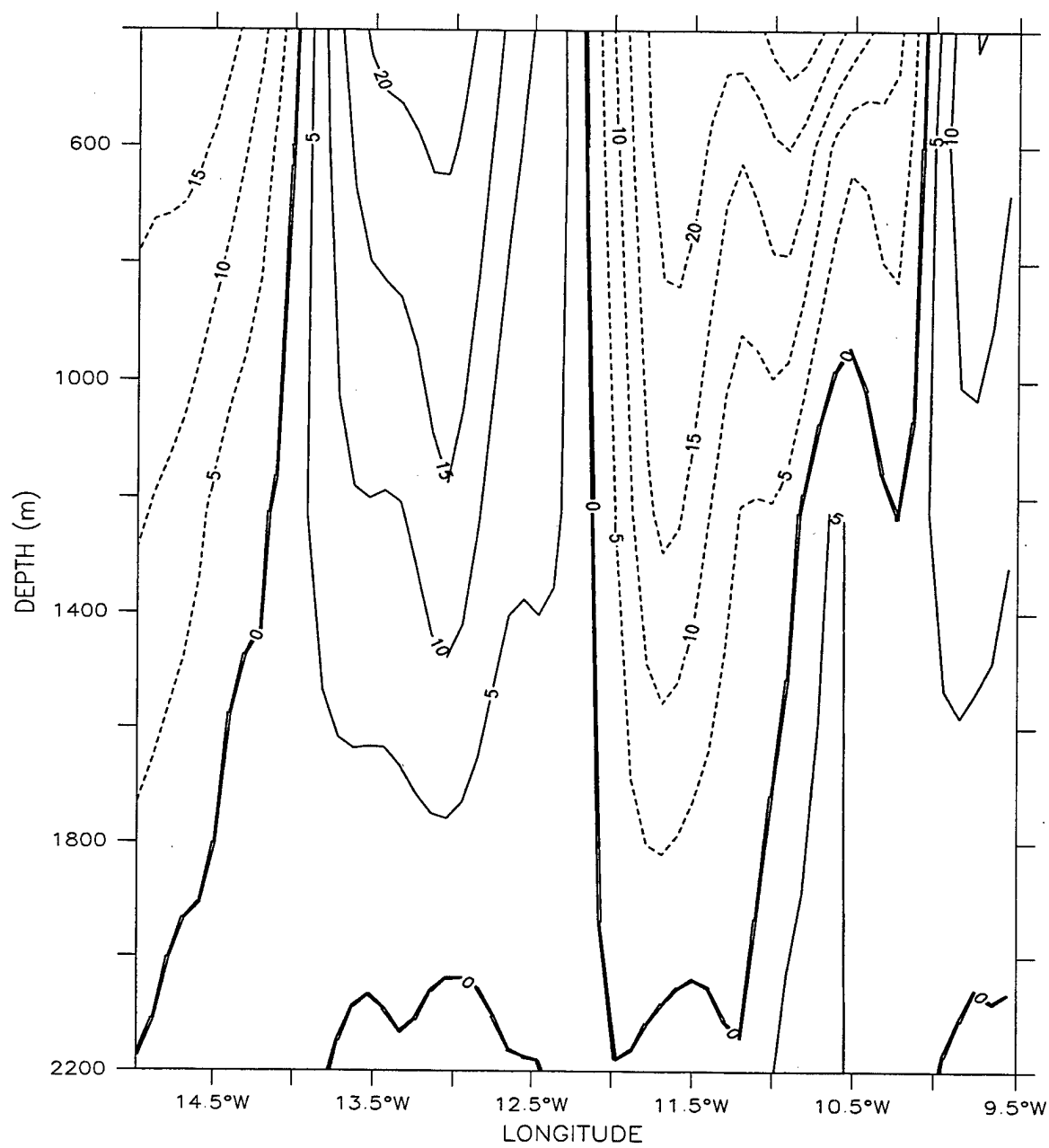


Figure 23a. . Velocity vectors at 1226 m depth for Experiment 4 at day 1068. Velocity vectors are plotted every second gridpoint in the cross-shore and alongshore directions. Maximum velocity vector is 20 cm/s. Meddy "A" is labeled.

LATITUDE : 37.7N
T (DAY) : 1068

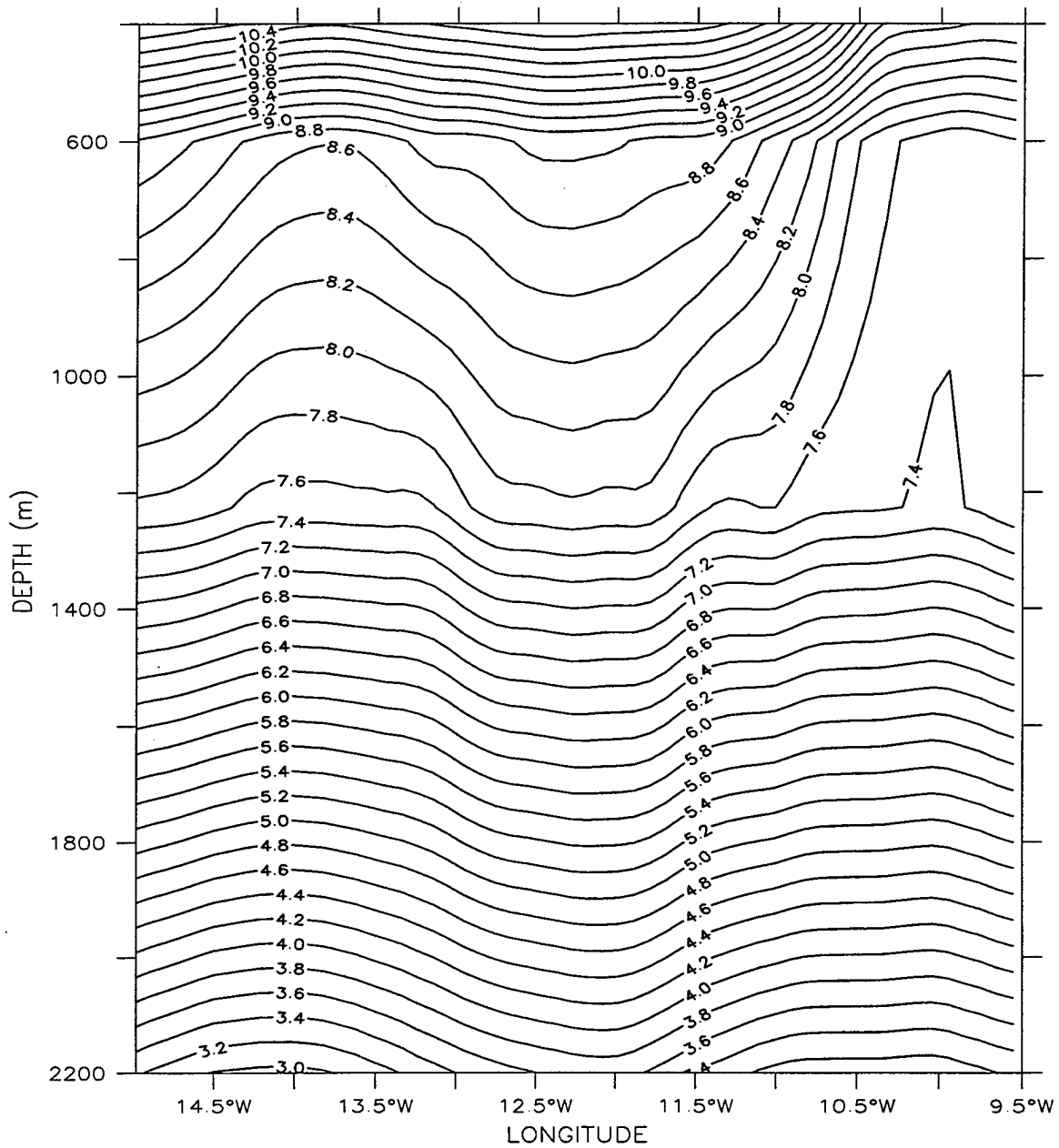


Meridional Velocity (cm/s)

(b)

Figure 23b. Cross-shore section of meridional velocity (v) at 37.7°N for Experiment 4 on day 1068. Contour interval is 5 cm/s for equatorward flow (dashed lines) and poleward flow (solid lines).

LATITUDE : 37.7N
T (DAY) : 1068



Temperature (deg C)
(c)

Figure 23c. Cross-shore section of temperature for Experiment 4 at 37.7°N on day 1068. The contour interval for temperature is 0.2 °C.

LATITUDE : 37.7N
T (DAY) : 1068

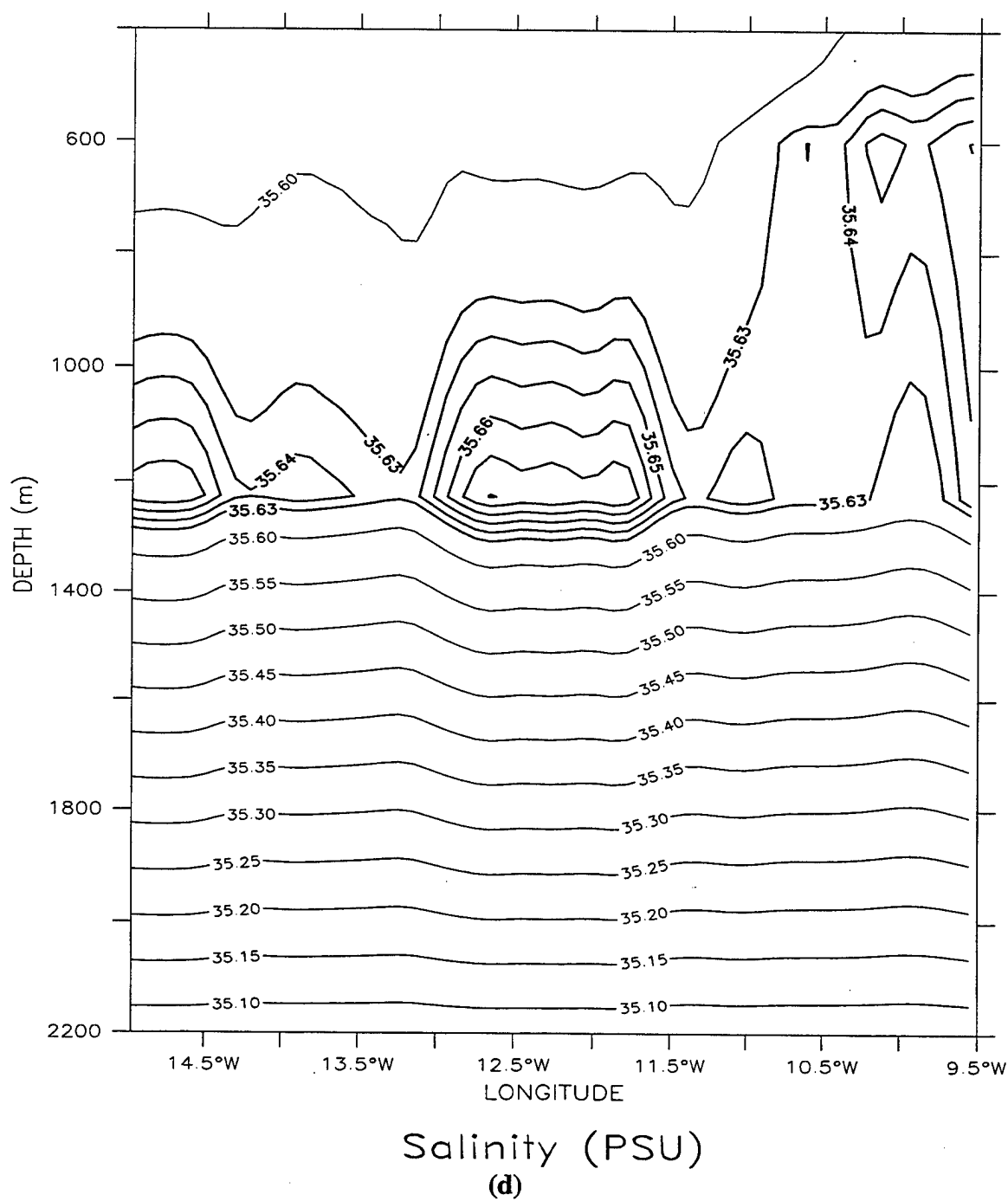


Figure 23d. Cross-shore section of salinity for Experiment 4 at 37.7°N on day 1068. The contour interval for salinity is 0.01 (0.05) above (below) 35.63 (35.60) values.

T (DAY) : 1068



Figure 23e. Temperature contours and velocity vectors for Experiment 4 at 1226 m depth on day 1068. The contour interval is 0.02°C. The maximum current velocity is 20 cm/s.

THIS PAGE INTENTIONALLY LEFT BLANK

Table 1. Summary of Batteen (1989) specific experimental design.

Cases	Coastline	Coriolis Parameterization	Type of Wind Stress (steady wind)
1	Straight	f -plane	constant
2	Straight	β -plane	constant
3	Straight	f -plane	alongshore-varying
4	Straight	β -plane	alongshore-varying

Table 2. Summary of Batteen (1997) specific experimental design.

Cases	Coastline	Coriolis Parameterization	Type of Wind Stress (steady wind)
1	Straight	β -plane	alongshore-varying
2a	Straight	f -plane	alongshore-varying
2b	Straight	f -plane	alongshore-varying
2c	Straight	f -plane	constant
2d	Straight	f -plane	constant (interior only)
3	Irregular	β -plane	alongshore-varying

Table 3. Summary of Batteen(2000) specific experimental design.

Cases	Coastline	Coriolis Parameterization	Annual Mediterranean Outflow and Thermohaline Forcing
1	Straight	β -plane	NO
2	Ideal Irregular	β -plane	NO
3	Realistic Irregular	β -plane	NO
4	Realistic Irregular	β -plane	YES

Table 4. Summary of specific experimental design in this study.

Cases	Coastline	Coriolis Parameterization	Thermohaline Gradients	Annual or Seasonal MO
1	Realistic Irregular	f -plane	YES	Annual
2	Realistic Irregular	β -plane	YES	Annual
3	Realistic Irregular	f -plane	YES	Seasonal
4	Realistic Irregular	β -plane	YES	Seasonal

Table 5. Values of constants used in the model

Constant	Value	Definition
T_0	278.2°K	Constant Reference Temperature
S_0	34.7	Constant Reference Salinity
ρ_0	1.0276 gm cm ³	Density of Sea Water At T_0 and S_0
α	$2.4 \times 10^{-4} (\text{°K})^{-1}$	Thermal Expansion Coefficient
β	7.5×10^{-4}	Saline Expansion Coefficient
K	10	Number of Levels In Vertical
Δx	9.0×10^5 cm	Cross-Shore Grid Spacing
Δy	1.1×10^6 cm	Alongshore Grid Spacing
H	4.5×10^5 cm	Total Ocean Depth
Δt	800 s	Time Step
f_0	$0.86 \times 10^4 \text{ s}^{-1}$	Mean Coriolis Parameter
g	980 cm s ²	Acceleration of Gravity
A_M	$2 \times 10^{17} \text{ cm}^4 \text{ s}^{-1}$	Bi-harmonic Momentum Diffusion Coefficient
A_H	$2 \times 10^{17} \text{ cm}^4 \text{ s}^{-1}$	Bi-harmonic Heat Diffusion Coefficient
K_M	$0.5 \text{ cm}^2 \text{ s}^{-1}$	Vertical Eddy Viscosity
K_H	$0.5 \text{ cm}^2 \text{ s}^{-1}$	Vertical Eddy Conductivity

Table 6: Annual salinity profiles for MO

Layer	(Depth in meters)	Salinity (psu)
1	10	36.07
2	30	36.05
3	75	36.05
4	150	36.05
5	250	36.05
6	400	35.75
7	600	35.75
8	1226	36.25

THIS PAGE INTENTIONALLY LEFT BLANK

LIST OF REFERENCES

- Ambar, I., Mediterranean influence off Portugal, in *Actual problems of oceanography in Portugal, Junta Nacional de Investigacao Cientifica e Tecnologica, Lisboa*, 73-87, 1982.
- Ambar, I., and M.R. Howe. Observations of the Mediterranean outflow – 1. Mixing in the Mediterranean outflow. *Deep-Sea Res.*, 26, 535-554, 1979.
- Arakawa, A. and V. R. Lamb, Computational design of the basic dynamical processes of the UCLA general circulation model, *Methods Comput. Phys.*, 17, 173-265, 1977.
- Barton, E.D., Eastern boundary of the North Atlantic: Northwest Africa and Iberia. In *The Sea, Vol. 11, The Global Coastal Ocean: Regional Studies and Syntheses*, K.H. Brink and A.R. Robinson, eds., Wiley, New York, Chap.22, 633-657, 1998.
- Batteen, M. L., Wind-forced modeling studies of currents, meanders, and eddies in the California Current System, *J. Geophys. Res.*, 102, 985-1009, 1997.
- Batteen, M. L. and Y. -J. Han, On the computational noise of finite difference schemes used in ocean models, *Tellus*, 33, 387-396, 1981.
- Batteen, M. L., J. R. Martinez, D. W. Bryan, and E. J. Buch, A modeling study of the coastal eastern boundary current system off Iberia and Morocco, *J. Geophys. Res.*, 2000, In press.
- Batteen, M. L., R. L. Haney, T. A. Tielking, and P. G. Renaud, A numerical study of wind forcing of eddies and jets in the California Current System, *J. Mar. Res.*, 47, 493-523, 1989.
- Camerlengo, A. L. and J. J. O'Brien, Open boundary conditions in rotating fluids, *J. Comput. Phys.*, 89, 12-35, 1980.
- Daniault, N., J. P. Maze, and M. Arhan, Circulation and mixing of Mediterranean Water west of the Iberian Peninsula, *Deep Sea Res.*, Part I, 41, 1685-1714, 1994.
- Defense Mapping Agency Hydrographic/Topographic Center (DMAH/TC), *Sailing Directions (Planning Guide) for the North Atlantic*, DMA Pub. No. 140, Washington D. C., 390 pp., 1988.
- Feliks, Y., On the Rossby radius of deformation in the ocean, *J. Phys. Oceanogr.*, 15, 1607-1685, 1985.

Fiuza, A. F. de G., The Portuguese coastal upwelling system, in *Actual problems of oceanography in Portugal*, Junta Nacional de Investigacao Cientifica e Tecnologica, Lisboa, 45-71, 1980.

Fiuza, A. F. de G., M. E. de Macedo, M. R. Guerreiro, Climatological space and time variation of the Portuguese coastal upwelling, *Oceanologica Acta*, Vol. 5, No. 1, 31-40, 1982.

Fiuza, A. F. de G., Hidrologia e dinamica das Aguas costeiras de Portugal. Dissertacao apresentada a Universidade de Lisboa para obtencao do grau de Doutor em Fisica, especializacao em Ciencias Geofisicas. Univ Lisboa, 294pp., 1984.

Fiuza, A. F. de G. and F. M. Sousa, Preliminary results of a CTD survey in the Coastal Transition Zone off Portugal during 1-9 September 1988, *Coastal Transition Zone Newsletter*, 4, 2-9, 1989.

Folkard, A. M., P. A. Davis, A. F. de G. Fiuza, and I. Ambar, Remotely sensed sea surface thermal patterns in the Gulf of Cadiz and the Strait of Gibraltar: Variability, correlations, and relationships with the surface wind field, *J. Geophys. Res.*, 102, 5669-5683, 1997.

Frouin, R., A. F. G. Fiuza, I. Ambar, and T. J. Boyd, Observations of a poleward surface current off the coasts of Portugal and Spain during Winter, *J. Geophys. Res.*, 95, 679-691, 1990.

Gill, A. E., Atmosphere-Ocean Dynamics. *Academic Press*, 662 pp., 1982.

Hagen, E., C. Zulicke, and R. Feistel, Near-surface structures in the Cape Ghir filament off Morocco, *Oceanol. Acta*, 19, 6, 577-598, 1996.

Haidvogel, D. B., A. Beckmann, and K. S. Hedstrom, Dynamical simulation of filament formation and evolution in the coastal transition zone, *J. Geophys. Res.*, 96, 15,017-15,040, 1991.

Haynes, R. and E. D. Barton, A poleward flow along the Atlantic coast of the Iberian Peninsula, *J. Geophys. Res.*, 95, 11425-11441, 1990.

Haynes, R., E. D. Barton, and I. Pilling, Development, persistence and variability of upwelling filaments off the Atlantic coast of Iberia, *J. Geophys. Res.*, 98, 22681-22692, 1993.

Holland, W. R., The role of mesoscale eddies in the general circulation of the ocean-Numerical experiments using a wind-driven quasi-geostrophic model, *J. Phys. Oceanogr.*, 8, 363-392, 1978.

Holland, W. R. and M. L. Batteen, The parameterization of subgrid scale heat diffusion in eddy-resolved ocean circulation models, *J. Phys. Oceanogr.*, 16, 200-206, 1986.

Ikeda, M., W. J. Emery, and L. A. Mysak, Seasonal variability in meanders of the California Current system off Vancouver Island, *J. Geophys. Res.*, 89, 3487-3505, 1984a.

Ikeda, M., L. A. Mysak, and W. J. Emery, Observations and modeling of satellite-sensed meanders and eddies off Vancouver Island, *J. Phys. Oceanogr.*, 14, 3-21, 1984b.

Iorga, M. C., and M. S. Lozier, Signatures of the Mediterranean outflow from a North Atlantic climatology, 1. Salinity and density fields, *J. Geophys. Res.*, 104, 25,985-26,009, 1999.

Kase, R.H., A. Beckmann, and H.H. Hinrichsen, Observational evidence of salt lens formation in the Iberian Peninsula, *J. Geophys. Res.*, 94, 4905-4912, 1989.

Levitus, S., and T. P. Boyer, World ocean atlas 1994, Vol. 4: Temperature, *NOAA Atlas NESDI 4*, 117 pp., U. S. Dept. of Commerce, Washington, D.C., 1994.

Levitus, S., R. Burgett, and T.P. Boyer, World ocean atlas, 1994, Vol. 3: Salinity, *NOAA Atlas NESDI 3*, 99 pp., U.S. Dept. of Commerce, Washington, D.C., 1994.

Lozier, M.S., W. B. Owens, and R. Curry, The climatology of the North Atlantic, *Prog. Oceanogr.*, 36, 1-44, 1995.

McCreary, J. P., A linear stratified ocean model of the coastal undercurrent, *Phil. Trans. Roy. Soc.*, A 302, 385-413, 1981.

McCreary, J. P., Y. Fukamachi, and P. K. Kundu, A numerical investigation of jets and eddies near an eastern ocean boundary, *J. Geophys. Res.*, 92, 2515-2534, 1991.

McCreary, J. P., P. K. Kundu, and S. Y. Chao, On the dynamics of the California Current system, *J. Mar. Res.*, 45, 1-32, 1987.

Meinke, J., G. Siedler, and W. Zenk., Some current observations near the continental slope off Portugal. *"Meteor" Forsch.-Ergebn.*, A, 16, 15-22, 1975.

Nelson, C. S., Wind stress and wind stress curl over the California Current, NOAA Tech Rep. NMFS SSFR-714, U. S. Dept. Commerce, 87 pp., 1977.

Pares-Sierra, A., W. B. White, and C. -K. Tai, Wind-driven coastal generation of annual mesoscale eddy activity in the California Current system: A numerical model, *J. Phys. Oceanogr.*, 23, 1110-1121, 1993.

Pichevin, T., and D. Nof, The eddy cannon, *Deep-Sea Res.*, 43, 1475-1507, 1996.

Prater, M. D., and T. B. Sanford, A Meddy off Cape St. Vincent. Part I: Description, *J. Phys. Oceanogr.*, 24, 1572-1586, 1994.

Richardson, P. L., and A. Tychensky, Meddy trajectories in the Canary Basin measured during the SEMAPHORE experiment, 1993-1995, *J. Geophys. Res.*, 103, 25,029-25,045, 1998.

Stammer, D., H. H. Hinrichsen, and R. H. Kase, Can Meddies Be Detected By Satellite Altimetry?, *J. Geophys. Res.*, 96, 7005-7014, 1991.

Tokmakian, R. T., and P. G. Challenor, Observations in the Canary Basin and the Azores Frontal Region Using Geosat Data, *J. Geophys. Res.*, 98, 4761-4773, 1993.

Tomczak, M. and J. S. Godfrey, *Regional Oceanography: An Introduction*, Pergamon Press, New York, 422 pp., 1994.

Trenberth, K. E., W. G. Large, J. G. Olsen, The mean annual cycle in global ocean wind stress, *J. Phys. Oceanogr.*, 20, 1742-1760, 1990.

Van Camp, L., L. Nykjaer, E. Mittelstaedt, and P. Schlittenhardt, Upwelling and boundary circulation off Northwest Africa as depicted by infrared and visible satellite observations, *Prog. Oceanogr.*, 26, 357-402, 1991.

Weatherly, G. L., A study of the bottom boundary layer of the Florida Current, *J. Phys. Oceanogr.*, 2, 54-72, 1972.

Wooster, W. S. and J. L. Reid, Jr., Eastern Boundary Currents. In *The Sea, Vol. 2*, M. N. Hill, Ed., Wiley International, New York, 253-280, 1963.

Wooster, W. S., A. Bakun, and D. R. McLain, The seasonal upwelling cycle along the eastern boundary of the North Atlantic, *J. Mar. Res.*, 34, 131-140, 1976.

Zenk, W., and L. Armi, The complex spreading pattern of Mediterranean Water off the Portuguese continental slope, *Deep Sea Res.*, 37, 1805-1823, 1990.

INITIAL DISTRIBUTION LIST

	No. Copies
1. Defense Technical Information Center.....2 8725 John J. Kingman Rd, STE 0944 Ft. Belvoir, VA 22060-6218	
2. Dudley Knox Library.....2 Naval Postgraduate School 411 Dyer Rd Monterey, CA 93943-5101	
3. Chairman (Code OC/Gd).....1 Department of Oceanography Naval Postgraduate School Monterey, CA 93943-5122	
4. Chairman (Code MR/Wx).....1 Department of Meteorology Naval Postgraduate School Monterey, CA 93943-5114	
5. Dr. Mary L. Batteen, (Code OC/Bv).....4 Department of Oceanography Naval Postgraduate School Monterey, CA 93943-5122	
6. Dr. Curtis A. Collins, (Code OC/Co)1 Department of Oceanography Naval Postgraduate School Monterey, CA 93943-5122	
7. LT Antonio Martinho, PON.....1 5200 Coe Avenue, Apt. 1155 Seaside, CA 93955	
8. LCDR Patrick J. Murray.....3 412 7 th Street Coronado, CA 92118	